

Some Aspects of Non-equilibrium Polymer Translocation Dynamics



A Thesis Submitted in Partial Fulfillment of the Requirements for the Degree of

Doctor of Philosophy

by

Bappa Ghosh

ID: 20143345

JUNE 2019

**Department of Chemistry
Indian Institute of Science Education and Research Pune**

To My Parents

Certificate

It is hereby certified that the work described in this thesis entitled “*Some Aspects of Non-equilibrium Polymer Translocation Dynamics*” submitted by *Mr. Bappa Ghosh* was carried out by the candidate, under my supervision. The work presented here or any part of it has not been included in any other thesis submitted previously for the award of any degree or diploma from any other university or institution.



Date: 3rd June, 2019

Dr. Srabanti Chaudhury

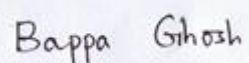
Supervisor

Email: srabanti@iiserpune.ac.in

Declaration

I declare that this written submission represents my ideas in my own words, and wherever other's ideas have been included; I have adequately cited and referenced the sources. I also declare that I have adhered to all principles of academic honesty and integrity and have not misrepresented or fabricated or falsified any idea/data/fact/source in my submission. I understand that violation of the above will cause for disciplinary action by the Institute and can also evoke penal action from the sources which have thus not been adequately cited or from whom proper permission has not been taken when needed.

Date: 3rd June, 2019



Bappa Ghosh

ID:20143345

Acknowledgments

My experience during my doctoral studies has been fulfilling due to many people I met and shared time during the journey. First and foremost, I convey my sincerest regards and gratitude to my supervisor Dr. Srabanti Chaudhury. She has been very encouraging and continuously supportive in all ups and downs throughout the journey. She is always a deeply involved person and first to respond to any issues regarding research. I am thankful for her guidance, and I will always cherish the freedom for doing research being one of the early students of the group.

I am grateful to my Research Advisory Committee (RAC) members Dr. Arnab Mukherjee (IISER Pune), Dr. Suman Chakrabarty (CSIR-NCL) and Dr. Durba Sengupta (CSIR-NCL) for their helpful suggestions not only during annual evaluation meetings but also at any time throughout the year. My collaborators Dr. Jalal Sarabadani and Prof. Tapio Ala-Nissila (Aalto University, Finland) provided me valuable research inputs in different joint ventures. I learned a lot from them during our numerous Skype conversations.

I feel very fortunate to have Divya as my labmate and a friend, who is always there to discuss and share anything between the earth and the sky. I would especially like to thank Avdhoot, Mahesh, and Meghna. I learned the importance of good lab-space in research life by sharing and being critical on many issues with them. The fun time and memories in the lab with Khushboo, Vaibhav, Megha, Ngawang, Kanika, Mayukh, Mrityunjay, Navoneel, Kinjal will always be with me. Subbu, Reman, Praveen, Indu, Rakesh, Mandar, Debasis, Hridya were always there for help and discussion on any issues related to studies and understanding. I want to express my heartfelt thanks to Prabhat for all the new and exciting ideas we shared during countless conversations.

I am thankful to all my friends for their support and encouragement, especially Sayantan, Pragati, Ajay, Ashoke, Chandan, Kamal, Madan, Sanjit, Shatruhan, Vinay, Turmoli, Yashwant, Anindita, Wasim, Avisikta, Debasis, Abhishek, and Sandip.

I am extremely thankful to IISER Pune for the fellowship, infrastructure, and necessary facilities. Mayuresh, Tushar, Sanjay, Sachin, Suresh, Shailesh, Neeta from academic office, and IT were always there to make life easier.

I have reached to this platform of doctoral studies all because of my beloved teachers from my school and college days. I feel blessed to be taught by them. I sincerely thank Dr. Bidhan Chandra Bag, Visva-Bharati University for motivating, teaching, encouraging and supporting the journey and implanting the seed to look for new things at the early days of my undergraduate studies.

Last but not the least, I want to express my sincere thanks to my parents and family members for their unconditional support and faith in this long journey.

IISER Pune

Bappa Ghosh

List of Publications

1. *Translocation Dynamics of Folded Polymer Pulled Through a Nanopore*, **B. Ghosh**, J. Sarabadani, S. Chaudhury, and T. Ala-Nissila, (Manuscript under preparation).
2. *Translocation Dynamics of an Asymmetrically Charged Polymer through a Pore under the Influence of Different pH Conditions*, **B. Ghosh** and S. Chaudhury, The Journal of Physical Chemistry B 123, 4318-4323 (2019).
3. *Dynamics of end-pulled polymer translocation through a nanopore*, J. Sarabadani, **B. Ghosh** and S. Chaudhury, and T. Ala-Nissila, EPL (Europhysics Letters) 120, 38004 (2018) .
4. *Influence of the Location of Attractive Polymer–Pore Interactions on Translocation Dynamics*, **B. Ghosh** and S. Chaudhury, The Journal of Physical Chemistry B 122, 360-368 (2017)
5. *Fluctuation theorems for total entropy production in generalized Langevin systems*, **B. Ghosh** and S. Chaudhury, Physica A: Statistical Mechanics and its Applications 466, 133-139 (2017).

Synopsis of the Thesis

Polymer translocation is an important biological process which has become an active field of research in recent past due to its potential application in DNA sequencing, drug design, virus injection, etc. This work aimed to study and understand the different aspects of the non-equilibrium phenomena observed in driven polymer translocation using computer simulations. In **Chapter 1**, we have introduced polymer translocation as a non-equilibrium phenomenon, its application, and scope. Next, the thesis has been broadly divided into two sections based on the application of the force on the polymer, namely the pore driven translocation and the end pulled translocation. In **Chapter 2** and **Chapter 3**, the role of polymer-pore interactions has been studied for the pore-driven translocation. In **Chapter 4** and **Chapter 5**, the end-pulled translocation has been studied for single and folded polymer movement through the pore. **Chapter 6**, considers a model particle in a viscous heat bath which is dragged with a harmonic potential and its total entropy production is calculated, which has implications in non-equilibrium thermodynamic principles in single molecule experiments.

Chapter 2 :

In this chapter, we consider a uniformly positive charged polymer chain translocating through a pore constructed with negatively charged regions at different spatial locations. This kind of model mimics the experimental condition when the pore is mutated with different amino acids in order to create charged electrostatic traps. We have studied the translocation times of such a polymer chain by varying the strength and location of the electrostatic traps, the magnitude of forces acting inside the pore and for varying the chain length of the polymer. The translocation time during different stages of the translocation has been calculated and is supported by a quasi-equilibrium free-energy calculations.

Chapter 3 :

In this section, both the charges on the polymer and the pore are varied to study the polymer translocation during different stages for pore-driven translocation. This kind of situation is important to tune the translocation of biological polymers by varying the charges on the surface of the polymer through a change in pH of the medium. The change in the pH of the

medium not only alters the charge decoration on the pore but also affects the charge on the polymer because the polymers are constituted by different amino acids. The simulation results on translocation times are again supported by similar quasi-equilibrium free energy calculations.

Chapter 4 :

In this chapter, we study the dynamics of end-pulled polymer translocation by applying very high force at one end of the polymer. Such kind of model study is important in optical tweezers or AFM experiments. The Langevin dynamics simulations revealed the propagation of the tension along the chain by measuring different quantities like waiting time distribution, the velocity of the monomers as a function of monomer number and as a function of distance during different stages of the translocation. From the simulations studies, one can find the total friction on the polymer and the propagation of the dynamic quantity “tension front” which was used to develop a quantitative theory for the end-pulled polymer translocation.

Chapter 5 :

In this part, the pulled polymer translocation is done for a folded chain. The translocation happened when two monomers crossed the pore simultaneously. It has implications in solid-state nanopore experiments where, unlike biological pores, the pore diameter could be varied to allow translocation of two monomers together. The waiting time distribution and velocity calculations revealed the dynamics of tension propagation along the two chain segment when chain segment lengths were varied. Further, the simulation results can be used to get a quantitative theory for the translocation of polymers with folded configurations.

Chapter 6 :

In this chapter, the dynamics of a single model particle in a heat bath subjected to a harmonic potential and dragged by a constant time-dependent external force is modeled using the generalizes Langevin equation(GLE) with colored noise. The total entropy production was calculated by considering the contribution of both the system and the surrounding on the total entropy production. This kind of analytical model is useful in obtaining a quantitative measure of thermodynamic quantities such as work done, entropy generation, etc. in many single-molecule experiments similar to polymer translocation which are away from thermodynamic equilibrium.

Contents

Certificate.....	iii
Declaration.....	iv
Acknowledgments.....	v
List of Publications	vii
Synopsis of the Thesis	viii
1. Introduction	1
1.1 Polymer Translocation	2
1.2 Experiments and Applications	4
1.3 Theoretical and Computational Studies	7
1.4 Simulation Methods	8
1.5 Overview of the thesis work	10
1.6 References.....	12
2. Pore-driven polymer translocation: Effect of pore charge distribution.....	15
2.1 Introduction.....	16
2.2 Model	17
2.3 Result and Discussion	19
2.4 Free Energy Calculation.....	26
2.5 Conclusion	31
2.6 References.....	32
3. Pore-driven polymer translocation: Effect of pore and polymer charge distribution ..	34
3.1 Introduction.....	35
3.2 Model	37
3.3 Results and Discussion	41
3.4 Conclusions.....	47
3.5 Appendix-3.1	47
3.6 References.....	51
4. End-pulled Polymer Translocation: Single Chain Dynamics	53
4.1. Introduction.....	54

4.2.	Model	56
4.3.	Result and Discussion	58
4.4.	Conclusion	62
4.5.	References.....	62
5.	End-pulled polymer translocation: Folded chain dynamics.....	64
5.1	Introduction.....	65
5.2	Model	66
5.3	Result and Discussion	68
5.4	Conclusion	76
5.5	References.....	76
6.	Fluctuation theorems for total entropy production in non-Markovian heat bath.....	78
6.1	Introduction.....	79
6.2	Model	81
6.3	Entropy Production Theorem.....	85
6.4	Total Entropy Distribution Function.....	87
6.5	Conclusions.....	89
6.6	References.....	90
7.	Conclusions.....	92
7.1	Conclusions and Future Outlook.....	93

List of Figures

Figure 1.1: Polymer translocation, stages and translocation time	3
Figure 1.2: (a) Experimental setup of polymer translocation and (b) Current drop profile in a typical voltage driven translocation experiment.	5
Figure 1.3: The schematic variables of the translocation process	5
Figure 1.4: The schematic of the optical trap induced end-pulled translocation	6
Figure 2.1: (a) Schematic representation of a polymer chain translocating through a pore of length $L=6$. (b) Representation of the different components of the total translocation time.	17
Figure 2.2: The distribution of translocation time for different attractive strength at (a) <i>cis</i> (b) <i>trans</i> (c) <i>cis-trans</i> side of the pore under the driving force of $F= 3.3$. The length of chain $N= 50$. $q_2= 0$ corresponds to a wild type pore with no pore- monomer interaction.....	20
Figure 2.3: Total translocation time and its components as a function of the attractive strength for interaction at (a) <i>cis</i> (b) <i>trans</i> and (c) <i>cis- trans</i> of the pore under the driving force $F=3.3$ and $N=50$	20
Figure 2.4: The total translocation time and its components as a function of the driving force for interaction strength $q_2= 0.05$ at (a) <i>cis</i> (b) <i>trans</i> and (c) <i>cis- trans</i> region of the pore with $N = 50$. $q_2=0$ corresponds to the wild type pore.	23
Figure 2.5: Free energy landscape for a polymer chain of length $N= 50$ translocating through a nanopore of length $L= 6$ with different attractive strengths at (a) <i>cis</i> (b) <i>trans</i> and (c) <i>cis- trans</i> region of the pore under the driving force $F= 0.3$	29
Figure 3.1: Schematic representation of the 36-bead polymer chain translocation from the <i>trans</i> to the <i>cis</i> side of the pore during (a) entry stage (b) exit stage. q_A and q_B are the charges on the entry and tail part of the chain and q_{ring} is the charge on the entry side of the pore. For S-I, $q_B= -12e$, $q_{ring}= -7e$, for S-II, $q_B= -4e$, $q_{ring}= 0$ and for S-III $q_B= -1e$, $q_{ring}= 6e$, $q_A= +12e$ for all the three systems.	40
Figure 3.2: The histogram of translocation time for different systems during the entry stage (a) pore filling, τ_1 (b) the first part of the transfer stage τ_{21} for a chain of length $N= 36$ and $E=4$; top horizontal axis is for S-I while the bottom horizontal axis is for S-II and S-III showing different utilized scales.	43

Figure 3.3: The histogram of translocation time for different systems during the exit stage (a) the second part of the transfer stage, τ_{22} (b) pore emptying stage, τ_3 for a chain of length $N=36$ and $E=0.1$ 44

Figure 3.4: Free energy landscape for the translocation of a polymer chain of length $N=36$ during the exit stage (τ_{22} and τ_3) translocating through a pore of length $L=26$ for S- II and S- III at $E=0.1$ 46

Figure 3.5: Free energy landscape for the translocation of a polymer chain of length $N=36$ during the entry stage ($\tau_1 + \tau_{21}$) translocating through a pore of length $L=26$ for S-I, S- II and S-III at $E=4$ 51

Figure 4.1: Schematic representation of end-pulled translocation..... 57

Figure 4.2: Various possible translocation scenarios during the tension propagation (TP) stage for the *trans* side strong stretching (SST) regime. The driving force f acts only on the head monomer of the polymer in the *trans* side. The length of the polymer is N_0 and the number of beads that have been already translocated into the *trans* side is denoted by s . The number of total beads influenced by the tension is $N=l+s$ (in the TP stage $N < N_0$). In panel (a) the *cis* side subchain is also in the SS regime (SSC) during the TP stage. (b) The translocation process when the tension front reaches the end of the chain on the *cis* side in the SSC regime (post propagation stage (PP), where $N=N_0$). Panels (c) and (e) are the same as panel (a) but for the stem-flower (SFC) and trumpet (TRC) regimes in the *cis* side, respectively. Panels (d) and (f) are the same as panel (b) but for SFC and TRC, respectively. (Figure Credit : Dr. Jalal Sarabadani) 58

Figure 4.3: The waiting time distribution for $N=100$, $f=100$ end-pulled polymer translocation. 59

Figure 4.4: Velocity vs monomer number for $N=100$, $f=100$. The maroon circles indicate the monomer bead which is at the pore. 60

Figure 4.5: Comparison of the waiting time distribution as a function of the translocation coordinate “ s ” from simulation and theory (Figure Credit : Dr. Jalal Sarabadani). 61

Figure 5.1: Schematic representation of the translocation of a polymer with a folded configuration (a) 51:51: symmetrical fold (b) 31:71 (c) 11:91 67

Figure 5.2: The translocation time distributions. (a) 51:51, (b) 31:71 and (c) 11:91 69

Figure 5.3: Waiting time distributions of the monomers. (a) 51:51, (b) 31:71 and (c) 11:91 72

Figure 5.4: The stages of the translocation. 73

Figure 5.5: The monomer velocities. (a) 51:51, (b) 31:71 and (c) 11:91 75

List of Tables

Table 2.1: Translocation times for chain length N and external driving force F traversing through a purely repulsive pore ($q=0$).....	21
Table 2.2 : Translocation times for chain length $N=50$ and $F=3.3$ traversing through a repulsive pore with polymer- pore interaction at different locations within the pore.	22
Table 2.3 : Translocation times for chain length $N=50$ and $q_2=0.05$ at different locations within the pore with varying magnitudes of externally applied field.	25
Table 2.4 : Translocation times for chain length $N=12$ and $F=4.8$ with polymer- pore interaction at different locations within the pore.	26
Table 3.1: Translocation times during entry stage.....	44
Table 3.2: Translocation times during exit stage	45
Table 5.1: Different translocation times of N_1 and N_2 with different branch ratios.	70

1. Introduction

1.1 Polymer Translocation

A single eukaryotic cell is filled with different components and machinery which function in harmony to manifest as life. The elements and machinery of the cell work in a compact and crowded environment.¹ Understanding the structure, dynamics, and function of a compact cell is very challenging due to the heterogeneity of the cellular environment. It is of foremost importance to separately study each of the components and machinery in a cell to order to gain a comprehensive understanding of the functioning of the cell.

A general outlook on the cellular components reveals that the polymeric materials such as cellulose and polypeptides are at the core as the structural basis and functioning of a cell. These polymers carry the information of life as ribonucleic acid (RNA), deoxyribonucleic acid (DNA), etc. The biological functionality is mostly governed by thousands of proteins which are very long polymers coiled into a particular shape. The fundamental understanding of the properties and dynamics of the polymers is thus crucial.²⁻³

The biological polymers such as DNA, RNA, polypeptides, inside the cell are needed to be moved from one place to another. Thus, polymer movement becomes one of the fundamental processes in life. Polymer translocation is the passage of polymers through a narrow hole mostly through different kinds of pores inside the cell. In the past three decades, polymer translocation has become the center of attention in terms of scientific curiosity to many people from the different arena of sciences. It has attracted physicist, biologist, chemist, engineers, and so on which made polymer translocation to be an interdisciplinary topic.

The translocation of a polymer through a membrane plays a vital role in many biological processes like the transport of RNA through the nuclear pore complex,⁴ the passage of DNA from a virus into a host cell (bacteriophage DNA ejection),⁵ transfer of proteins across membranes and so in. The key concepts and recent development of polymer translocation are given in the book by Muthukumar⁶ and the review by Metzler *et al.*⁷ Polymer translocation have a variety of technological applications such as the detection of nucleobases in RNA and DNA chains,⁸ fast and cheap DNA sequencing,⁹ virus injection,¹⁰ gene therapy,¹¹ and drug delivery.⁷

The process of polymer translocation is shown as a schematic in Figure 1.1. A polymer is present on the one side of a wall and reaches the other side through a pore. It is a simple depiction of the complex biological translocation process. The polymer in this schematic can be

a DNA, RNA or polypeptides. The wall here is the cell membrane or nuclear membrane. Different membrane proteins like alpha-hemolysin constitute the pore.

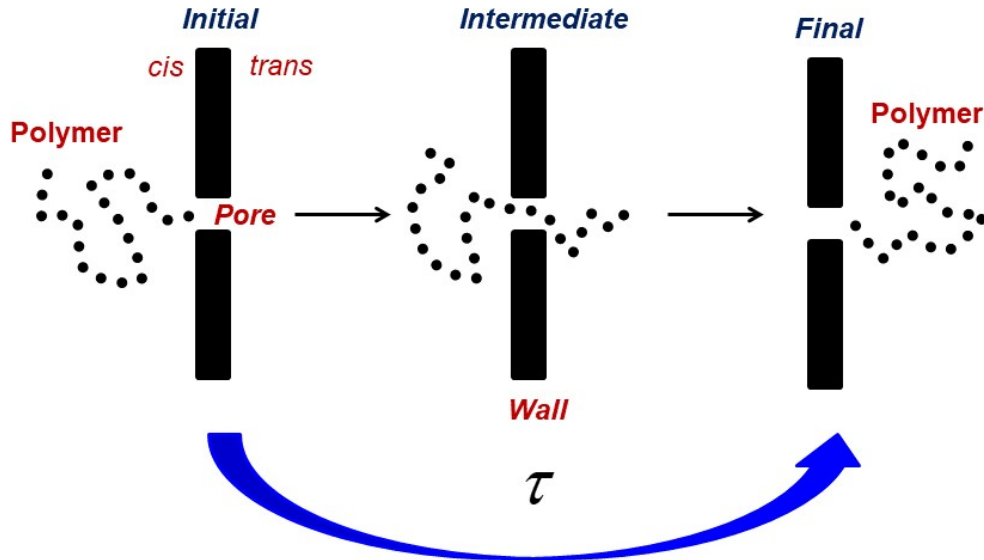


Figure 1.1: Polymer translocation, stages and translocation time

The passage of the polymer through the narrow hole happens when the diameter of the hole is tiny compared to the size of the polymer which is usually denoted by its radius of gyration (R_g). When the polymer enters the pore, it has to uncoil first and then pass through the narrow pore. The number of allowed conformations of the polymer is reduced when it enters the pore, and the polymer faces a free energy (entropic) barrier. Thus the problem of polymer translocation can be envisaged as a ‘barrier crossing’ phenomenon which is relevant to the physicist and chemist from the statistical thermodynamics point of view. To overcome this entropic barrier, a driving force facilitates the movement of the polymer across the pore. Due to the long relaxation time of polymer chains in solution, in the presence of a driving force, the translocation happens much before the equilibration of the polymer chain in the solution.¹²⁻¹⁴ Thus from the thermodynamics perspective, forced polymer translocation is an out of equilibrium phenomena.

With the advent of sophisticated technologies, single molecule experimental techniques have gone through a massive leap in the past few decades. Harnessing the single-molecule experimental methods, it was possible to detect picoampere electrical signals of the single molecule passage of molecules through nanopores. This was first shown by the landmark experiment from J.J. Kasianowicz *et al.*¹⁵ in 1996 through the biological protein pore alpha-hemolysin. In **Section 1.2**, a brief overview of this experiment and other subsequent developments of the single molecule techniques are discussed in brief. These experiments give a clear understanding of the polymer translocation and the scope of theoretical and computational studies.

1.2 Experiments and Applications

The experiment by J.J. Kasianowicz *et al.*¹⁵ studied the phenomena of polymer translocation of a single-stranded RNA/DNA threaded through protein nanopore inserted in a lipid bilayer membrane. In the experimental setup, the convenient protein used to model polymer translocation is the α -hemolysin from *Staphylococcus aureus*. It forms a heptameric pore about 10nm long and 2nm wide across a biological membrane that separates the set up into two chambers, one is called *cis* side, and another is called the *trans* side. Protein nanopores have smaller inner diameters that allow only single-file polymer translocations. With the progress in material development, the biological membranes proteins were replaced with solid-state nanopores, which are constituted of silicon dioxide or graphene-based materials. The solid-state nanopores are more stable to different ranges of voltage, pH changes, and other chemical conditions compared to the biological pores. In the polymer translocation experiments, a voltage difference is applied across the pore, and subsequent ionic current is measured through the pore. A current blockage occurs when the ssDNA translocates in the α -HL channel. Once the polymer enters the pore from the *cis* side, it blocks the ionic current through the pore. As a result, the original current drops to a minimum, and this drop persists till the polymer exits the pore from the *trans* side. The experimental schematic and current drop profiles are shown in **Figure 1.2 (a) and (b)**.^{11, 16} This drop in the current and the duration of the fall depends on the polymer length.

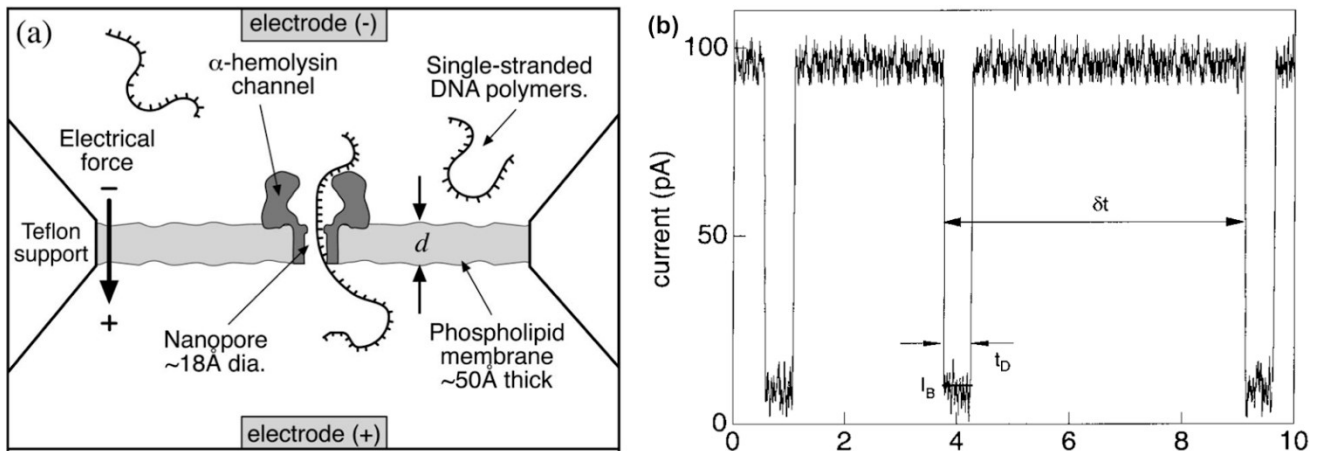


Figure 1.2: (a) Experimental setup of polymer translocation and (b) Current drop profile in a typical voltage driven translocation experiment (taken from reference 11 and reference 16).^{11,16}

Dependence of the translocation time on system parameters

The translocation time depends on many variables like the polymer length (N), pore length (L), pore width (W), the strength of applied force (F), polymer-pore interaction (U), etc. It is schematically shown in Figure 1.3.

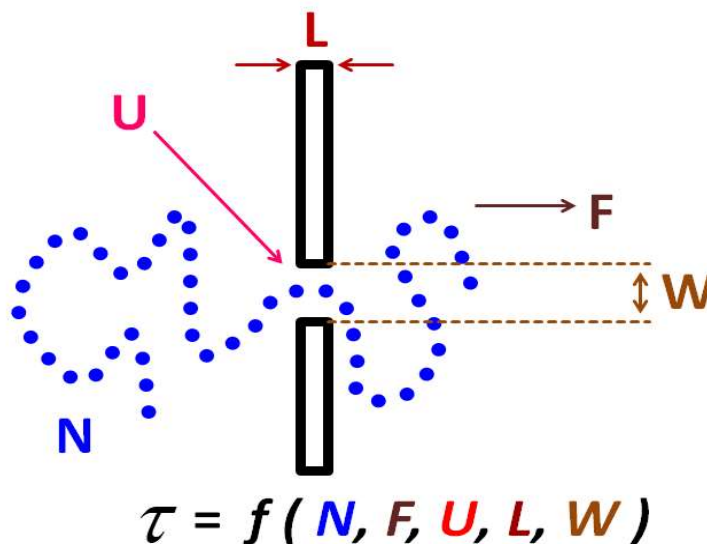


Figure 1.3: The schematic variables of the translocation process

Based on the application of external force, the polymer translocation is categorized into two broad divisions. One is called the ‘unbiased’ or ‘unforced’ translocation, and the other one is called the ‘biased’ or ‘forced’ translocation. While the unforced polymer translocation is mainly of theoretical interests, the forced translocation is of practical and experimental relevance. The forced translocation is again divided into two categories.¹⁷⁻¹⁹ The first one (as in **Figure 1.2 (a) and (b)**) is known as ‘voltage-driven translocation’ or ‘pore-driven translocation.’⁷ Here the effective force on the polymer is felt by the monomers within the pore during translocation. It happens as the effective ionic concentration difference across the pore is mainly at the pore. Virtually, the monomers which are situated at the pore will experience the force due to the chemical potential difference across the pore. The other type of forced polymer translocation is called the ‘end-pulled translocation where the polymer is pulled through the nanopore through optical or magnetic tweezers^{10, 20-21} and atomic force microscopy²² (as shown in Figure 1.4)

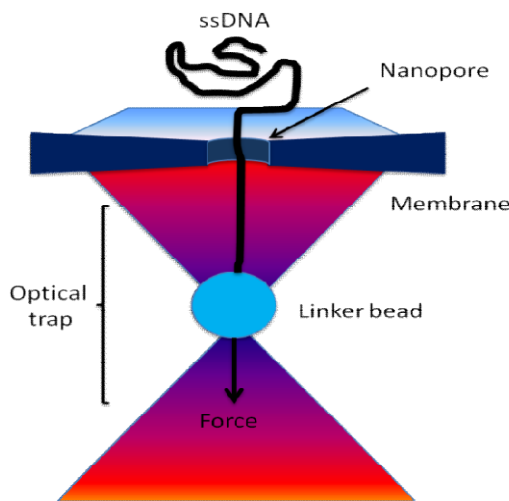


Figure 1.4: The schematic of the optical trap induced end-pulled translocation

The study by Dekker *et al.*²¹ showed that if a polymer is pulled through the pore, it can give similar current signals as that of voltage-driven translocation. Although this technique is relatively difficult to implement in experiments compared to voltage driven studies, it provides with more precision and control in the polymer translocation studies. Better controlled polymer translocation is crucial in technological applications like rapid DNA sequencing, gene therapy,⁸⁻⁹ and human genome project,²³ etc.

Again ‘force’ is only one variable which controls the translocation process. There are several other factors which can change the translocation scenario. For example, it was found experimentally that the translocation time distribution of polydeoxyadenylic (poly (dA)) acid and polydeoxycytidylic acid DNA molecules are different. The origin of the different behavior was attributed to a stronger attractive interaction of poly(dA) with the pore. In a recent experiment by Krasilnikov *et al.*,²⁴ it was found that for a single poly (ethylene glycol) (PEG) polymer translocating through a protein nanopore, the residence time in the channel has a nonmonotonic dependence on the polymer molecular weight in the limit of a strong, attractive polymer-pore attraction. Further development on the understanding of this complex translocation process from theoretical perspectives based on these variables is discussed in the next section.

1.3 Theoretical and Computational Studies

The first theoretical study on polymer translocation was reported by Sung and Park²⁵ and later developed by Muthukumar²⁶ for the case of unbiased translocation. They considered the translocation process as a one-dimensional diffusion problem where the reaction coordinate is the number of monomers on the trans side of the pore. It is assumed that the translocation process is sufficiently slow and the polymer is at an equilibrium state during the translocation. The dynamics of the system is captured by the Fokker–Planck equation and the mean translocation time as a function of the chain length scales as was found be $\tau \sim N^2$ for unbiased translocation whereas τ scales as $N/\Delta\mu$ for the driven translocation scaled as in the absence of hydrodynamic interactions.²⁷ Later Kantor and Kardar showed from 2D lattice simulations that the translocation time scales as $N^{2.5}$ for unimpeded motion²⁸ and $\tau \sim N^{1.53}/\Delta\mu$ when polymer experience a chemical potential difference $\Delta\mu$ across the membrane.²⁹ In all these simulation studies, the equilibrium assumption was questioned since the translocation time of the unbiased case is of the same order of magnitude as the diffusion time of a polymer in bulk solution without a barrier. For the case of biased translocation, the polymer does not have enough time to relax to its equilibrium configuration. The translocation problem has been studied using different approaches such as the generalized Langevin equation (GLE) formulation by Chaudhury *et al.*³⁰ to describe the anomalous translocation dynamics and calculate the scaling laws for the average translocation time as a function of N at weak and strong force regimes. The fractional Fokker Planck equation (FFPE) method by Metzler and Klafter³¹ studies the stochastic evolution of a particle under a non-linear external force in a heat bath. Their one-dimensional

model based on the FFPE formalism could account for anomalous diffusive behavior relevant to complex biological environments. Using this same FFPE formalism, Dubbeldam *et al*³² studied translocation of polymer through a narrow pore using extensive molecular dynamics simulation. The effect of thermal fluctuations on the diffusive nature of the translocating polymer was estimated by invoking scaling theory. In this work, the polymer was Vocks *et al*³³ that in the presence of an external field across the pore in three dimensions, the origin of the scaling behavior can be attributed to the local memory effects at the vicinity of the pore. Also, several other investigations for the scaling exponents for translocation were reported.³⁴⁻³⁵ Nevertheless, there is so far no clear knowledge regarding the scaling exponents. All these studies showed the importance of analytical models as well as computer simulations for studying the translocation process in elucidating the complex nature of the process. It showed that a quantitative description of the process was needed. A quantitative theory that takes into account the non-equilibrium aspect of the driven translocation was given by Sakaue³⁶⁻³⁸ based on *tension propagation theory* (TPT) and later developed and compared with molecular dynamic simulation.³⁹⁻⁴¹

In most cases, the non- equilibrium aspects of driven translocation are hidden in simple theories but can be well manifested by molecular dynamics simulations. Simple free energy calculations considering polymer translocation as a quasi-equilibrium process is insufficient to be quantitatively compared with the simulations. The simulations serve as a tool to mimic experiments that can be used to come up with theories of a process. The Langevin dynamics simulation method used in our work is described in the next section.

1.4 Simulation Methods

The key computational technique used here to study polymer translocation is the Langevin dynamics simulation where solvent interactions are implicitly included in the equation of motion. Along with this, the particles of the system feel random thermal kinetic energy. Depending on the context of the problem, changes have been incorporated into the equation of motion. These changes are discussed in the respective chapters. The general method which applies to all the cases is discussed here.

The polymer beads are modeled by a bead-spring chain. The beads experience excluded volume interaction given by the repulsive LJ interaction potential

$$U_{LJ}(r) = 4\epsilon \left[\left(\frac{\sigma}{r} \right)^{12} - \left(\frac{\sigma}{r} \right)^6 \right] + \epsilon, \text{ if } r \leq 2^{1/6}\sigma \quad \dots[\text{Eq. 1.1}]$$

$$U_{LJ}(r) = 0, \quad \text{if } r > 2^{1/6}\sigma \quad \dots[\text{Eq. 1.2}]$$

where r is the distance between two monomer beads, ϵ is the interaction strength and σ is the diameter of the monomer. The cut-off, $r_c = 2^{1/6}\sigma$. Only the repulsive part of the LJ potential is considered by including the ϵ term in Eq. 1.1. This is known as Weeks-Chandler-Anderson potential. This assures that the polymer is in a good solvent. The consecutive beads are connected by finitely extensible nonlinear elastic (FENE) springs. The pair potential of the corresponding polymer is-

$$U_{FENE}(r) = -\frac{kR_0^2}{2} \ln\left(1 - \frac{r^2}{R_0^2}\right) \quad \dots[\text{Eq. 1.3}]$$

where k is the spring constant, and R_0 is the maximum bond length. Newton's equation of motion is solved starting from some initial coordinates and velocities of the polymer configuration. The equation is solved to predict the next set of the coordinates, velocities. It includes conservational, frictional and random forces. These forces on each of the i th particle can be written as -

$$m\ddot{r}_i = -\nabla(U_{LJ} + U_{FENE}) + F_{ext} + F_i^F + F_i^R \quad \dots[\text{Eq. 1.4}]$$

where the frictional force $F_i^F = -\eta v_i$, v_i is the monomer velocity, η is the friction coefficient, F_i^R is the random force with a zero mean $\langle F_i^R(t) \rangle = 0$ and satisfies the fluctuation-dissipation theorem $\langle F_i^R(t) F_j^R(t') \rangle = 6\eta K_B \delta_{ij} \delta(t - t')$. The contribution F_{ext} comes from the external force acting on the monomers. The temperature was taken to be $1.2\epsilon/k_B$. The parameters of our MD simulations in LJ units have been chosen as $\sigma = 1$, $\epsilon = 1$, $R_0 = 1.5\sigma$, $k = 30$, and $\eta = 0.7$. Here, $k_B T = 1.2$, $m = 1.0$. The mass of each bead corresponds to 936 amu for the actual DNA, its size corresponds approximately to the Kuhn length of a single-stranded DNA, which is about $\sigma = 1.5\text{nm}$, and the interaction strength is 3.39×10^{-21} J at room temperature ($T = 295\text{K}$). Therefore, the time and the force scales in LJ units are 32.1 ps and 2.3 pN, respectively.

In a general set up of the simulation, first, a wall is constructed consisting of LJ particles in XY-plane. Usually, a pore is created on the wall. The first monomer of a polymer is threaded on the pore. The simulation was carried out in three stages. First two stages were equilibration steps, and the third stage was the translocation step. During the equilibration of the polymer, the radius of gyration value of the chain reaches a constant value. In the first stage, the first monomer was kept frozen at the pore keeping all other monomers free at $\eta = 0.1$. After this, the chain was

further equilibrated at a higher $\eta = 0.7$, keeping all the conditions and constraints fixed. In the third stage, the constraint on the first monomer was lifted, and a force was applied to the polymer chain by various methods so as it to carry out the translocation. Throughout the simulations, the wall coordinates were kept frozen, and they interact with the polymer only via LJ potential. In general, at $t=0$, which marks the start of the translocation process, the head monomer is at the pore. The translocation process is terminated when the last bead of the chain enters to the trans side, and the translocation time is noted. If the chain escapes from the pore to the cis side, we neglect that, and a new translocation event is restarted from a new equilibrium configuration at $t=0$. The molecular dynamics calculations were performed using GROMACS⁴² and LAMMPS⁴³ simulation packages.

1.5 Overview of the thesis work

The main aim of this work was to study and understand the different aspects of the non-equilibrium phenomena observed in driven polymer translocation using computer simulations. In **Chapter 1**, we have introduced polymer translocation a non-equilibrium polymer dynamics problem, its application, and scope. Next, the thesis has been broadly divided into two sections based on the application of the force on the polymer, namely the pore driven translocation and the end pulled translocation. In **Chapter 2** and **Chapter 3**, the role of polymer-pore interactions has been studied for the pore-driven translocation. In **Chapter 4** and **Chapter 5**, the end-pulled translocation has been studied for single and folded polymer movement through the pore. **Chapter 6**, considers a model particle in a viscous heat bath which is dragged with a harmonic potential and its total entropy production is calculated, which has implications in non-equilibrium thermodynamic principles in single molecule experiments.

Chapter 2:

In this chapter, we consider a uniformly positive charged polymer chain translocating through a pore constructed with negatively charged regions at different spatial locations. This kind of model mimics the experimental condition when the pore is mutated with different amino acids in order to create charged electrostatic traps. We have studied the translocation times of such a polymer chain by varying the strength of the electrostatic traps, the magnitude of forces acting inside the pore and varying the chain length of the polymer. The translocation time is

calculated during different stages of the translocation and is supported by quasi-equilibrium free-energy calculations.

Chapter 3:

In this section, both the charges on the polymer and the pore are varied to study the polymer translocation during different stages for pore-driven translocation. This kind of situation is important to tune the translocation of biological polymers by varying the charges on the surface of the polymer through a change in pH of the medium. The change in the pH of the medium not only alters the charge decoration on the pore but also affects the charge on the polymer because the polymers are constituted by different amino acids. The simulation results on translocation times are again supported by similar quasi-equilibrium free energy calculations.

Chapter 4:

In this chapter, we study the dynamics of end-pulled polymer translocation by applying very high force at one end of the polymer. Such kind of model study is important in optical tweezers or AFM experiments. The Langevin dynamics simulations revealed the propagation of the tension along the chain by measuring different quantities like the waiting time distribution, the velocity of the monomers as a function of monomer number and as a function of distance during different stages of the translocation. From the simulations studies, one can find the total friction on the polymer and the propagation of the dynamic quantity “tension front” which was used to develop a quantitative theory for the end-pulled polymer translocation.

Chapter 5:

In this part, the pulled polymer translocation is done for a folded chain. The translocation happened when two monomers crossed the pore simultaneously. It has implications in solid-state nanopore experiments where, unlike biological pores, the pore diameter could be varied to allow translocation of two monomers together. The waiting time distribution and velocity calculations revealed the dynamics of tension propagation along the two chain segment when chain segment lengths were varied. Further, the simulation results can be used to get a quantitative theory for the translocation of polymers with folded configurations.

Chapter 6:

In this chapter, the dynamics of a single model particle in a heat bath subjected to a harmonic potential and dragged by a constant time-dependent external force is modeled using the generalized Langevin equation (GLE) with colored noise. The total entropy production was calculated by considering the contribution of both the system and the surrounding on the total entropy production. This kind of analytical model is useful in obtaining a quantitative measure of thermodynamic quantities such as work done, entropy generation, etc. in many single-molecule experiments similar to polymer translocation which are away from thermodynamic equilibrium.

1.6 References

1. Boyle, J., *Molecular Biology of the Cell*, 5th Edition by B. Alberts, A. Johnson, J. Lewis, M. Raff, K. Roberts, and P. Walter. *Biochemistry and Molecular Biology Education* **2008**, 36, 317-318.
2. Doi, M.; Edwards, S. F., *The Theory of Polymer Dynamics*; Clarendon: Oxford, 1986.
3. De Gennes, P. G., *Scaling Concepts in Polymer Physics*; Cornell University Press: Ithaca, NY, 1979.
4. Kabachinski, G.; Schwartz, T. U., The Nuclear Pore Complex – Structure and Function at a Glance. *J. Cell Sci.* **2015**, 128, 423.
5. Fay, N.; Panté, N., Nuclear Entry of DNA Viruses. *Front. Microb.* **2015**, 6, 467.
6. Muthukumar, M., *Polymer Translocation*; CRC Press: Boca Raton, Florida, 2011.
7. Palyulin, V. V.; Ala-Nissila, T.; Metzler, R., Polymer Translocation: The First Two Decades and the Recent Diversification. *Soft Matter* **2014**, 10, 9016-9037.
8. Manrao, E. A.; Derrington, I. M.; Laszlo, A. H.; Langford, K. W.; Hopper, M. K.; Gillgren, N.; Pavlenok, M.; Niederweis, M.; Gundlach, J. H., Reading DNA at Single-Nucleotide Resolution with a Mutant MspA Nanopore and Phi29 DNA Polymerase. *Nat. Biotech.* **2012**, 30, 349.
9. Branton, D., et al., The Potential and Challenges of Nanopore Sequencing. *Nat. Biotech.* **2008**, 26, 1146.
10. Smith, D. E.; Tans, S. J.; Smith, S. B.; Grimes, S.; Anderson, D. L.; Bustamante, C., The Bacteriophage Φ 29 Portal Motor Can Package DNA against a Large Internal Force. *Nature* **2001**, 413, 748-752.
11. Meller, A.; Nivon, L.; Branton, D., Voltage-Driven DNA Translocations through a Nanopore. *Phys. Rev. Lett.* **2001**, 86, 3435-3438.
12. Lubensky, D. K.; Nelson, D. R., Driven Polymer Translocation through a Narrow Pore. *Biophys. J.* **1999**, 77, 1824-1838.
13. Metzler, R.; Luo, K., Polymer Translocation through Nanopores: Parking Lot Problems, Scaling Laws and Their Breakdown. *Euro. Phys. J. Spec. Top.* **2010**, 189, 119-134.
14. Slonkina, E.; Kolomeisky, A. B., Polymer Translocation through a Long Nanopore. *J. Chem. Phys.* **2003**, 118, 7112-7118.
15. Kasianowicz, J. J.; Brandin, E.; Branton, D.; Deamer, D. W., Characterization of Individual Polynucleotide Molecules Using a Membrane Channel. *Proc. Nat. Acad. Sci.* **1996**, 93, 13770.
16. Meller, A.; Branton, D., Single Molecule Measurements of DNA Transport through a Nanopore. *Electrophoresis.* **2002**, 23, 2583-2591.

17. Polson, J. M.; McCaffrey, A. C. M., Polymer Translocation Dynamics in the Quasi-Static Limit. *J.Chem. Phys.* **2013**, 138, 174902.
18. de Haan, H. W.; Slater, G. W., Using an Incremental Mean First Passage Approach to Explore the Viscosity Dependent Dynamics of the Unbiased Translocation of a Polymer through a Nanopore. *J.Chem. Phys.* **2012**, 136, 204902.
19. Steiglitz, K.; Rand, D., Photon Trapping and Transfer with Solitons. *Phys. Rev. A* **2009**, 79, 021802.
20. Sischka, A.; Spiering, A.; Khaksar, M.; Laxa, M.; König, J.; Dietz, K.-J.; Anselmetti, D., Dynamic Translocation of Ligand-Complexed DNA through Solid-State Nanopores with Optical Tweezers. *J. Phys.: Cond. Matt.* **2010**, 22, 454121.
21. Keyser, U. F.; Koeleman, B. N.; van Dorp, S.; Krapf, D.; Smeets, R. M. M.; Lemay, S. G.; Dekker, N. H.; Dekker, C., Direct Force Measurements on DNA in a Solid-State Nanopore. *Nat. Phys.* **2006**, 2, 473.
22. Ritort, F., Single-Molecule Experiments in Biological Physics: Methods and Applications. *J. Phys.: Cond. Matt.* **2006**, 18, R531-R583.
23. Bates, G. W., Chapter 26 Electroporation of Plant Protoplasts and Tissues. In *Methods in Cell Biology*, Galbraith, D. W.; Bourque, D. P.; Bohnert, H. J., Eds. Academic Press: 1995; Vol. 50, pp 363-373.
24. Krasilnikov, O. V.; Rodrigues, C. G.; Bezrukov, S. M., Single Polymer Molecules in a Protein Nanopore in the Limit of a Strong Polymer-Pore Attraction. *Phys. Rev. Lett.* **2006**, 97, 018301.
25. Sung, W.; Park, P. J., Polymer Translocation through a Pore in a Membrane. *Phys. Rev. Lett.* **1996**, 77, 783.
26. Muthukumar, M., Polymer Translocation through a Hole. *J. Chem. Phys.* **1999**, 111, 10371-10374.
27. Wong, C. T. A.; Muthukumar, M., Polymer Capture by Electro-Osmotic Flow of Oppositely Charged Nanopores. *J. Chem. Phys.* **2007**, 126, 164903.
28. Chuang, J.; Kantor, Y.; Kardar, M., Anomalous Dynamics of Translocation. *Phys. Rev. E.* **2001**, 65, 011802.
29. Kantor, Y.; Kardar, M., Anomalous Dynamics of Forced Translocation. *Phys. Rev. E.* **2004**, 69, 021806.
30. Chaudhury, S.; Cherayil, B. J., A Model of Anomalous Chain Translocation Dynamics. *J. Phys. Chem. B* **2008**, 112, 15973-15979.
31. Metzler, R.; Barkai, E.; Klafter, J., Anomalous Diffusion and Relaxation Close to Thermal Equilibrium: A Fractional Fokker-Planck Equation Approach. *Phys. Rev. Lett.* **1999**, 82, 3563-3567.
32. Dubbeldam, J. L. A.; Rostiashvili, V. G.; Milchev, A.; Vilgis, T. A., Driven Translocation of a Polymer: Fluctuations at Work. *Phys. Rev. E.* **2013**, 87, 032147.
33. Vocks, H.; Panja, D.; Barkema, G. T.; Ball, R. C., Pore-Blockade Times for Field-Driven Polymer Translocation. *J. Phys.: Cond. Matt.* **2008**, 20, 095224.
34. Menais, T., Polymer Translocation under a Pulling Force: Scaling Arguments and Threshold Forces. *Phys. Rev. E* **2018**, 97, 022501.
35. Milchev, A., Single-Polymer Dynamics under Constraints: Scaling Theory and Computer Experiment. *Journal of Physics: Cond. Matt.* **2011**, 23, 103101.
36. Sakaue, T., Nonequilibrium Dynamics of Polymer Translocation and Straightening. *Phys. Rev. E.* **2007**, 76, 021803.

37. Saito, T.; Sakaue, T., Dynamical Diagram and Scaling in Polymer Driven Translocation. *Euro. Phys. J. E* **2011**, 34, 135.
38. Saito, T.; Sakaue, T., Process Time Distribution of Driven Polymer Transport. *Phys. Rev. E* **2012**, 85, 061803.
39. Ikonen, T.; Bhattacharya, A.; Ala-Nissila, T.; Sung, W., Unifying Model of Driven Polymer Translocation. *Phys. Rev. E* **2012**, 85, 051803.
40. Ikonen, T.; Shin, J.; Sung, W.; Ala-Nissila, T., Polymer Translocation under Time-Dependent Driving Forces: Resonant Activation Induced by Attractive Polymer-Pore Interactions. *J. Chem. Phys.* **2012**, 136, 205104.
41. Sarabadani, J.; Ikonen, T.; Ala-Nissila, T., Iso-Flux Tension Propagation Theory of Driven Polymer Translocation: The Role of Initial Configurations. *J. Chem. Phys.* **2014**, 141, 214907.
42. Abraham, M. J.; Murtola, T.; Schulz, R.; Páll, S.; Smith, J. C.; Hess, B.; Lindahl, E., Gromacs: High Performance Molecular Simulations through Multi-Level Parallelism from Laptops to Supercomputers. *SoftwareX* **2015**, 1-2, 19-25.
43. Plimpton, S., Fast Parallel Algorithms for Short-Range Molecular Dynamics. *J. Comp. Phys.* **1995**, 117, 1-19.

2. Pore-driven polymer translocation: Effect of pore charge distribution

(Rights and Permission)

Reprinted (adapted) with permission from (*J. Phys. Chem. B.* **2018**, 122, 1, 360-368). **Copyright ©
2017 American Chemical Society.**

2.1 Introduction

There are many basic questions related to the problem of polymer translocation. Few of them are the dependence of the translocation time on the system parameters such as the length of the polymer chain,¹ the length,² and width of the pore, the secondary structure, the salt concentration, the driving force, and the polymer pore interaction.³⁻⁷ The dependence of translocation time on many such quantities has been shown schematically in Figure 1.3. It has been shown experimentally that the translocation of cationic polypeptides can be altered by modifying the distribution of charge in the alpha-hemolysin pore.⁸⁻⁹ Two-dimensional Langevin dynamics simulations by Luo *et al.* have shown that an attractive interaction can increase the translocation probability, but the average translocation time decreases with the increase in the attractive strength.¹⁰ In most of the earlier studies, it was assumed that the charge density along the pore is constant. Foster *et al.* have performed two-dimensional molecular dynamics simulations to study the effect of the location of the attractive region on the translocation time for both short and long polymers.¹¹ Their simulation results are in good qualitative agreement with the experimental findings by Meller *et al.* on the translocation of a single-stranded DNA through the alpha-hemolysin pore. Katkar and Muthukumar³ have performed three-dimensional Langevin dynamics simulations to study the effect of placing alternate charged and uncharged regions of different lengths along the nanopore on the translocation dynamics of a negatively charged flexible polyelectrolyte passing through solid-state nanopore¹²⁻¹³ under the influence of a constant electric field. The simulation results are quantitatively supported by a theory based on the Fokker Planck formalism.¹⁴ Chen *et al.* have studied the effect of attractive polymer-pore interaction on the translocation dynamics of a polyelectrolyte by performing Monte Carlo simulations with a 2D lattice bond fluctuation model.⁴

In this chapter, we discuss about three-dimensional Langevin dynamics simulations for the translocation of a charged polymer moving through an interacting channel. We show that the translocation dynamics is strongly influenced not only by the presence of an attractive polymer-pore interaction but also depends on the location of the interaction region. In our work, we use a coarse-grained description to exclusively study the role of the strength and location of the attractive polymer pore interaction within the pore in the presence of an external field on the

translocation dynamics of the polymer moving from the left to right side of the pore (cis to trans).

2.2 Model

The movement of the polymer chain through a narrow channel is studied by Langevin dynamics simulations using the GROMACS package.¹⁵ The system consists of a membrane, a pore, and a charged polymer chain. The neutral part of the polymer is modeled according to the method described in Section 1.4. The membrane separating the *cis* and the *trans* side is created by LJ particles in *yz*- plane with the pore oriented along the *x*-axis. The cylindrical pore is constructed of six consecutive rings of uncharged beads, where each ring consists of 16 monomer beads of diameter σ such that the length of the pore is $L=6\sigma$ and width $W=3\sigma$ as shown in Figure 2.1(a) and 2.1(c).

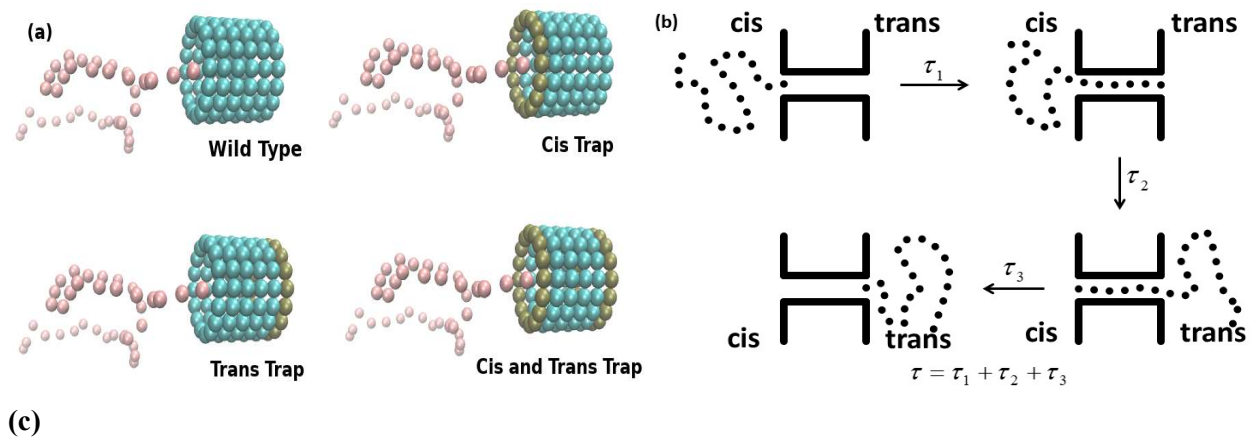


Figure 2.1: (a) Schematic representation of a polymer chain translocating through a pore of length $L=6$. (b) Representation of the different components of the total translocation time. (c) Cross-sectional view of the pore.

The wall coordinates were frozen during the simulations, and they interact with the polymer chain only via the LJ force. The bonded and non-bonded interactions modeled according to the method described in Section 1.4. The electrostatic potential between charged beads are modeled by the Coulomb potential-

$$U_{coul}(r) = \frac{q_i q_j}{4\pi\epsilon_0 r} \quad , \quad \dots[\text{Eq. 2.1}]$$

where ϵ_0 is the dielectric constant of the medium, q_i , and q_j are the charges on the beads i and j that are separated at a distance r . The charges of all the polymer beads are equal and the same is true for charges on the pore beads. The magnitude of charge in pore and polymers beads are different and opposite in sign.

The electrostatic interaction calculations are done by simple Coulomb cut-off from Eq. 2.1. The $r_{\text{cut-off}} = 2.0$ beyond which all the electrostatic interactions are neglected. The electrostatic calculations in a periodic system based on Particle-Mesh Ewald (PME) method or Particle-Particle, particle-mesh method approaches that require charge neutrality in the system are not used here.

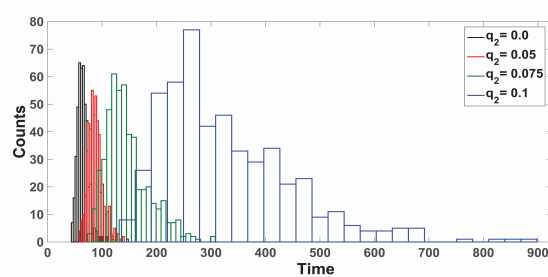
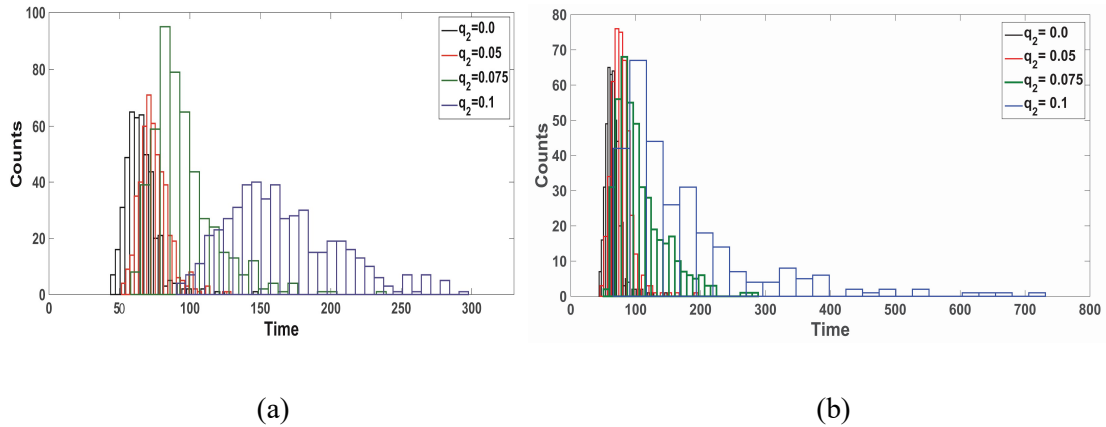
In Langevin dynamics simulations, a polymer of $N=12$ to 50 are considered in a $108 \times 54 \times 54$ unit box dimension without periodic boundary conditions. Each monomer is subjected to conservative, frictional, and random forces, as described in Eq.1.4. F_{ext} is the external force due to an external electric field, $F_{ext} = F \hat{x}$ where F is the external force acting on the monomers inside the pore and \hat{x} is the unit vector along the axis of the pore. The details of the simulation are described in Chapter 1. The integration time step is set to $dt = 0.005$ units. The results reported in this work are obtained by averaging over 500-1500 independent simulation runs. For each successful translocation event, the translocation time is defined as the time between the entrance of the first bead into the pore from the *cis* side and the exit of the last monomer bead from the *trans* side. In the present work, all quantities are expressed in dimensionless LJ unit of energy, length and mass scales as described in Section 1.4.

In order to study how the location of the interacting region can affect the translocation dynamics, we introduce charges either on the entry side (*cis*) or on the exit side (*trans*) or on both sides (*cis* and *trans*) of the pore. In order to introduce an attractive interaction at the *cis* side of the pore, a charge of $-q_2 e$ is introduced on all the 16 beads that form the first ring of the pore on the entry side. Similarly, interactions on both sides of the pore can be initiated by introducing

charges on the beads that form the first and the last ring of the pore. For a given set of parameter values, the translocation time distribution for all the successful translocation events with attractive interactions at different positions is obtained from which the mean translocation time can be computed and compared.

2.3 Result and Discussion

The unit of charge in one nucleotide of a DNA is $-0.094e$. One bead is considered to be composed of three units of nucleotides. So, the charge on each beads is $3 \times 0.094e = 0.282e$. This fact comes from the situation that the phosphate backbone of the DNA is partially negatively charged.²²⁻²³ In order to mimic the DNA in real biological environments; we consider a positively charged polymer chain of N beads, assuming that there are three unit charges per bead and an effective charge of $0.094e$ for each unit charge. The external driving force F is set between 2.5 and 5 such that it corresponds to the range of voltages used in the experiments. Figure 2.2 shows the translocation time distribution calculated for a chain of length $N=50$ moving from the *cis* to the *trans* side of the pore with an attractive interaction placed within the pore at different locations and at an external field strength of $F=3.3$.



(c)

Figure 2.2: The distribution of translocation time for different attractive strength at (a) *cis* (b) *trans* (c) *cis-trans* side of the pore under the driving force of $F=3.3$. The length of chain $N=50$. $q_2=0$ corresponds to a wild type pore with no pore- monomer interaction.

For attractive regions on either the *cis*, or *trans* or both sides of the pore, the histogram of the translocation times deviates from a Gaussian distribution to a long-tailed behavior with an increase in the value of q_2 thereby leading to a slower translocation. From these distributions, we calculate the first moment and this corresponds to the mean translocation time, τ . The translocation time of the polymer τ , as defined in the Section 2.1 involves three different time scales as shown in Figure 2.1(b): τ_1 that corresponds to the filling of the pore, τ_2 that involves the movement from the *cis* to *trans* side of the pore and τ_3 that is associated with the emptying of the pore. The mean translocation time τ is a sum of their averages.

Figure 2.3 shows that the total translocation time τ increases with the increase in q for all the different types of partially charged pores.

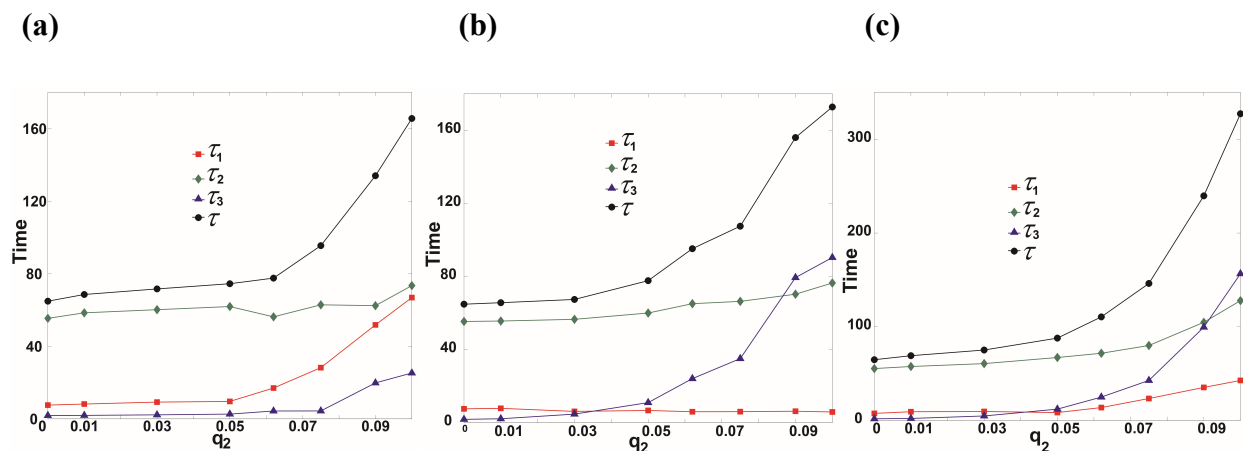


Figure 2.3: Total translocation time and its components as a function of the attractive strength for interaction at (a) *cis* (b) *trans* and (c) *cis-trans* of the pore under the driving force $F=3.3$ and $N=50$.

For a wild-type pore ($q_2=0$), the translocation time depends on the length of the polymer chain N and the strength of the external driving force F (Table 2.1). Under the influence of an strong attractive force, the mean translocation time shows a nonmonotonic behavior with a sharp

increase in τ as compared to the case of weak attractive pore interaction placed at either the *cis* or *trans* or *cis-trans* region of the pore. (Table 2.2).

N	F	τ_1	τ_2	τ_3	$\tau = \tau_1 + \tau_2 + \tau_3$
50	2.5	10.7	72	2.25	85
50	2.9	9.45	64.24	2.13	75.82
50	3.3	7	55.4	1.85	65
50	3.7	6.46	51.62	1.66	59.75
50	4.5	5.57	43.32	1.43	50.32
50	4.8	5.44	39.7	1.3	46.5
35	4.8	5.27	22.32	1.34	28.93
20	4.8	5.39	9.44	1.23	16.06
12	4.8	4.81	4.4	1.25	10.5

Table 2.1: Translocation times for chain length N and external driving force F traversing through a purely repulsive pore ($q_2=0$).

We perform simulations in order to investigate how the three individual time scales τ_1, τ_2, τ_3 are affected as a function of the polymer- pore interaction q positioned at different locations of the pore. As shown in Figure 2.3, the position of the attractive region has an impact on the translocation time. Under the effect of strong attractive force on the *cis* (entry) side of the pore, the mean translocation time τ is dominated by the pore filling stage, τ_1 (Figure 2.3(a), Table 2.2 (a)).

(a) Cis trap

q_2	τ_1	τ_2	τ_3	$\tau = \tau_1 + \tau_2 + \tau_3$
0.01	8.2	58.5	1.92	68.6
0.03	9.24	60.2	2.21	71.63
0.05	9.61	61.9	2.63	74.5
0.062	16.99	56.23	4.34	77.58
0.075	28.23	62.9	4.37	95.5

0.09	51.79	62.40	19.81	134.00
0.1	66.85	73.5	26	165

(b) *Trans* trap

Q	τ_1	τ_2	τ_3	$\tau = \tau_1 + \tau_2 + \tau_3$
0.01	7.9	55.65	2.2	65.7
0.03	6.2	56.6	4.71	67.5
0.05	6.71	60	11	77.8
0.062	6.00	65.14	24.12	95.26
0.075	6.05	66.42	35.1	107.56
0.09	6.29	70.34	79.44	156.08
0.1	5.89	76.5	90.4	172.8

(c) *Cis-Trans* trap

Q	τ_1	τ_2	τ_3	$\tau = \tau_1 + \tau_2 + \tau_3$
0.01	9.4	57.6	2.2	69.16
0.03	9.63	60.7	4.86	75.2
0.05	8.5	67.24	12.15	87.9
0.062	13.82	71.74	25	110.56
0.075	23.45	80	42.75	146.22
0.09	35.31	104.77	99.57	239.66
0.1	42.75	127.9	156.6	327.3

Table 2.2: Translocation times for chain length $N= 50$ and $F= 3.3$ traversing through a repulsive pore with polymer- pore interaction at different locations within the pore.

With a strong, attractive interaction on the *trans* side, τ is determined by the pore emptying time, τ_3 (Figure 2.3(b), Table 2.2 (b)). Thus τ_1 dominates at a strong polymer-pore interaction on the *cis* side and τ_3 dominates when there is a strong attractive interaction on the *trans* side of the pore. An attractive force on both the *cis* and *trans* side will affect the pore filling as well as the

emptying stage (Table 2.2(c)). As a result of this, a pore with a strong attractive polymer-pore interaction both at the entry and exit side of the pore will have a maximum effect on the total translocation time τ for a given driving force. The slowest translocation occurs when there is a strong attractive interaction present on both sides of the pore. This is verified when Figure 2.3(c) is compared with Figure 2.3(a) and (b) at high values of q_2 . These findings are in good agreement with previous experiments and simulations.^{5-6, 10} Thus, the distribution of charge along the pore has a significant effect on the mean translocation time.^{3, 8}

The dependence of the average translocation time of a polymer chain on the applied electric field at a given polymer- pore interaction positioned at either the *cis* or *trans* or *cis-trans* region of the pore are presented in Figure 2.4. In all the three cases, the translocation becomes faster with the increase in the strength of the applied field.

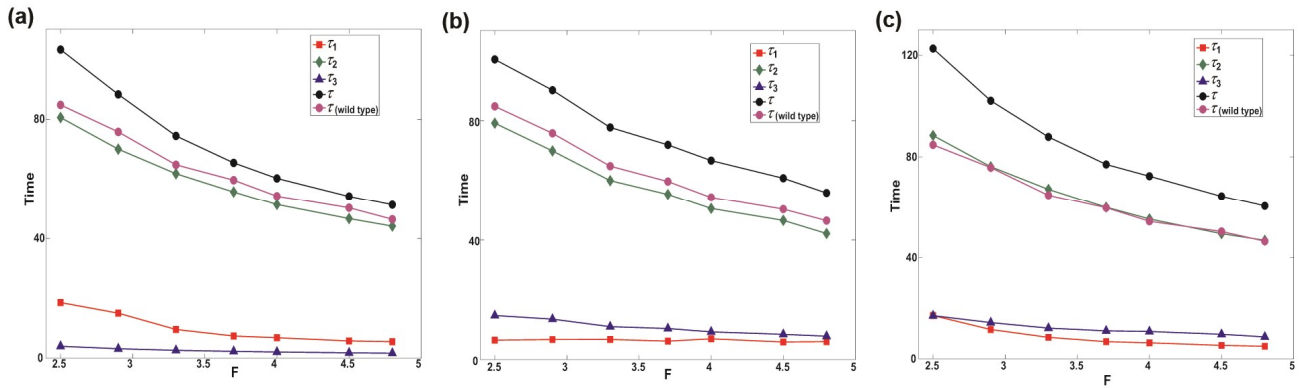


Figure 2.4: The total translocation time and its components as a function of the driving force for interaction strength $q_2 = 0.05$ at (a) *cis* (b) *trans* and (c) *cis-trans* region of the pore with $N = 50$. $q_2 = 0$ corresponds to the wild type pore.

The translocation time decays non-monotonically with the increased applied field. The decay behaviors of the τ s' with and without the polymer-pore interaction also suggest that the effect of the polymer- pore interaction is decreased with an increase in the strength of the external electric field. This is evident from the comparison of the translocation time at different driving forces for the wild type (Table 2.1) and the partially charged pores (Table 2.3). The difference between the translocation time of the wild-type and charged pore decreases with an

increase in the external driving force (the magenta and the black circles come closer to each other with the increase in F).

(a) *Cis* trap:

F	τ_1	τ_2	τ_3	$\tau = \tau_1 + \tau_2 + \tau_3$
2.5	18.6	80.6	4	103.2
2.9	15.05	70.08	3.17	88.30
3.3	9.61	61.9	2.63	74.5
3.7	7.42	55.79	2.29	65.51
4	6.85	51.42	2.06	60.34
4.5	5.78	46.69	1.81	54.29
4.8	5.51	44.2	1.67	51.36

(b) *Trans* trap

F	τ_1	τ_2	τ_3	$\tau = \tau_1 + \tau_2 + \tau_3$
2.5	6.5	79.2	14.72	100.4
2.9	6.68	70	13.51	90.14
3.3	6.71	60	11	77.8
3.7	6.16	55.42	10.37	71.96
4.0	6.93	50.53	9.26	66.72
4.5	5.86	46.53	8.43	60.84
4.8	6	42.13	7.8	55.93

(c) *Cis-trans* trap

F	τ_1	τ_2	τ_3	$\tau = \tau_1 + \tau_2 + \tau_3$
2.5	17.1	88.5	17.06	122.7
2.9	11.59	76.2	14.34	102.13
3.3	8.5	67.24	12.15	87.9
3.7	6.79	59.95	11.07	77.07
4	6.33	55.29	10.82	72.43
4.5	5.33	49.45	9.7	64.47

4.8	5	46.8	8.7	60.5
-----	---	------	-----	------

Table 2.3: Translocation times for chain length $N= 50$ and $q_2= 0.05$ at different locations within the pore with varying magnitudes of externally applied field.

Simulations are also performed for shorter chain lengths ($N= 12, 20,$ and 35). In the presence of a strong driving force, $F= 4.8$ and at a moderate to high attractive polymer- pore interaction of $q_2= 0.05$ and $q_2= 0.1$ respectively on the *cis* end of the pore, τ_1 is roughly comparable to that observed for longer chains ($\tau_1^{cis}(N = 12) \approx \tau_1^{cis}(N = 50)$). But τ_2 decreases significantly with the decrease in the chain length (Table 2.4) thereby decreasing the total translocation time.

(a)Cis trap

N	τ_1	τ_2	τ_3	$\tau = \tau_1 + \tau_2 + \tau_3$
12 ($q=0.05$)	5.69	4.56	1.50	11.75
12 ($q_2=0.1$)	5.40	5	1.89	12.3
20 ($q_2=0.05$)	4.85	10.13	1.60	16.59
35($q_2=0.05$)	4.81	23.67	1.73	30.2
50($q_2=0.05$)	5.51	44.2	1.67	51.36

(b)Trans trap

N	τ_1	τ_2	τ_3	$\tau = \tau_1 + \tau_2 + \tau_3$
12($q_2 =0.05$)	4.7	4.2	2.06	10.9
12($q_2 =0.1$)	4.4	4	43.7	56
20($q_2= 0.05$)	4.59	8.94	7.64	21.2
35($q_2= 0.05$)	5.1	23.23	7.46	35.8
50($q_2 =0.05$)	6	42.13	7.8	56

(c)Cis-trans trap

N	τ_1	τ_2	τ_3	$\tau = \tau_1 + \tau_2 + \tau_3$
12 ($q_2=0.05$)	5.75	4.4	2.57	12.72
12 ($q_2=0.1$)	4.4	4.5	64.1	72.89
20 ($q_2=0.05$)	4.64	9.54	9.21	23.29
35 ($q_2=0.05$)	4.53	24.8	7.96	37.39
50 ($q_2=0.05$)	5	46.8	8.7	60.5

Table 2.4: Translocation times for chain length $N=12$ and $F= 4.8$ with polymer- pore interaction at different locations within the pore.

Thus τ_1 is independent of the chain length and the translocation process is dominated by τ_2 for polymer chains of different length but experiencing same attractive interaction on the *cis* side of the pore. When a strong interaction is present at the *trans* side, τ_3 is longer for longer chains ($\tau_3^{trans}(N = 12) < \tau_3^{trans}(N = 50)$). For relatively short chains and strong interaction strength at the exit side or on both sides of the pore, τ_3 increases significantly and has a greater effect on the total translocation time (for $N=12$, $\tau_3^{trans}(q = 0.05) \ll \tau_3^{trans}(q = 0.1)$). The translocation time is independent of the presence of attractive polymer- pore interaction on the *cis* side of the pore.¹⁶

2.4 Free Energy Calculation

The effect of the translocation time on the strength of the polymer- pore interaction is explained qualitatively in the context of the free energy landscape.^{4, 10-11} In general, this free energy barrier of a polymer translocation event is dependent on the strength of the polymer pore interaction q ^{10, 14, 17-19} the length of the chain N ¹¹ and the strength of the applied external field, F .^{18, 20} Assuming that polymer translocation is a quasi-equilibrium process, the free energy of the polymer is equal to $U-TS$, where S is the conformational entropy $S = k_B \ln \Omega$, Ω is the conformational number of the polymer. The internal energy U has two components (a) the energy U_{int} that arises due to the polymer- pore electrostatic interaction and (b) the energy U_{ext} due to the externally applied field F . For a polymer chain that is partially or entirely within the pore, and having a *cis* trap, the electrostatic interaction energy is given by-

$$U_{int}^{cis}(a, b) = \frac{N_r q_1 q_2 (1)}{4\pi\epsilon_0} \sum_{i=a}^b \frac{1}{r(i,1)}, \quad \dots [\text{Eq. 2.2a}]$$

where (b-a) monomers are within the pore, q_1 is the charge on the monomer beads, N_r is the number of pore beads that form the charged ring on the *cis* side and $q_2(1)$ is the charge in each of these pore beads and $r(i, 1)$ is the distance between the i^{th} monomer bead and the charged pore ring at entry side. For a trap on the trans end, the electrostatic interaction energy is given by

$$U_{int}^{trans}(a, b) = \frac{N_r q_1 q_2(L)}{4\pi\epsilon_0} \sum_{i=a}^b \frac{1}{r(i, L)} \quad , \quad \dots[\text{Eq. 2.2b}]$$

where $q_2(L)$ is the charge in each of the pore beads on the last ring at the end of the pore and $r(i, L)$ is the distance between the i^{th} monomer bead and the pore ring at exit side. The contribution to U_{ext} due to the external electric field is given as

$$U_{ext}(a, b) = \sum_{x=a}^b Fx \quad \dots[\text{Eq. 2.3}]$$

The contribution from entropy is given by

$$U_{ent}(n) = k_B T \ln \Omega(n) \quad . \quad \dots[\text{Eq. 2.4}]$$

For n number of monomers at the *cis* or *trans* side of the pore, $\Omega(n) = n^{\gamma-1}$, where $\gamma = 0.69$ for a 3D polymer chain. Considering that the chain inside the channel is straight, $\Omega = 1$ for monomers within the channel. The entropic contribution to the polymer chain can be derived from its partition function Z , which corresponds to the number of conformations that the chain can take. $S = -k_B T \ln Z$. The partition function scales like $Z \sim q^N N^{\gamma-1}$. The q^N term appears through the chemical potential. This term is absorbed through the chemical potential difference between the two chambers. The free energy of the polymer is expressed in the unit of $k_B T$. During all the three stages of translocation, U_{int} , U_{ext} , and U_{ent} will contribute to the free energy of the system, $E = U_{int} + U_{ext} - U_{ent} = U_{int} + U_{ext} + k_B T(1 - \gamma) \ln(n)$. Using these relations, one can construct the free energy landscape for a translocation coordinate m based on the method described by Katkar and Muthukumar.³ These three energy terms contribute to the total free energy during the filling, transfer and escape stage for different spatial distribution of the attractive regions within the pore.

For a polymer chain with N monomer beads translocating through a nanopore of length $L=6$, during the pore filling stage m number of monomers are within the pore and rest $N-m$ is on the *cis* side of the pore ($0 < m < L$). In the transfer stage L monomers are within pore, $N-m$ number of monomers on the *cis* side and $m-L$ monomers on the *trans* side of the pore ($L < m < N$). During the escape stage, $m-N$ monomers are on the *trans* side and the rest are within the pore ($N < m < N + L$). Using these limits, one can construct the free energy landscape with

attractive interactions on cis, trans or both sides of the pore.

When the attraction is present at the cis side of the pore,

$$E_{filling}(m) = \frac{N_r q_1 q_2(1)}{4\pi\epsilon_0} \sum_{i=0}^m \frac{1}{r(i,1)} + U_{ext}(0, m) + k_B T(1 - \gamma) \ln(N - m) \quad , \quad \dots[\text{Eq. 2.5a}]$$

$$E_{transfer}(m) = \frac{N_r q_1 q_2(1)}{4\pi\epsilon_0} \sum_{i=0}^6 \frac{1}{r(i,1)} + U_{ext}(0,6) + k_B T(1 - \gamma) (\ln(N - m) + \ln(m - L)), \quad \dots[\text{Eq. 2.5b}]$$

$$E_{escape}(m) = \frac{N_r q_1 q_2(1)}{4\pi\epsilon_0} \sum_{i=m-N}^L \frac{1}{r(i,1)} + U_{ext}(m - N, L) + k_B T(1 - \gamma) \ln(m - L) \quad \dots[\text{Eq. 2.5c}]$$

With an attractive interaction on the trans end of the pore,

$$E_{filling}(m) = \frac{N_r q_1 q_2(L)}{4\pi\epsilon_0} \sum_{i=0}^m \frac{1}{r(i,L)} + U_{ext}(0, m) + k_B T(1 - \gamma) \ln(N - m) \quad \dots[\text{Eq. 2.6a}]$$

$$E_{transfer}(m) = \frac{N_r q_1 q_2(L)}{4\pi\epsilon_0} \sum_{i=0}^6 \frac{1}{r(i,L)} + U_{ext}(0,6) + k_B T(1 - \gamma) (\ln(N - m) + \ln(m - L)), \quad \dots[\text{Eq. 2.6b}]$$

$$E_{escape}(m) = \frac{N_r q_1 q_2(L)}{4\pi\epsilon_0} \sum_{i=m-N}^L \frac{1}{r(i,L)} + U_{ext}(m - N, L) + k_B T(1 - \gamma) \ln(m - L) \quad \dots[\text{Eq. 2.6c}]$$

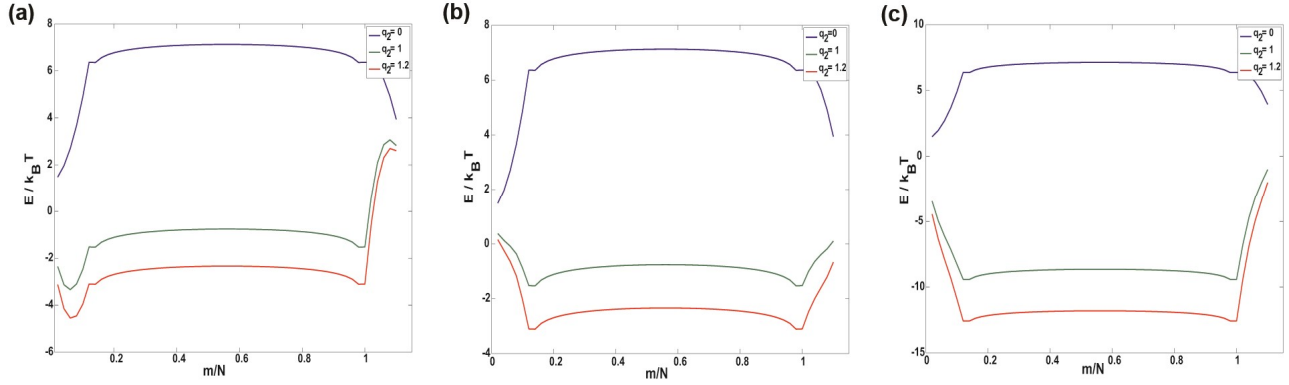
When attractive interactions are present on both ends, contributions to the free energy are as follows

$$E_{filling}(m) = \frac{N_r q_1}{4\pi\epsilon_0} \left(\sum_{i=0}^m \frac{q_2(L)}{r(i,L)} + \sum_{i=0}^m \frac{q_2(1)}{r(i,1)} \right) + U_{ext}(0, m) + k_B T(1 - \gamma) \ln(N - m) \quad \dots[\text{Eq. 2.7a}]$$

$$E_{transfer}(m) = \frac{N_r q_1}{4\pi\epsilon_0} \left(\sum_{i=0}^m \frac{q_2(L)}{r(i,L)} + \sum_{i=0}^m \frac{q_2(1)}{r(i,1)} \right) + U_{ext}(0,6) + k_B T(1 - \gamma) (\ln(N - m) + \ln(m - L)), \quad \dots[\text{Eq. 2.7b}]$$

$$E_{escape}(m) = \frac{N_r q_1}{4\pi\epsilon_0} \left(\sum_{i=0}^m \frac{q_2(L)}{r(i,L)} + \sum_{i=0}^m \frac{q_2(1)}{r(i,1)} \right) + U_{ext}(m - N, L) + k_B T(1 - \gamma) \ln(m - L) \quad \dots[\text{Eq. 2.7c}]$$

Using the above equations, we construct the free energy profile at charges $q_2 = 1, 1.2$ and external force ($F= 0.3$) as shown in Figure 2.5. When a polymer chain enters the pore, there is a



decrease in the entropy due to the decrease in the number of available configurations of the chain.

Figure 2.5: Free energy landscape for a polymer chain of length $N= 50$ translocating through a nanopore of length $L= 6$ with different attractive strengths at (a) *cis* (b) *trans* and (c) *cis-trans* region of the pore under the driving force $F= 0.3$

For a wild-type pore ($U_{int} = 0$), in order to enter the pore, the polymer experiences a force due to the external driving force that counterbalances the entropy loss due to confinement. As shown in Figure 2.5(a), a polymer- pore interaction on the *cis* side of the pore creates a free energy well on the *cis* side. The polymer chain is trapped inside this well making it difficult for the chain to fill up the pore ($\tau_1(q_2 = 0) \ll \tau_1^{cis}(q_2 = 0.1)$). The stronger the attraction on the *cis* side, deeper is the free-energy well and higher is the contribution from U_{int}^{cis} that prevents the polymer from filling the pore. This is also evident from Table 2.2(a) where a *cis* trap increases τ_1 . During the escape stage, the external driving force and the entropy gain due to deconfinement need to overcome this interaction energy for the polymer to escape from the pore. Since the effect of the attractive charges present on the *cis* side is weak during the pore emptying stage, it does not show any significant effect on the pore emptying time. Hence the free energy profile at the end of the pore does not change with the change in the strength of the *cis* attraction. A *trans* trap creates a wide free energy well for translocation that prevents the polymer to escape from the pore ($\tau_3^{trans}(q_2 = 0) \ll \tau_3^{trans}(q_2 = 0.1)$). A stronger interaction on the *trans* side increases the depth of this free energy well (contribution from U_{int}^{trans} increases, Figure 2.5(b)). During the

escape stage, only a few monomers are present inside the pore and U_{ext} goes on decreasing. Since charges are present near the pore end, the attractive force increases. The electric driving force is insufficient to overcome this attractive force U_{int}^{trans} and causes the trapping of the polymer within the pore thereby increasing τ_3 . When traps are present on both ends of the pore, for a given attractive strength, the free energy is more negative indicating that the effect of the attractive interactions increases (Figure 2.5(c), $\tau^{trans}(q_2, N) < \tau^{cis-trans}(q_2, N)$ as seen in Table 2.2(b) and 2.2(c)). The polymer first overcomes the free energy on the *cis* side and fills up the pore. During the transport stage, the tail part of the chain that was outside the pore enters the pore and the head monomeric part leaves the pore from the *trans* side. The presence of *trans* trap attracts the positively charged monomers confined within the pore towards the pore end; also U_{ext} goes on decreasing. Since there is no effect of the external force on the monomer beads that have already translocated through the pore, these beads on the *trans* side of the pore are also attracted towards the trap thereby causing crowding near the pore end.¹¹ This crowding effect affects the monomers confined within the pore and the monomers near the pore exit. Thus in the emptying stage, there is a significant trapping of the polymer at the *trans* end of the pore. This suggests that the effect of an attractive electrostatic interaction on the *trans* side is high compared to the *cis* side if all other parameters are kept fixed. As shown in Figure 2.5(c) the free energy cost during the filling stage is less than the free energy cost during the emptying stage. This intuition is also supported by our simulation results. For a given chain length and at an optimum polymer-pore interaction present on both sides of the pore, the increase in translocation time due to *trans* side trap is more compared to the *cis* side trap ($\tau_1^{cis-trans}(q_2, N) < \tau_3^{cis-trans}(q_2, N)$), Table 2.2(c)). The free energy landscape is also dependent on the strength of the driving force F . A stronger driving force can tilt the landscape and can make the translocation process faster.¹⁷ Though an attractive polymer pore interaction at either or both ends of the pore causes trapping of the polymer inside the pore, increasing the strength of the applied voltage facilitates the translocation process (at $q_2=0.05$, $\tau^{cis,trans,cis-trans}(F = 3.3) > \tau^{cis,trans,cis-trans}(F = 4.8)$). As a result of this, with an increase in the external driving force, the effect of the polymer-pore interaction decreases. For chain lengths longer than the length of the pore ($N=12, 20, 35$ and $N=50$), the filling time τ_1 is almost constant. This is because, during the filling stage, the numbers of monomers confined within the pore is roughly the same for all chain lengths. This number corresponds to the maximum number of monomers that can be accommodated within the

pore. Thus, the presence of a *cis* trap does not influence τ_1 for chains of different length (Table 2.4 (a)). During the transfer stage, the last polymer bead needs to reach the *cis* end of the pore. This process is longer for chains of longer length; hence τ_2 increases with increase in the chain length. When the trap is at the *trans* end, the crowding effect felt by the monomers confined within the pore is same for both chain lengths. But for smaller chains, there is less number of monomer beads that are already on the *trans* side and are attracted towards the pore wall. Hence it is easier to overcome this barrier during the emptying stage for short chains and τ_3 increases with chain length as reported in Table 2.4(b).

We find that the free energy landscape estimated from the equation $E = U - TS$ provides a satisfactory qualitative explanation of our results from the Langevin dynamics simulations on the effect of the strength and spatial distribution of the attractive charges along the pore. From the free energy landscape, one can also use a Fokker Planck formalism to theoretically calculate the translocation time of the polymer by assuming a position independent diffusion coefficient.²¹ But quantitative comparison between the theoretical and numerical results is not possible since the formula used for estimating the free energy is valid in the quasi-equilibrium assumption, but in reality, polymer translocation is an out-of-equilibrium process that can be adequately captured only in our simulations. Also, the crowding effect at *trans* end of the pore is not accounted for in the free energy calculations. The position-dependent and interaction dependent diffusion properties that are neglected in the theoretical calculations of the translocation time are included in our simulations.

Experiments on polymer translocation are quite complicated where one needs to take care of the hydrophobicity of the polypeptide, the polypeptide sequence, the ionic strength of the aqueous phase, the transmembrane potential; all of which have not been explicitly taken into account in our numerical simulations. Hence it is not possible to relate our simulations results directly to an experimental setup. Our model is a coarse-grained picture where we intend to capture the sole effects of the polymer-pore interaction in the translocation of the polymer from one side of the membrane to other.

2.5 Conclusion

To summarize, in this chapter, we have studied the role of attractive polymer interaction in translocation process and show that the location of the polymer- pore interaction plays a crucial role in the pore driven translocation of a charged polymer chain. The position of the electrostatic

interaction causes variation in the dependence of the total translocation time as a function of the attractive interaction strength, the external field, and the chain length. For a given chain length and in the presence of an externally applied field, the translocation time τ , which is, composed of three different time scales τ_1 , τ_2 and τ_3 increases non-monotonically with the increase in the polymer-pore interaction. With the increase in the attractive strength on the *cis* side of the pore, τ_1 contributes dominantly to τ whereas τ is determined by τ_3 when the interaction is on the *trans* side. The translocation is slowest when a strong polymer-pore interaction is present on both sides of the pore. Also, the effect of the polymer-pore interaction decreases with the increase in the strength of the external field. From our simulation results, we also study the dependence of the translocation time on the location of attractive regions for chains of different lengths.

The effect of polymer pore interaction on the translocation of a polymer is explained by qualitatively by constructing the free energy landscape of polymer translocation. Polymer translocation is essentially an out-of-equilibrium process, which is a big challenge for theoretical calculations. Our simulations provide an important tool to understand polymer translocation in the presence of attractive polymer pore interactions. Our conclusions are based on a coarse-grained description of the translocation dynamics by explicitly considering the individual contributions of the filling, transfer, and escape stage to the translocation time, which is difficult to follow in experiments. In governing the translocation time, incorporation of an electrostatic attractive trans trap can be more effective compared to cis trap. The effect is more when the chain lengths are shorter. Our results show that the translocation dynamics can be modified and tuned by altering the strength and spatial distributions of attractive polymer pore interaction.

2.6 References

1. Meller, A.; Nivon, L.; Branton, D. P., Voltage-Driven DNA Translocations through a Nanopore. *Phys. Rev. Lett.* **2001**, *86*, 3435.
2. Luo, K. F.; Ala-Nissila, T.; Ying, S. C., Polymer Translocation through a Nanopore: A Two-Dimensional Monte Carlo Study. *J. Chem. Phys.* **2006**, *124*, 034714.
3. Katkar, H. H.; Muthukumar, M., Effect of Charge Patterns Along a Solid-State Nanopore on Polyelectrolyte Translocation. *J. Chem. Phys.* **2014**, *140*, 135102.
4. Chen, Y.-C.; Wang, C.; Zhou, Y. L.; Luo, M.-B., Effect of Attractive Polymer-Pore Interactions on Translocation Dynamics. *J. Chem. Phys.* **2009**, *130*, 054902.
5. Meller, A.; Branton, D., Single Molecule Measurements of DNA Transport through a Nanopore. *Electrophoresis* **2002**, *23*, 2583-2591.

6. Meller, A.; Nivon, L.; Brandin, E.; Golovchenko, J. A.; Branton, D., Rapid Nanopore Discrimination between Single Polynucleotide Molecules. *Proc. Natl. Acad. Sci. U.S.A.* **2000**, *97*, 1079-1084.
7. Mirigian, S.; Wang, Y.; Muthukumar, M., Translocation of a Heterogeneous Polymer. *J. Chem. Phys.* **2012**, *137*, 064904.
8. Wolfe, A. J.; Mohammad, M. M. C., S.; Bayley, H.; Movileanu, L., Catalyzing the Translocation of Polypeptides through Attractive Interactions. *J. Am. Chem. Soc.* **2007**, *129*, 14034-14041.
9. Mohammad, M. M.; Prakash, S.; Matouschek, A.; Movileanu, L., Controlling a Single Protein in a Nanopore through Electrostatic Traps. *J. Am. Chem. Soc.* **2008**, *130*, 4081-4088.
10. Luo, K.; Ala-Nissila, T.; Ying, S.-C.; Bhattacharya, A., Influence of Polymer-Pore Interactions on Translocation. *Phys. Rev. Lett.* **2007**, *99*, 148102.
11. Piguet, F.; Foster, D. P., Translocation of Short and Long Polymers through an Interacting Pore. *J. Chem. Phys.* **2013**, *138*, 084902.
12. Kowalczyk, S. W.; Wells, D. B.; Aksimentiev, A.; Dekker, C., Slowing Down DNA Translocation through a Nanopore in Lithium Chloride. *Nano Lett.* **2012**, *12*, 1038-1044.
13. Chen, P.; Gu, J.; Brandin, E.; Kim, Y.-R.; Wang, Q.; Branton, D., Probing Single DNA Molecule Transport Using Fabricated Nanopores. *Nano Lett.* **2004**, *4*, 2293-2298.
14. Muthukumar, M., Polymer Escape through a Nanopore. *J. Chem. Phys.* **2003**, *118*, 5174.
15. Abraham, M. J.; Murtola, T.; Schulz, R.; Páll, S.; Smith, J. C.; Hess, B.; Lindahl, E., Gromacs: High Performance Molecular Simulations through Multi-Level Parallelism from Laptops to Supercomputers. *SoftwareX* **2015**, *1-2*, 19-25.
16. Sun, L. Z.; Luo, M. B., Langevin Dynamics Simulation on the Translocation of Polymer through A-Hemolysin Pore. *J Phys Condes Matter* **2014**, *26*, 415101.
17. Luo, N.-B.; Cao, W.-P., Influence of Polymer-Pore Interaction on the Translocation of a Polymer through a Nanopore. *Phys. Rev. E* **2012**, *86*, 031914.
18. Wang, C.; Chen, Y. C.; Zhou, Y. L.; Luo, M. B., Escape of Polymer Chains from an Attractive Channel under Electrical Force. *J. Chem. Phys.* **2011**, *134*, 064905.
19. Sun, L. Z.; Cao, W. P.; Luo, M. B., Free Energy Landscape for the Translocation of Polymer through an Interacting Pore. *J. Chem. Phys.* **2009**, *131*, 194904.
20. Muthukumar, M., Polymer Translocation through a Hole. *J. Chem. Phys.* **1999**, *111*, 10371.
21. Zhang, S.; Wang, C.; Sun, L.-Z.; Li, C.-Y.; Luo, M.-B., Polymer Translocation through a Gradient Channel. *J. Chem. Phys.* **2013**, *139*, 044902.
22. Luo, K.; Ala-Nissila, T.; Ying, S.-C.; Bhattacharya, A., Sequence Dependence of DNA Translocation through a Nanopore. *Phys. Rev. Lett.* **2008**, *100*, 058101.
23. Jerome, M.; Hasina, V.; Virgile, V.; Yitzhak, R.; Amit, M., Nanopore Unzipping of Individual DNA Hairpin Molecules. *Biophys. J.* **2004**, *87*, 3205-3212

3. Pore-driven polymer translocation: Effect of pore and polymer charge distribution

(Rights and Permission)

Reprinted (adapted) with permission from (*J. Phys. Chem. B.* **2019**,123,19, 4318-4323). **Copyright**

© **2019 American Chemical Society.**

3.1 Introduction

In chapter 2, the effect of altering the pore charge due to mutation is studied by incorporating charged beads at different locations of the pore. To control the polymer translocation, tuning the charge distribution on the pore is crucial. Since biological polymers like peptides are constituted with different kinds of amino acids, their protonation states at the C and N terminal depends on the pH of the medium. This opens up a new way to modulate the charge distribution on the polymer, which is translocating. In this regard, few experiments are carried out to study translocation.

A change in the salt concentration gradient or a pH difference can lead to a change in the polymer-pore interaction. It has been shown by Wong and Muthukumar that the charges at the constriction region and the end of the beta-barrel of the pore can be changed by altering the pH.¹ In a recent experimental report by Jeon and Muthukumar,² the translocation of a macromolecule from the *cis* to the *trans* side of the pore has been studied under various salt concentrations at two different pH conditions (pH 4.5 and 7.5). Their main finding is that the electrostatic interaction between the end of the beta-barrel of the pore and the polymer end can be modulated by changing the pH of the solution near the ring region from neutral to more acidic values.² Thus the electrophoretic transport of charged polymers can be controlled by altering the pH gradients across a protein pore. Using all-atom molecular dynamics simulations, it has been shown that the alteration in the pH of the solution has a significant effect on both electroosmotic flow and the anionic selectivity of the pore.³ The experimental findings were explained theoretically by performing free energy calculations and calculating the translocation time from the free energy profile of the polymer.^{1, 4-7} As discussed in Chapter 2, we have studied the effect of the strength and spatial distribution of charges across a nanopore using extensive molecular dynamics

simulations.⁸ By using a polycationic peptide-PNA probe as the carrier, a nanopore can selectively capture and detect the target miRNA.⁹ Also, by applying the dielectrophoretic principle, DNA, and RNA molecules can be detected selectively by using an engineered biological nanopore.¹⁰ In an experimental study by Luchian and coworkers, it was shown that the capture and transfer of a polypeptide across the nanopore could be controlled by placing oppositely charged amino acid residues at both the chain ends.¹¹ The experimental results were validated by a simple mathematical model for the free-energy profile along the translocation process and also verified by coarse-grained simulations by considering a polymer with oppositely charged segments at the two ends. As an extension of this work, Luchian and coworkers have examined the role of charge asymmetry induced by pH differences on the capture and escape of a peptide containing oppositely charged segments at the *N*- and *C*-termini into the α -HL pore and translocating through the nanopore.¹² A pH gradient can alter both the magnitude of the charge on the peptide and the pore, thereby controlling the magnitude of peptide- α -HL interactions. The charge asymmetry factor has also been taken into account in a work reported by Chinappi and coworkers where they have proposed a nanopore tweezing approach to study the translocation of asymmetrically and unsymmetrically charged cylindrical rod by adding a positive and a negative tail at the two ends and controlling its residence time by tuning the applied voltage.¹³ These experimental techniques have been used to discriminate between neutral amino acid residues from the primary structure of a polypeptide.¹⁴

In our work, we have performed extensive simulation studies to understand the role of pore-polymer interaction in the translocation of a polymer from *trans* (beta barrel side) to the *cis* side of the pore where the electrostatic interaction between pore entrance and the two ends of the chain is modulated by altering the *trans* pH. We consider a coarse-grained picture, and the

details about the simulation set up are discussed in Section 3.2. In Section 3.3, we discuss our simulations and explain our numerical results based on the free energy landscape. Finally, in Section 3.4, we summarize our results.

3.2 Model

The model is similar to the system described in chapter 2. The system under study consists of a membrane, a pore, and a charged polymer chain. The polymer chain is composed of $N=36$ spherical beads each of diameter σ . The consecutive monomer beads are connected by finitely extensible non-linear elastic (FENE) springs and the excluded volume interactions between beads are modeled by using a short-range repulsive Lennard-Jones(LJ) potential according to Eq. 1.1 and Eq. 1.2 in Chapter 1. The wall separating the *cis* and *trans* regions is created by LJ particles in *yz*- plane with the pore oriented along the *x*-axis. Our system of study is not a true polypeptide in the sense that many characteristic features of a polypeptide in terms of folds, torsion angles, and interactions are not taken into account in our current model. In experiments or in vivo condition, the scenario is complicated by atomic charges,¹ electro hydrodynamic interactions,¹⁵⁻¹⁶ electrophoresis,^{15, 17} protonation-deprotonation due to variation in pH,¹⁷⁻¹⁹ etc. During translocation, most of the time the polymer remains in extended form. The backbone of the peptide can thus be considered as the single file motion of the polymer through the pore. Such simple polymer models are well established in previous simulation studies on polymer translocation.^{4, 8, 20-21}

In this work, we consider only the single-file motion of long polymer containing symmetric or asymmetric charged patches at the two ends and a central neutral segment across the pore. In general, the electrostatic interaction between charged particles (polymer-polymer, polymer-pore) is given by the Debye-Hückel screened Coulombic potential

$$U_{coul}(r) = \frac{q_i q_j e^{-\kappa r}}{4\pi\epsilon_0 r} \quad \dots[\text{Eq. 3.1}]$$

q_i and q_j are charges on beads i and j separated at a distance r . The Debye length $\kappa^{-1} = 0.19\text{nm}$ corresponding to a 2M KCl salt concentration. This small Debye length leads to a strong screening effect,²² as a result of which the electrostatic interaction among the monomer beads of the polymer chain can be neglected. In our calculations, we only compute the pair-wise electrostatic interactions between the pore-polymer beads.

For an α -HL pore which is used as a model system to study translocation, there is a spacious vestibule and the β -barrel connected by a narrow constriction. Wong and Muthukumar have estimated the effective charge of the constriction and the ring at the end of the β -barrel as a function of pH.¹ At a pH= 7.5 the constriction is neutral while the ring at the mouth of the β -barrel has a charge of $-7e$. On lowering the pH, the pore interior becomes more and more positively charged and the pore becomes more anionic-selective due to the presence of an excess of positive charges on its internal surface.^{3, 23} The charged state of the constriction and vestibule regions of the α -HL pore is invariant to the change of pH imposed on the *trans* side of the pore. Due to the high anion selectivity at low pH values, the entry of protons into the pore does not alter the protonation state of the residues located at the constriction- or vestibule region. In Ref. 3 and 12, the charge on the *trans* entrance of the pore changed with the change in pH but the charge on the *cis* entrance and the constriction region remain unaltered. Our model is a simplified case of the α -HL pore, where the explicit consideration of barrel, constriction, and vestibule regions are not being included. We mainly focus on the *cis* and the *trans* entrance of a cylindrical pore and the net charge on these regions at different pH gradients. In our simulations, we construct a cylindrical pore which is composed of 26 consecutive rings of uncharged beads where each ring consists of 16 monomer beads of diameter σ such that the length of the pore is

$L= 26\sigma$ and width $W= 3\sigma$. The overall charge on the *cis* entrance of the pore is taken to be equal to zero at all conditions. The simulation box is of $110 \times 100 \times 100$ unit without any periodic boundary condition. In experiments, a pH gradient is created by changing the pH of the *trans* buffer thereby altering the net charge on the pore entrance and the charge on the tail part of the polymer added from the *trans* side. This changes the strength of the electrostatic interactions between the polymer and the pore and also the electrical forces acting on the charged monomers within the pore.¹² The *trans* pH also induces asymmetry in the charge on the peptide chain. In our simulations, as shown in Figure 3.1, the charged patch on the first 12 beads are referred to as the A termini, and the charged path the chain end is referred to as B termini. We mimic pH gradients by considering three types of systems, as shown in Figure 3.1. In the first case (S-I), we introduce a positive unit charge on each of the first 12 beads of the chain ($q_A=12e$, $e = 1.60217646 \times 10^{-19}$ C is the elementary charge), the central 12 beads are neutral and then a unit of negative charge on each of the last 12 beads, ($q_B= -12e$). A charge of $-7e$ is distributed among all the 16 beads that form the first ring of the pore on the entry side (q_{ring}) as shown in Figure 3.1. This arrangement of charges on the polymer and the pore roughly corresponds to a pH=7.3 on the *trans* side. In the 2nd and 3rd system(S-II and S-III respectively), the charge at the end of the polymer(last 12 monomer beads of the chain) entering the pore from the *trans* side is changed from $-4e$ to $-1e$ and the charge on the first ring of the pore is changed from $q_{ring}= 0$ to $q_{ring}= +6e$ corresponding to roughly pH ~ 3.7 and pH ~ 3.1 respectively.¹² Based on the discussion in the Appendix 3.1 of Ref. 12, we assume that for a given system, the charges on the N terminal beads do not change as the chain moves from *trans* to *cis* side of the pore.

We simulate the translocation of this partially charged polymer²⁴ through a nanopore using Langevin dynamics simulations by using the LAMMPS package.²⁵ In Langevin dynamics

simulations, each monomer is subjected to conservative, frictional, and random forces, F_i^C , F_i^F , and F_i^R respectively according to Eq. 1.4 where $F_{ext} = q_i E$ is the external force acting parallel to the pore axis on the i^{th} monomer inside the pore due to the presence of an external electrical field, E .

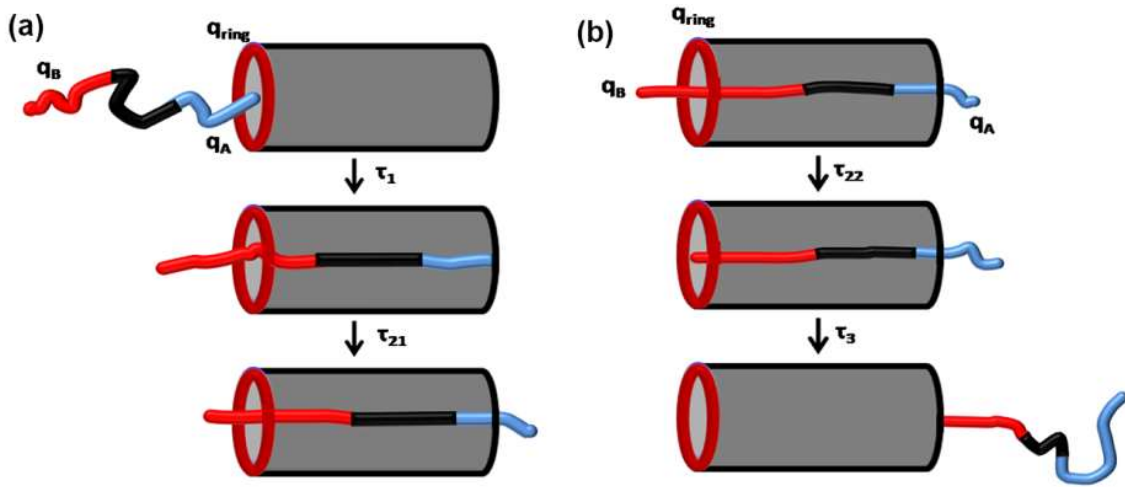


Figure 3.1: Schematic representation of the 36-bead polymer chain translocation from the *trans* to the *cis* side of the pore during (a) entry stage (b) exit stage. q_A and q_B are the charges on the entry and tail part of the chain and q_{ring} is the charge on the entry side of the pore. For S-I, $q_B = -12e$, $q_{ring} = -7e$, for S-II, $q_B = -4e$, $q_{ring} = 0$ and for S-III $q_B = -1e$, $q_{ring} = 6e$, $q_A = +12e$ for all the three systems.

In our simulations, all quantities are expressed in dimensionless LJ unit of energy, length, and mass scales as described in Chapter 1. The parameter values used in our simulations are in the range of benchmark parameters reported in previous translocation studies and were effective in explaining experimental results.^{4, 8, 26-27} In our simulations, the external electric field E is set over a range between 0.1 to 4. This corresponds to the applied voltage of 14 to 560 mV across the pore. The upper limit of the applied voltage in our simulations is higher than values of applied voltage utilized in typical experiments (30-200 mV). As discussed in the results section below, in

order to monitor the capture and filling up of the pore in our simulations here, we required a strong electric field to avoid the escape through the *trans* side.

The equilibration and translocations steps are followed, as discussed in Chapter 1. As described in some previous simulation studies,^{8,27} the average translocation time of the polymer τ involves three different time scales: the pore filling time (τ_1), the transfer time from the *trans* to *cis* side of the pore (τ_2) and the pore emptying time (τ_3). In our current study, τ_2 is further divided into two regimes (τ_{21} and τ_{22}) as shown in Figure 3.1. The timescale τ_{21} is the time required for the middle bead of the polymer chain to reach the center of the pore. This corresponds to the situation when an equal number of positively and negatively charged monomer beads are arranged symmetrically within the pore. As shown in Figure 3.1, τ_1 and τ_{21} correspond to the *entry* stage of the translocation process. We start from this configuration and record the time for the transfer stage (τ_{22}) to be completed. The timescale τ_{22} followed by τ_3 correspond to the *exit* stage. The integration time step is set to $dt= 0.0005$ units. For a given set of parameter values for each system, we perform 200 simulation runs and the histogram of the distributions is constructed from the successful simulation runs using which the average translocation times are obtained. Failed translocation events are rejected and excluded from the statistics. In Figure 3.2 and 3.3, the normalized counts on the vertical axis refer to the ratio of the number of successful translocation events in each bin and the total number of successful translocation events. The probability density distributions of the translocation time are normalized to unity.

3.3 Results and Discussion

We consider the translocation of this partially charged polymer chain from the *trans* to *cis* side of the pore. In order to mimic the effect of pH gradients across the pore on the

translocation properties, we fix the charge at the *cis* end of the pore to be zero (corresponding to *cis*-pH = 7.3) and alter the magnitude of the net charge of the polymer's *A*-end and the *trans* end of the pore corresponding to a drop of the *trans*-pH from 7.3 to 3.17. This allows us to control the sign and the strength of the electrostatic interaction between the charged polymer and the entry side of the pore.

Once the polymer enters the pore, the external electric field drives it from the *trans* to the *cis*-side of the pore. The greater the magnitude of the applied trans-membrane potential, the greater the chance of the polymer to fill the pore. For S-I, during the entry stage, the electrostatic attraction between the positively charged beads that have entered the pore and the negatively charged ring at the pore entry ($q_{ring} = -7e$) can slow down the translocation process, and the polymer may escape from the *trans* side itself. To avoid this, the simulations are performed at a strong electric field of $E = 4$, where the electric field effects are significant enough to overcome the electrostatic attractions. For S-II and S-III, the attractive interaction between the *A*-end moiety and the pore ring decreases, and one would expect that the pore to be filled up faster. But as electric field effects dominate and the charge on the end beads that fill up the pore remains invariant for all three systems, in the presence of a strong electric field, the external electric force acting on the monomers inside the pore is the same for all cases. Therefore there is no significant change in the pore filling time, as seen in Table 3.1. Figure 3.2 shows the translocation time distribution for the polymer chain of length $N = 36$ units for the three different systems that roughly correspond to three different pH gradients.

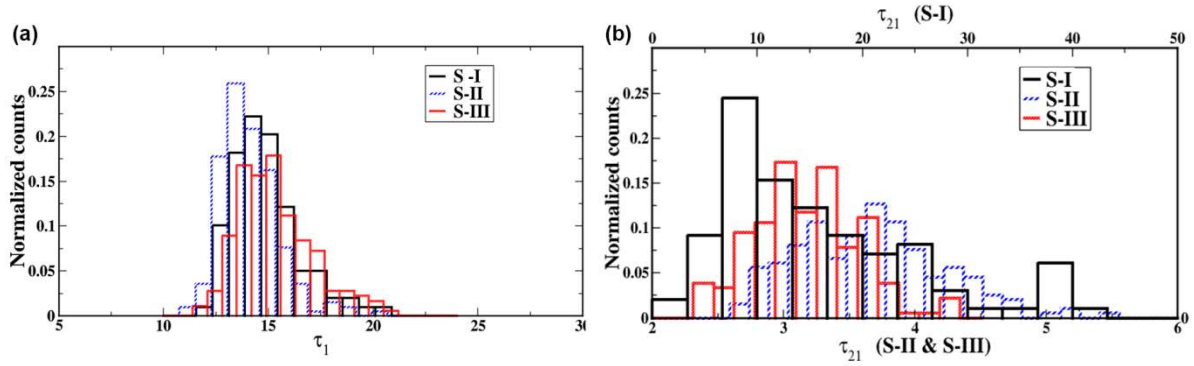


Figure 3.2: The histogram of translocation time for different systems during the entry stage (a) pore filling, τ_1 (b) the first part of the transfer stage τ_{21} for a chain of length $N=36$ and $E=4$; top horizontal axis is for S-I while the bottom horizontal axis is for S-II and S-III showing different utilized scales.

As shown in Figure 3.2a, the translocation time distribution for τ_1 is found to have a slightly asymmetric distribution for all the systems. After the pore filling stage, positively charged residues exit from the *cis* side and negative residues enter from the *trans* side of the pore. This gives rise to a charge asymmetry on the pore-trapped chain. Since the charges on the end beads of the polymer decrease for less acidic values, the negative field that pulls back the polymer towards the entrance side is highest for S-I corresponding to a slower translocation and results in a long-tailed distribution as shown in Figure 3.2b. For S-II and S-III, the peptide trapped inside the pore is effectively positively charged and is driven to the *cis* end thereby making transfer faster as shown in Table 3.1 and leads to slightly asymmetric type distribution plots.

E	Systems	τ_1	τ_{21}
4.0	S- I	14.78±0.16	15.84±0.98
	S- II	14.08±0.10	3.66±0.04
	S- III	15.34±0.13	3.18±0.03

Table 3.1: Translocation times during entry stage

During the exit stage, the pore-trapped polymer is becoming more negatively charged. A strong electric field will pull back the monomers towards the *trans* end, thereby decreasing the probability of a successful translocation event. As a result of this, the simulations during this stage are performed at smaller values of the electric field to prevent escape on the *trans* side. As shown in Figure 3.3, we perform simulations to obtain the distributions and calculate the transfer time and pore emptying time at $E=0.1$. For all the systems, the translocation time distributions for τ_{22} is along tail distribution whereas τ_3 shows an asymmetric broad behavior.

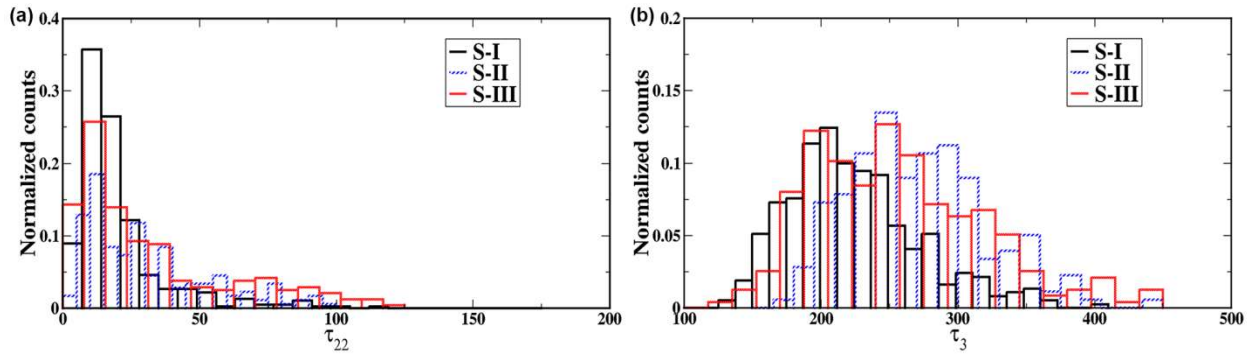


Figure 3.3: The histogram of translocation time for different systems during the exit stage (a) the second part of the transfer stage, τ_{22} (b) pore emptying stage, τ_3 for a chain of length $N=36$ and $E=0.1$.

For S-I, the electrostatic interaction between the polymer ($q_B=-12e$) and the pore ($q_{ring}=-7e$) is

repulsive that facilitates the transfer process. For S-II and S-III, the tail part (B end) of the polymer is less negatively charged, and the charge on the pore ring becomes positive which gives rise to attractive electrostatic interaction and τ_{22} increases as shown in Table 3.2. Based on these arguments, during the escape stage on the sole basis of the electrostatic interactions, we would expect τ_3 to increase as we go from S-I to S-III.

E	Systems	τ_{22}	τ_3
0.08	S- I	19.54±0.67	192.52±1.94
	S- II	35.77±1.63	215.43±3.23
	S- III	39.91±1.87	209.81±3.18
0.1	S- I	20.30±0.88	203.37±2.39
	S- II	31.11±1.70	241.39±4.12
	S- III	32.42±1.89	224.21±4.29

Table 3.2: Translocation times during exit stage

But our simulations show that this trend is not entirely followed (Table 3.2). The escape time for S-III is less than at S-II. The same trend is also observed in the experiments.¹² For S-II and S-III, the pore captured chain experience asymmetrical electrical forces acting oppositely on it. This unbalance of the net charge is more for S-III than for S-II. Thus the pore-captured polymer is more prone to escape from the pore from the *cis* end for S-III than for S-II. This observed phenomenon could be explained qualitatively from our free energy calculations. The free-energy E is plotted as a function of the progress variable Q defined as $Q=N_{cis}-N_{trans}$ where N_{cis} and N_{trans} are the number of monomers on the *cis* and *trans* side of the pore. $N=-35$ corresponds to the beginning of translocation when the first bead is on the *trans* entrance of the pore, and $N= 35$ corresponds to the end of the translocation event when the last bead is on the *cis* entrance of the

pore. The free energy has three contributions: a contribution due to configurational entropy, a contribution due to the electrostatic interaction and a contribution from the external electric field.^{4, 11-12} Following the method used in Ref. 11 and 12 the free energy profile can be constructed as a function of the coordinate Q , as shown in Appendix 3.1. Figure 3.4 shows the free energy landscape for the translocation of a polymer during the pore emptying stage for S-II and S-III. The asymmetry in the charge distribution on the chain results in a decrease of the free-energy barrier at the *cis* end during the emptying stage thereby reducing τ_3 for the latter case.

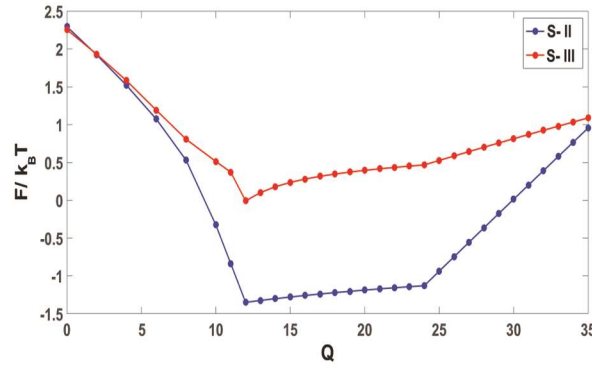


Figure 3.4: Free energy landscape for the translocation of a polymer chain of length $N = 36$ during the exit stage (τ_{22} and τ_3) translocating through a pore of length $L = 26$ for S- II and S-III at $E = 0.1$.

Similarly, the free energy landscape for the entry stage can also be constructed and is reported in Fig. 3.5 in Appendix 3.1. The free energy landscape shows that the energy barrier is almost similar for all the three systems during the pore filling stage (τ_1) and τ_{21} decreases from I to III which agrees qualitatively with the trend shown in Table 3.1. Also as shown in Table 3.2, for each system, the residence time of the polymer within the pore (τ_3) increases with the increase in the applied electric field. Our simulation results are in qualitative agreement with experiments that show that the residence time of the polymer within the pore increases with the increase in the applied voltage.¹²⁻¹³

3.4 Conclusions

In this study, we have performed extensive molecular dynamics simulations to study the effect of polymer-pore interactions on the translocation process by changing the charge distribution of the polymer and the pore to mimic the pH change of the solutions in experimental situations. Experimentally it has been shown that changing the pH alters the charge on the tail part of the polypeptide as well as the charge on the mouth of the β -barrel pore thereby modulating the electrostatic interactions between the pore and either of the two ends of the peptide. Our simulations show that in the presence of a strong externally applied field, the effect of the electrostatic interactions between the polymer and the pore is minimized during the entry stage of the translocation process. The pore entry time τ_1 is independent of the interactions between the polymer and the pore. During the exit stage of the translocation, the pore emptying time τ_3 plays a dominant role. In the presence of a weak electric field, the polymer-pore interactions are important and the pore-trapped polymer is expected to be more prone to exit the pore for S-I due to the repulsion between the negatively charged beads at polymer tail and the negatively charged ring at the pore entrance. At the same time, our simulations show that the unbalanced electric forces acting on both ends of the pore-captured polymer cannot be ignored and plays a crucial role during the pore emptying stage. This is manifested by the fact that the pore trapped polymer exits the pore faster for S- III than for S- II. Thus our simulations could capture the dynamics during different stages of the translocation process. The simulation results are also qualitatively supported and explained by free energy calculations.

3.5 Appendix-3.1

Free energy calculation for translocation

We have a polymer chain with N monomer beads translocating through a nanopore of length $L=26$. We define a translocation coordinate $Q = N_{cis} - N_{trans}$ where N_{cis} and N_{trans} are the number of monomer beads on the *cis* and *trans* side of the pore respectively. During the onset of the translocation process, the first monomer bead is at the entrance of the pore ($N_{cis}=0$, $N_{trans} = 35$, $Q = -35$) The translocation continues with an increase in the number of monomer beads filling up the pore (at the end of pore filling stage at $N_{cis}=0$, $N_{trans}=26$, $Q=-26$) followed by the transfer of the polymer across the pore. As the transfer stage continues, the number of beads on the *cis* side of the pore increases and on the *trans* side decreases, leading to the increase in the value of Q . At the end of the entry stage, an equal number of charged residues is present within the pore as well as an equal number of beads is present on either side of the pore as shown in Figure 3.1. ($N_{cis}=5$, $N_{trans}=5$, $Q=0$). Once the transfer stage ends, there are no monomer beads on the *trans* side of the pore ($N_{trans}=0$, $N_{cis}= 10$, $Q=10$) and after this, the value of Q is only determined by the value of N_{cis} . During the pore emptying stage, N_{cis} increases and reaches its maximum value ($Q=36$) when all the monomers are on the *cis* side of the pore. Between the limits of $Q=-36$ to 0 and $Q= 0$ to 36, one can construct the free energy landscape for the entry stage and exit stage respectively for the different systems under consideration. The free energy of this system has three major components in it: the electrostatic interaction between the polymer and the pore-polymer (F_{elec}), the contribution due to an externally applied electric field (F_{ext}), and the entropy of the chain (F_{ent}). To calculate the electric field contribution, we used the protocol employed in Ref. 11 and 12.¹¹⁻¹² The contribution due to the external electric field E is given by the work done by the electric field E acting only the monomers within the pore moving along pore axis from the *cis* to the *trans* side:

$$F_{ext} = aE(N_+q_1 + N_-q_2) \quad \dots[\text{Eq. A3.1}]$$

where N_+ and N_- correspond to the number of positively and negatively charged residues within the pore with charges q_1 and q_2 respectively. Here q_1 is always $1e$, and q_2 is negative whose magnitude changes with changes for different systems. As mentioned in Ref. 11 and 12, “ a ” is a “function that connects the variation in the progress variable Q to the average movement of the mass center of the peptide.” “ a ” is a function of Q and attains a fixed value over two different ranges of Q . In our case $a=1$ when the pore is fully occupied by the polymer with $N_{cis} \neq 0$ and $N_{trans} \neq 0$ which corresponds to a Q value within the range -8 to 8 . For all other values of Q , $a=0.5$.

In addition to the contribution from the external electric field, we also consider a contribution of the electrostatic interaction between the polymer and pore.^{4, 8} The free energy contribution due to the pore-polymer electrostatic interaction is given by a screened Coulombic interaction

$$F_{elec} = \frac{N_r q_{ring}}{4\pi\epsilon_0} \left(\sum_i \frac{q_1}{x(i,1)} e^{-\kappa x(i,1)} + \sum_j \frac{q_2}{x(j,1)} e^{-\kappa x(j,1)} \right) \quad \dots[\text{Eq. A3.2}]$$

where $(i, 1)$ is the distance between the i^{th} bead of the A end with charge q_1 and $x(j, 1)$ is the distance between the j^{th} bead of the B end with charge q_2 from the pore ring with charge q_{ring} . The cylindrical pore is made up of 26 consecutive rings such that $L=26$. The symbol “1” in the parenthesis denotes the position of the first ring along the pore axis. As seen in Figure 3.1, q_{ring} is situated at the mouth/ entrance of the pore on the *trans* side. Note that the sums over index i and j is performed on the location of each of the N_+^{th} and N_-^{th} bead respectively along the pore axis with respect to the ring at the entrance of the pore. The number of N_+ and N_- beads changes as well as for a given N_+^{th} or N_-^{th} bead, $x(i,1)$ or $x(j,1)$ changes as translocation progresses (variable Q changes). There can be an attractive or repulsive interaction between the *trans* side of the pore and the pore confined polymer depending upon the magnitude of charges on the pore ring and

the charges on both tails of the polymer. Also, the number of the attractive or repulsive term that contributes to the electrostatic energy within the summation depends on the number of N_+ and N_- beads, which changes Q . In Eq. A3.1 and A3.3, N_+ or N_- or both determine the value of Q and the progress of the translocation process with respect to Q . Thus, F_{ext} and F_{elec} are implicit functions of the variable Q . There is also an entropic contribution given by

$$F_{\text{ent}} = k_B T \ln \Omega(n) \quad \dots[\text{Eq. A3.3}]$$

where n is the number of monomers at the *cis* or *trans* side of the pore which is a measure of the value of Q . $\Omega(n) = n^{\gamma-1}$, where $\gamma = 0.69$ for a 3D polymer chain.²⁸ A free energy landscape is constructed including all the above components with appropriate limits as a function of the translocation coordinate Q .

During the beginning of the exit stage, for example, when $Q=2$, there are 8 monomers on the *cis* side and 6 on the *trans* side with $N_{\text{cis}}=6$ and $N_{\text{trans}}=4$, $N_+=6$ and $N_-=8$, the free energy is given by

$$F(Q = 2) = \frac{q_{\text{ring}}}{4\pi\epsilon_0} \left(\sum_{j=0}^7 \frac{q_2}{x(j,1)} + \sum_{i=20}^{25} \frac{q_1}{x(i,1)} \right) + Ea(6q_1 + 8q_2) + k_B T(1 - \gamma)(\ln(4) + \ln(6)) \quad \dots[\text{Eq. A3.4}]$$

Since q_1 corresponds to the charge on the A end, it is always positive. q_2 is negative on the B patch, and its magnitude will depend on the pH of the system. Also the sign and magnitude of q_{ring} changes from S-I to S-III. Based on this, one can construct the free energy landscape during different stages of the translocation process. Figure 3.5 shows the free energy during the entry stage and Figure 3.4 in the manuscript shows the free energy diagram during the exit stage of the translocation.

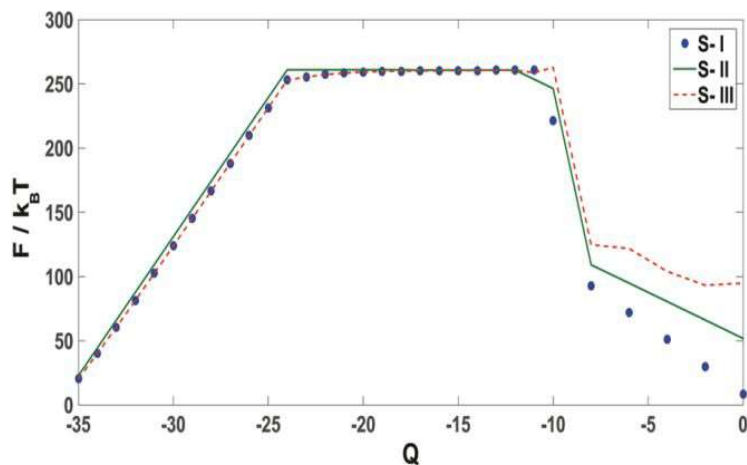


Figure 3.5: Free energy landscape for the translocation of a polymer chain of length $N = 36$ during the entry stage ($\tau_1 + \tau_{21}$) translocating through a pore of length $L = 26$ for S-I, S-II and S-III at $E = 4$.

3.6 References

1. A.T.C., W.; Muthukumar, M., Polymer Translocation through Alpha-Hemolysin Pore with Tunable Polymer-Pore Electrostatic Interaction. *J. Chem. Phys.* **2010**, 133, 045101.
2. Jeon, B.; Muthukumar, M., Electrostatic Control of Polymer Translocation Speed through A-Hemolysin Protein Pore. *Macromolecules* **2016**, 49, 9132-9138.
3. Bonome, E. L.; Cecconi, F.; Chinappi, M., Electroosmotic Flow through an Alpha-Hemolysin Nanopore. *Microfluidics and Nanofluidics* **2017**, 21, 96.
4. Katkar, H. H.; Muthukumar, M., Effect of Charge Patterns Along a Solid-State Nanopore on Polyelectrolyte Translocation. *J. Chem. Phys.* **2014**, 140, 135102.
5. Sun, L. Z.; Cao, W. P.; Luo, M. B., Free Energy Landscape for the Translocation of Polymer through an Interacting Pore. *J. Chem. Phys.* **2009**, 131, 194904.
6. Chen, Y.-C.; Wang, C.; Zhou, Y. L.; Luo, M.-B., Effect of Attractive Polymer-Pore Interactions on Translocation Dynamics. *J. Chem. Phys.* **2009**, 130, 054902.
7. Zhang, S.; Wang, C.; Sun, L.-Z.; Li, C.-Y.; Luo, M.-B., Polymer Translocation through a Gradient Channel. *J. Chem. Phys.* **2013**, 139, 044902.
8. Ghosh, B.; Chaudhury, S., Influence of the Location of Attractive Polymer-Pore Interactions on Translocation Dynamics. *J. Phys. Chem. B* **2018**, 122, 360-368.
9. Tian, K.; He, Z.; Wang, Y.; Chen, S. J.; Gu, L. Q., Designing a Polycationic Probe for Simultaneous Enrichment and Detection of Micrnas in a Nanopore. *ACS Nano* **2013**, 7, 3962-3969.
10. Tian, K.; Decker, K.; Aksimentiev, A.; Gu, L. Q., Interference-Free Detection of Genetic Biomarkers Using Synthetic Dipole-Facilitated Nanopore Dielectrophoresis. *ACS Nano* **2017**, 11, 1204- 1213.

11. Asandei, A.; Chinappi, M.; Lee, J.; Seo, C. H.; Mereuta, L.; Park, Y.; Luchian, T., Placement of Oppositely Charged Aminoacids at a Polypeptide Termini Determines the Voltage-Controlled Braking of Polymer Transport through Nanometer-Scale Pores. *Sci. Rep.* **2015**, *5*, 10419.
12. Asandei, A.; Chinappi, M.; Kang, H.-K.; Chang, H. S.; Mereuta, L.; Park, Y.; Luchian, T., Acidity-Mediated, Electrostatic Tuning of Asymmetrically Charged Peptides Interactions with Protein Nanopores. *ACS Appl. Mater. Interfaces* **2015**, *7*, 16706-16714.
13. Chinappi, M.; Luchian, T.; Cecconi, F., Nanopore Tweezers: Voltage-Controlled Trapping and Releasing of Analytes. *Phys. Rev. E* **2015**, *92*, 032714.
14. Asandei, A.; Rossini, E.; Chinappi, M.; Park, Y.; Luchian, T., Protein Nanopore-Based Discrimination between Selected Neutral Amino Acids from Polypeptides. *Langmuir* **2017**, *33*, 14451-14459.
15. Luan, B.; Aksimentiev, A., Electric and Electrophoretic Inversion of the DNA Charge in Multivalent Electrolytes. *Soft Matter* **2010**, *6*, 243-246.
16. Ghosal, S., Effect of Salt Concentration on the Electrophoretic Speed of a Polyelectrolyte through a Nanopore. *Phys. Rev. Lett.* **2007**, *98*.
17. Buyukdagli, S.; Ala-Nissila, T., pH-Mediated Regulation of Polymer Transport through Sin Pores. *EPL* **2018**, *123*, 38003.
18. Buyukdagli, S.; Ala-Nissila, T., Controlling Polymer Translocation and Ion Transport Via Charge Correlations. *Langmuir* **2014**, *30*, 12907-12915.
19. Buyukdagli, S.; Ala-Nissila, T., Controlling Polymer Capture and Translocation by Electrostatic Polymer-Pore Interactions. *J. Chem. Phys.* **2017**, *147*, 114904.
20. Hsiao, P.-Y., Polyelectrolyte Threading through a Nanopore. *Polymers* **2016**, *8*, 73.
21. Sarabadani, J.; Ikonen, T.; Ala-Nissila, T., Iso-Flux Tension Propagation Theory of Driven Polymer Translocation: The Role of Initial Configurations. *J. Chem. Phys.* **2014**, *141*, 214907.
22. Oukhaled, G.; Bacri, L.; Mathe, J.; Pelta, J.; Auvray, L., Effect of Screening on the Transport of Polyelectrolytes through Nanopores. *EPL* **2008**, *82*, 48003.
23. Aksimentiev, A.; Schulten, K., Imaging A-Hemolysin with Molecular Dynamics: Ionic Conductance, Osmotic Permeability, and the Electrostatic Potential Map. *Biophys. J.* **2005**, *88*, 3745-3761.
24. Ghosh, B.; Chaudhury, S., Translocation Dynamics of an Asymmetrically Charged Polymer through a Pore under the Influence of Different pH Conditions. *J. Phys. Chem. B* **2019**, *123*, 4318-4323.
25. Plimpton, S., Fast Parallel Algorithms for Short-Range Molecular Dynamics. *Journal of computational physics* **1995**, *117*, 1-19.
26. Sarabadani, J.; Ghosh, B.; Chaudhury, S.; Ala-Nissila, T., Dynamics of End-Pulled Polymer Translocation through a Nanopore. *EPL* **2017**, *120*, 38004.
27. Luo, K.; Ala-Nissila, T.; Ying, S. C.; Bhattacharya, A., Influence of Polymer-Pore Interactions on Translocation. *Phys. Rev. Lett.* **2007**, *99*, 148102.
28. Flory, P., *Principles of Polymer Chemistry*; Cornell University Press, 1953.

4. End-pulled Polymer Translocation: Single Chain Dynamics

4.1. Introduction

End-pulled translocation is an important type of forced translocation where the polymer is pulled from one end through the pore. In experiments, the end-pulled translocation is performed by applying force on one end of the polymer using an optical or a magnetic tweezer or by atomic force microscopy.¹⁻⁵ End-pulled translocation is thought to be an effective method for carrying out the translocation in a more controlled and slow way. In general, the polymer translocation events in experiments are very short lived. A controlled and slow translocation process allows better detection and resolution of the current signals. In this regard, end-pulled translocation is promising for cheap and rapid DNA sequencing.⁶⁻⁸

Over the past few years, there is a continuous effort to understand pore-driven polymer translocation and develop a quantitative theory.⁹⁻¹⁵ Driven translocation is a far-from-equilibrium phenomenon, and the first non-equilibrium treatment was given by Sakaue using a tension propagation (TP) theory.¹⁶ Till now the case of end-pulled translocation has not been treated theoretically beyond simple scaling arguments and due to its non-equilibrium dynamics, only scaling arguments cannot describe the physics behind this process. To this end, in this chapter, we present a proper theoretical treatment of the end-pulled translocation based on extensive molecular dynamics (MD) simulations and augmented with the iso flux tension propagation theory which we will discuss in the next section.

The key idea of the TP theory¹⁰ is that the translocation process constitutes two stages, the tension propagation (TP) and post propagation (PP) stages. During the TP stage, a tension propagates through the chain backbone, and the cis side of the subchain can be divided into two distinct domains. The first domain includes the monomers that have been set into motion by the external force applied on the monomers inside the pore, the first few monomers sets into motion. The rest of the chain remains at rest on an average. At any stage of the translocation, the chain is divided into a moving, and a non-moving (on an average) segments and the junction between them is called *tension front*. As the translocation proceeds, the *tension front* moves along the chain with time, including more and more monomers into the moving part. With the inclusion of more monomers into the moving part, the effective friction on the chain increases. The tension propagation ends when the last monomer sets into motion. After a certain instant of time known

as the tension propagation time, the front reaches the last bead, and the tension propagation process ends. The *tension propagation* is analogous to the situation when a coiled rope is pulled from one end where first the rope uncoils, and then it starts moving as a whole. After this time, referred to as the PP stage, the chain starts moving as a whole towards the *trans* side. In the TP model, the translocation process is given by the translocation coordinate(s) that defines the position of a monomer with respect to the pore and the location of the tension front. The equation of motion of the translocation coordinate(s) can be written as-

$$\Gamma(t) \frac{ds}{dt} = f_{total} \quad \dots[\text{Eq. 4.1}]$$

where s is the monomers on the trans side of the pore, $\Gamma(t)$ is the effective friction and f_{total} is the total force acting on the polymer. However, this theory was implemented in the asymptotic limit of long chains, which is out of reach of experiments and numerical simulations. Also, the interaction between the pore and the polymer was neglected.

Nissila and coworkers have modified the TP formalism by combining tension propagation with the iso-flux assumption.¹⁷ According to the iso-flux approximation, the monomer flux on the mobile domain of the cis and trans sides and through the pore is constant in space but evolves in time. This modified theory is known as the iso-flux tension propagation theory^{10, 13-14} incorporates finite chain lengths by including the pore-polymer interactions to the TP equations. Here the effective friction was divided into two parts, namely, the friction of the moving chain, and the friction due to the pore. This was given as –

$$\Gamma(t) = \eta_{cis}(t) + \eta_p \quad \dots[\text{Eq. 4.2}]$$

where $\eta_{cis}(t)$ and η_p are the cis side subchain and pore friction

The IFTP theory provides exact analytic scaling forms of the average translocation time as a function of the chain length in the appropriate limits, including the influence due to the pore friction. Since the *trans* side of the chain was static, the friction on the trans side chain was neglected. The main assumption of the TP theory was that the effect of the *trans* side subchain on the non-equilibrium dynamics is small and hence, its contribution to the effective total friction is neglected. However, for example, for semi-flexible polymer chains,¹⁴ the influence of the *trans* side chain on the dynamics is non-negligible. It has been shown that an additional time-dependent *trans* side friction due to the stiffness of the chain plays an important role, especially

for shorter chains. In the case of end-pulled translocation,¹⁸ the effect of the trans side friction needs to be incorporated in the effective friction. The effective friction can be written as –

$$\Gamma(t) = \eta_{cis}(t) + \eta_p + \eta_{trans}(t) \quad \dots[\text{Eq. 4.3}]$$

$\eta_{trans}(t)$ is the time-dependent trans side friction.

The coarse-grained Langevin dynamics simulations for end pulled translocation are important to obtain the quantitative value of the total chain friction, the position of the *tension front*, and the tension propagation time during translocation. Further, based on the findings of these two quantities, the IFTP theory for the end-pulled polymer translocation is developed. The details of the model and parameters are explained in the next section.

4.2. Model

The general approach of the simulation is described in the introduction chapter of the thesis. Here, the modification and particulars of this study have been given. A polymer of $N=100$ was considered where the successive beads were connected by the finitely extensible nonlinear elastic (FENE) spring interaction, which was given in Eq. 1.2 where k is the spring constant and R_0 is the maximum allowed distance between neighboring beads. The Eq. 1.3 was used for the excluded-volume interaction between the beads, where σ is the diameter of each bead, ϵ is the potential well depth, and r is the distance between the beads. Using the repulsive LJ interaction

$$U_{LJ}(r) = 4\epsilon \left[\left(\frac{\sigma}{r} \right)^9 - \left(\frac{\sigma}{r} \right)^3 \right] \quad \dots[\text{Eq. 4.4}]$$

the physical wall at $x = 0$ and is parallel to the yz -plane, is constructed. The region of space with $x > 0$ is the *trans* side, and with $x < 0$ is the *cis* side.

The pore is constructed by 16 beads (each bead with a diameter of σ) that are placed on a circle with a diameter of $d = 3\sigma$. The pore is parallel to the wall, and its center is at $x = 0$, which is given in Figure-4.1. The pore thickness is σ , and the interaction between pore particles and monomers is repulsive LJ interaction with the same parameters as of the excluded-volume interactions between the beads of the polymer. The simulation box is of $200 \times 200 \times 200$ units without a periodic boundary condition. The box dimension is such that the polymer remains inside the box when the translocation ends.

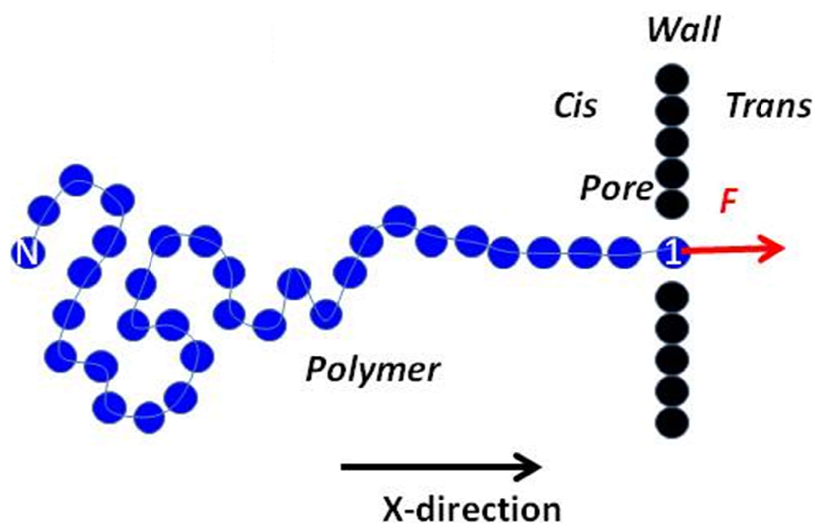


Figure 4.1: Schematic representation of end-pulled translocation

The external driving force, f , which is in the positive x -direction, only acts on the head bead of the polymer. The equation of motion is similar to Equation-1.4 for the i -th bead where now the external force acts on the first monomer bead of the polymer chain. The parameters of our MD simulations are in LJ units and have been given in Chapter 1. Since the force scales in LJ units as 2.3 pN, a pulling force of $f=100$ in our LJ units correspond to 230 pN, which is well in the range that can be realized with the AFM technique.³⁻⁵ The equilibration is done by fixing the first bead at the pore the details for which are given in Chapter 1. The constraint on the first monomer was lifted, and a force of $f=100$ was applied on the first bead to carry out the translocation. With the application of the force on the first monomer, the chain started moving according to the IFTP theory described in Section 4.1.1.

Also, the IFTP theory has revealed that for the pore-driven case there are three different regimes of translocation dynamics depending on the different driving force strengths, namely the strong stretching (SS) limit of high forces, the stem-flower (SF) regime of intermediate forces, and the trumpet (TR) regime of weak forces shown in Figure 4.2.¹⁸ For end pulled polymers, there are different combinations of the chain configurations both on the cis and trans sides. Here we will consider only the case of high driving forces such that the trans side subchain is fully straightened at all times during the translocation process, i.e., the trans chain is in the strong

stretching (SST) regime.

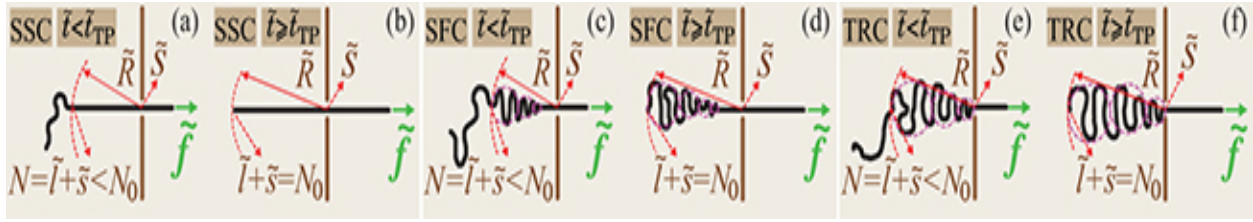


Figure 4.2: Various possible translocation scenarios during the tension propagation (TP) stage for the *trans* side strong stretching (SST) regime. The driving force \tilde{f} acts only on the head monomer of the polymer in the *trans* side. The length of the polymer is N_0 and the number of beads that have been already translocated into the *trans* side is denoted by \tilde{s} . The number of total beads influenced by the tension is $N = \tilde{l} + \tilde{s}$ (in the TP stage $N < N_0$). In panel (a) the *cis* side subchain is also in the SS regime (SSC) during the TP stage. (b) The translocation process when the tension front reaches the end of the chain on the *cis* side in the SSC regime (post propagation stage (PP), where $N=N_0$). Panels (c) and (e) are the same as panel (a) but for the stem-flower (SFC) and trumpet (TRC) regimes in the *cis* side, respectively. Panels (d) and (f) are the same as panel (b) but for SFC and TRC, respectively. (Figure Credit : Dr. Jalal Sarabadani)¹⁸

In order to get the total friction on the chain, first, the tension front on the chain was calculated. This was done from the waiting time distribution calculations followed by a few other calculations discussed in the following sections.

4.3. Result and Discussion

a) Waiting Time Distribution

Waiting time is generally referred to the time spent by each of the monomers on the pore of during translocation. Mathematically, waiting time of monomer s is the time between the s^{th} and $(s+1)^{\text{th}}$ monomer exiting the pore. From the Langevin dynamics simulations, this time was approximated by as the number of times s appears on pore multiplied by the time step where s was the translocation coordinate denoting the progress of the translocation. For each monomer, the waiting time is an average quantity of several simulation runs. In our case, the waiting time

distribution was calculated from 2000 trajectories of successful translocation runs shown in Figure 4.3.

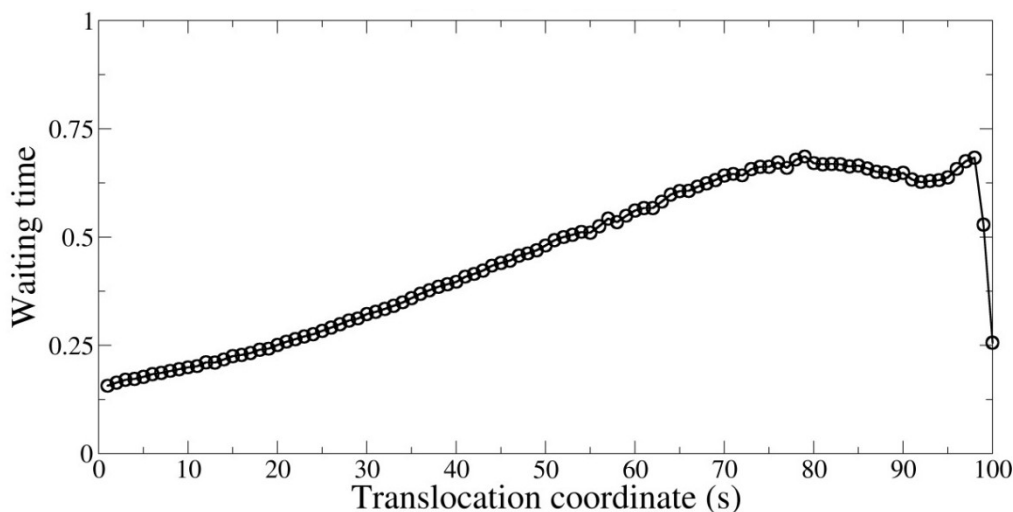


Figure 4.3: The waiting time distribution for $N=100$, $f=100$ end-pulled polymer translocation.

From Figure 4.3, the waiting time is plotted as a function of the translocation coordinate. During the TP stage, the tension propagates along more and more mobile monomers on the backbone of the chain. Consequently, the friction increases, the dynamics of the system gets slower, and the waiting time increases. The waiting time becomes maximum when the tension reaches the chain end. In Figure 4.3, the waiting time for the monomers is maximum at $s=80$. Thus the area in the waiting till $s=80$ is the tension propagation time. In the TP stage, all monomers of *cis* side subchain move with some velocity and contribute to the friction. As time passes the *cis* sub-chain is sucked into the pore, the number of mobile monomers in the *cis* side decreases, and consequently, the friction decreases. The plateau region in the figure denotes the post propagation stage of the translocation. To find out the chain configuration during different stages of the translocation, and the time-dependent friction on the chain, the velocity of the monomer was calculated.

b) Monomer Velocity Calculation:

The monomer velocities (averaged over 2000 successful translocation runs) were calculated in the strong force limit from molecular dynamics simulation to study the dynamics at different stages of the translocation. The individual monomer velocities perpendicular to the wall (velocity in the direction of the applied driving force, here x-axis) is plotted against the monomer number in Figure 4.5.

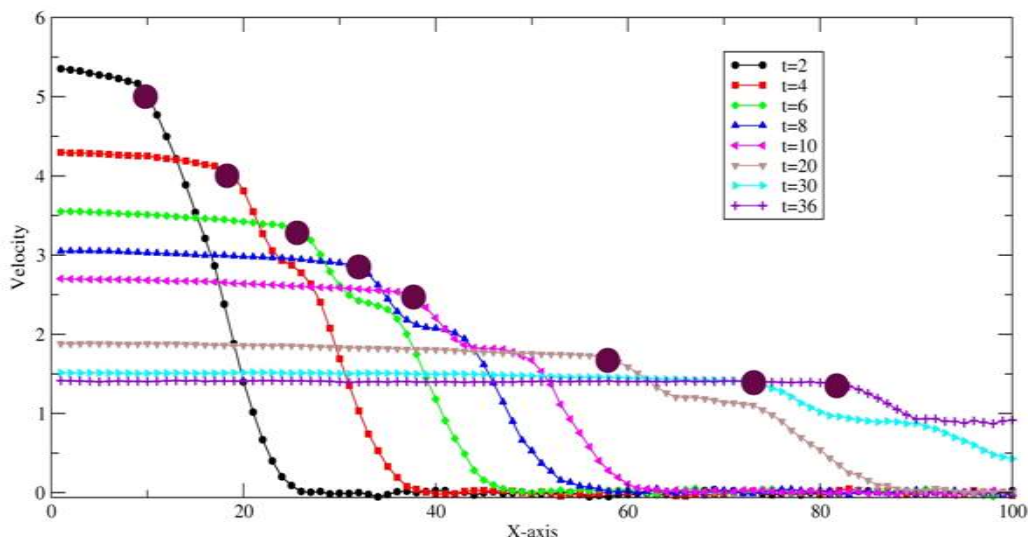


Figure 4.4: Velocity vs. monomer number for $N=100$, $f=100$. The maroon circles indicate the monomer bead which is at the pore.

At each time, the velocities of the monomers on the *trans* side of the pore have a constant value and drops immediately close to the pore entrance on the *cis* side. This drop in velocity in the TP stage is due to the reorientation of the mobile part of the chain in the *cis* side when force is applied on the chain end, and finally, for the non-moving part of the chain, the velocity is zero. With the progress of time, during the PP stage, all the monomers start with a constant non-zero velocity and finally it becomes equal to that of the *trans* side sub chain.

For example in Figure 4.4 around $t=4$, the 20th bead is roughly at the pore, the tension has propagated almost till the 40th bead, and the rest part of the chain is still in the static domain. Whereas at $t=36$, the 80th bead is roughly at the pore, but the tension front has propagated till the

last bead as a result of which all the beads on the cis side of the pore are moving with some non-zero velocity. Our simulations showing the drop in velocity on the cis side subchain at different times further strengthens the fact that the chain on the cis side is not in the SS regime, rather it is a combination of the SSC and SST regimes.

c) Mean Waiting Times: Simulation and theory:

To test the validity of the IFTP theory for the end-pulled case in Figure 4.6, the monomer waiting time distribution $w(s)$ is plotted as a function of the translocation coordinate s .

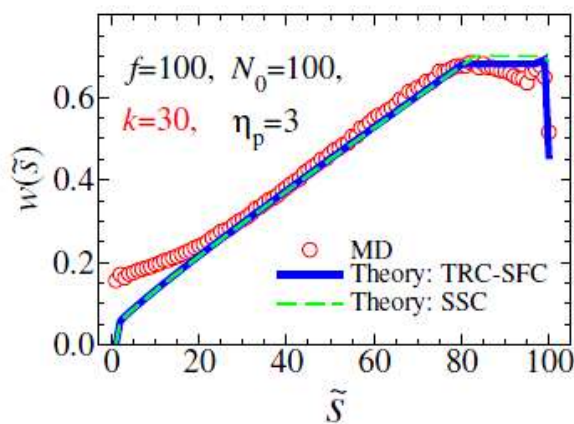


Figure 4.5: Comparison of the mean waiting times as a function of the translocation coordinate “s” from simulation and theory (Figure Credit: Dr. Jalal Sarabadani).¹⁸

The red circles show the MD data obtained using the bead-spring model. The solid blue line comes from the IFTP theory when the equations of motion are solved with a combination of the SSC, SFC, and TRC regime. This part of the work on the IFTP theory has been done by Dr. Jalal and Prof. Tapio. For small values of s , the solution of the IFTP theory underestimates the waiting time. This occurs mostly because of bond stretching and also due to the beginning of the reorientation of the mobile part on the *cis* side, which can be captured accurately from our simulations. This discrepancy between theory and simulation exists only for small values of s and the main contribution of the waiting time and consequently the translocation time comes from the larger s almost at the end of the tension propagation stage, and over the whole post propagation stage, the IFTP theory correctly predicts the overall behavior of the translocation process.

4.4. Conclusion

We have studied the dynamics end-pulled polymer translocation through a nanopore by extensive simulations which reveal the existence of a complicated scenario depending on the strength of the driving force. Even in the case where the force is high enough such that the trans side of the chain is straight, our simulations show that there are three different regimes depending on the conformation of the cis side subchain. The waiting time distribution and velocity calculations described the nature of the end-pulled translocation in the tension propagation and post propagation regimes. Using the analytical IFTP theory, we have derived the corresponding equations of motion for the tension front propagation explicitly including the trans side friction. The theory shows excellent agreement with MD simulations for the waiting time distribution of the monomers.

4.5. References

1. Smith, D. E.; Tans, S. J.; Smith, S. B.; Grimes, S.; Anderson, D. L.; Bustamante, C., The Bacteriophage Φ 29 Portal Motor Can Package DNA against a Large Internal Force. *Nature* **2001**, 413, 748-752.
2. Keyser, U. F.; Koeleman, B. N.; van Dorp, S.; Krapf, D.; Smeets, R. M. M.; Lemay, S. G.; Dekker, N. H.; Dekker, C., Direct Force Measurements on DNA in a Solid-State Nanopore. *Nat. Phys.* **2006**, 2, 473.
3. van Dorp, S.; Keyser, U. F.; Dekker, N. H.; Dekker, C.; Lemay, S. G., Origin of the Electrophoretic Force on DNA in Solid-State Nanopores. *Nat. Phys.* **2009**, 5, 347.
4. Bulushev, R. D.; Steinbock, L. J.; Khlybov, S.; Steinbock, J. F.; Keyser, U. F.; Radenovic, A., Measurement of the Position-Dependent Electrophoretic Force on DNA in a Glass Nanocapillary. *Nano Lett.* **2014**, 14, 6606-6613.
5. Bulushev, R. D.; Marion, S.; Petrova, E.; Davis, S. J.; Maerkl, S. J.; Radenovic, A., Single Molecule Localization and Discrimination of DNA-Protein Complexes by Controlled Translocation through Nanocapillaries. *Nano Lett.* **2016**, 16, 7882-7890.
6. Ollila, S. T. T.; Luo, K. F.; Ala-Nissila, T.; Ying, S. C., Polymer Translocation in a Double-Force Arrangement. *Euro. Phys. J. E* **2009**, 28, 385-393.
7. Huopaniemi, I.; Luo, K.; Ala-Nissila, T.; Ying, S.-C., Polymer Translocation through a Nanopore under a Pulling Force. *Phys.Rev. E* **2007**, 75, 061912.
8. Kantor, Y.; Kardar, M., Anomalous Dynamics of Forced Translocation. *Phys. Rev. E* **2004**, 69, 021806.
9. Sarabadani, J.; Ikonen, T.; Ala-Nissila, T., Theory of Polymer Translocation through a Flickering Nanopore under an Alternating Driving Force. *J. Chem. Phys.* **2015**, 143, 074905.

10. Sarabadani, J.; Ikonen, T.; Ala-Nissila, T., Iso-Flux Tension Propagation Theory of Driven Polymer Translocation: The Role of Initial Configurations. *J. Chem. Phys.* **2014**, 141, 214907.
11. Ikonen, T.; Bhattacharya, A.; Ala-Nissila, T.; Sung, W., Influence of Pore Friction on the Universal Aspects of Driven Polymer Translocation. *EPL* **2013**, 103, 38001.
12. Ikonen, T.; Shin, J.; Sung, W.; Ala-Nissila, T., Polymer Translocation under Time-Dependent Driving Forces: Resonant Activation Induced by Attractive Polymer-Pore Interactions. *J. Chem. Phys.* **2012**, 136, 205104.
13. Ikonen, T.; Bhattacharya, A.; Ala-Nissila, T.; Sung, W., Unifying Model of Driven Polymer Translocation. *Phys. Rev. E* **2012**, 85, 051803.
14. Sarabadani, J.; Ikonen, T.; Mökkönen, H.; Ala-Nissila, T.; Carson, S.; Wanunu, M., Driven Translocation of a Semi-Flexible Polymer through a Nanopore. *Sci. Rep.* **2017**, 7, 7423.
15. Ikonen, T.; Bhattacharya, A.; Ala-Nissila, T.; Sung, W., Influence of Non-Universal Effects on Dynamical Scaling in Driven Polymer Translocation. *J. Chem. Phys.* **2012**, 137, 085101.
16. Sakaue, T., Nonequilibrium Dynamics of Polymer Translocation and Straightening. *Phys. Rev. E* **2007**, 76, 021803.
17. Rowghanian, P.; Grosberg, A. Y., Force-Driven Polymer Translocation through a Nanopore: An Old Problem Revisited. *J. Phys. Chem. B* **2011**, 115, 14127-14135.
18. Sarabadani, J.; Ghosh, B.; Chaudhury, S.; Ala-Nissila, T., Dynamics of end-pulled polymer translocation through a nanopore. *EPL* **2018**, 120, 38004

5. End-pulled polymer translocation: Folded chain dynamics

5.1 Introduction

In chapter 2 and 3, we have discussed about the role of polymer-pore interaction in the context of pore driven translocation.¹⁻² The theoretical work is based on experimental studies of polymer translocation where charged polymers are electrically driven through pores whose typical diameters range from nanometers to tens of nanometers. In most experiments, the alpha-hemolysin pore complex is used in common to study the translocation process.³⁻⁵ The alpha-hemolysin pore has a diameter much less than 2nm such that only single-stranded DNA/RNA molecules are restricted to thread through these protein channels. In the experiment by Kasionawicz and coworkers, the ionic current through the voltage biased alpha-hemolysin pore can detect the translocation of single-stranded molecules pulled through the narrow pore under the influence of an external field.³ One of the main challenges in DNA sequencing is to construct pores with a diameter comparable to the diameter of the polymer that allows translocation of double-stranded DNA molecules. Experiments on double-strand DNA translocation using silicon oxide nanopores have been reported by Dekker and coworkers.⁶⁻⁹ Such synthetic pores have a lot of advantages over biological pores. For example, the pore size can be tuned, and such pores are stable under experimental conditions such as high temperature and extreme voltage and pH values.¹⁰⁻¹⁴ Since the solid-state pore diameters can range from 5 to 15 nm, and experimentally, it has observed that the polymer can undergo not only single file motion through the pore but also in different folded states.¹⁵ The formation of double-stranded DNA hairpins undergoing voltage-driven translocation through nanopores located in synthetic membranes has been studied using coarse-grained Langevin dynamics of translocation.¹⁶ Kotsev, and Kolomeisky have studied the translocation dynamics of polymer with folded configurations using simple discrete stochastic models.¹⁷

In this chapter, we investigate the translocation dynamics of polymers with folds using coarse grain Langevin dynamics simulation by implementing the concept of end pulled translocation introduced in Chapter 4.¹⁸ Experimental results on solid-state nanopores show that the translocation of polymers with more than one fold is negligible.¹⁵ Hence one considers the polymer chain to have a single fold such that the chain will have two equal or unequal length segments, as shown in Figure 5.1. The polymer may pass through the pore in either single file or folded configuration. The details of the model for our simulations are given in the next section, and the simulation results are discussed in Sec 5.3.

5.2 Model

We study the translocation of a single chain of N monomers through the pore with any one of the intermediate bead placed on the pore that divides the chain into two folded segments: the shorter segment containing N_1 monomers and the longer segment shorter N_2 monomers ($N_1: N_2$) with $N_1 < N_2$. As shown in Figure 5.1, we consider a chain of an odd number of monomer beads $N = 101$ with the bead connecting the two segments placed at the pore. We consider a chain of different segment lengths of (a) 51:51 (b) 31: 71 (c) 11: 91. The simulation box is of $200 \times 200 \times 200$ unit without a periodic boundary condition. The folded polymer is driven through the nanopore by pulling any intermediate bead placed in the pore by an external driving force. The translocation dynamics of this folded chain involves two events: one is the motion of both the folded segments through the channel followed by the linear motion of the longer segment of the polymer through the pore.

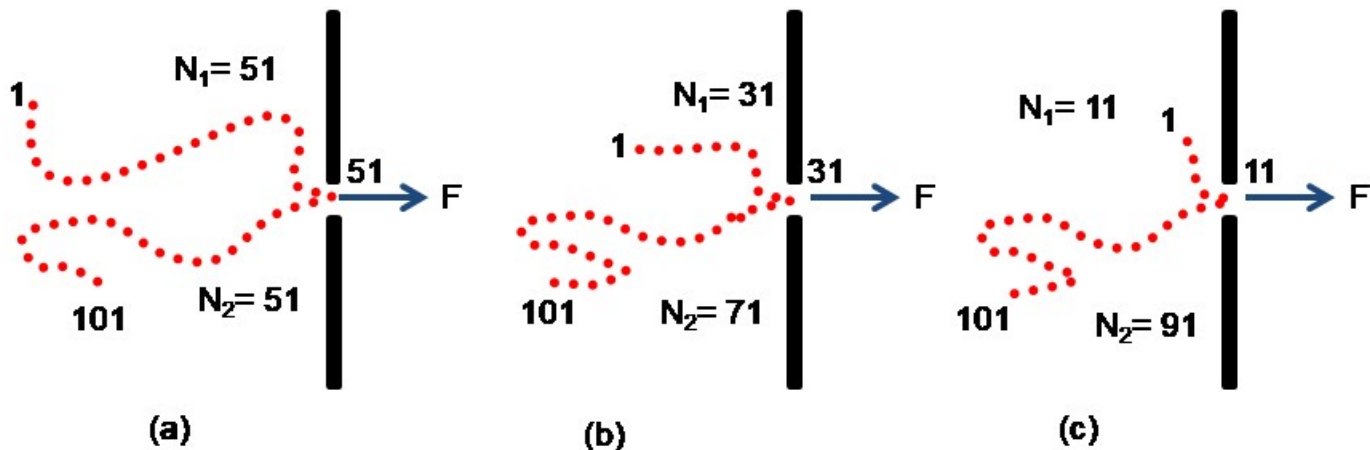


Figure 5.1: Schematic representation of the translocation of a polymer with a folded configuration (a) 51:51: symmetrical fold (b) 31:71 (c) 11:91

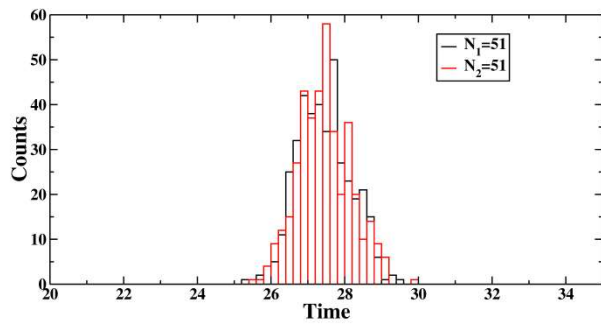
As discussed in Chapter 1 and the previous chapters, the successive beads are connected by the finitely extensible nonlinear elastic (FENE) spring interaction and the excluded-volume interaction between the beads, is given by the repulsive LJ interaction. All other simulation details follow the same set up as used in Chapter 4 for end pulled translocation. We assume that the length of the pore is small so that only one (for a linear chain) or two (for a folded chain) monomers can be present inside the channel. In the first stage of the simulation, any intermediate monomer bead that divides the chain into the two segments/folds are fixed at the pore, and the chain is equilibrated in the absence of any applied force. In the next step, this constraint is removed, and the equilibrated chain is allowed to transfer through the pore following the Langevin equation of motion by applying a strong pulling force on this bead. The pulling force is high such that the chain is straight on the *trans* side of the pore. Once the entire chain moves to the *trans* side of the pore, we record the translocation time, and we begin the next independent simulation run. The simulation results are averaged over 300-500 independent runs. The average

translocation time of the chain is the difference in time when this intermediate bead that divided the chain into folds is at the pore and the time when the last bead (N^{th} bead) of the polymer leaves the pore. In order to calculate the total friction on the chain, we use the concept of the tension propagation theory discussed in Chapter 4. First, we calculate the time evolution of the tension front on the individual folds of the chain. This was done from the waiting time distribution calculations followed by a few sets of calculations of the monomer velocity that describes the time evolution of the tension front, as discussed in the result section.

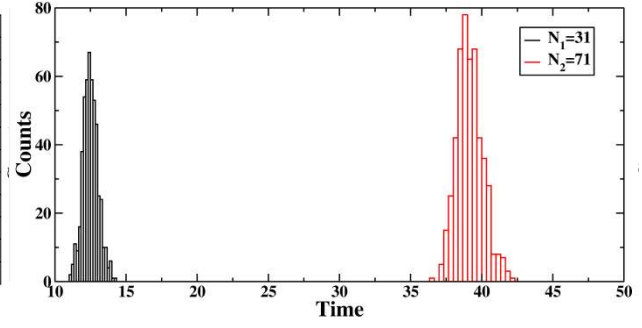
5.3 Result and Discussion

(a) Translocation time distribution

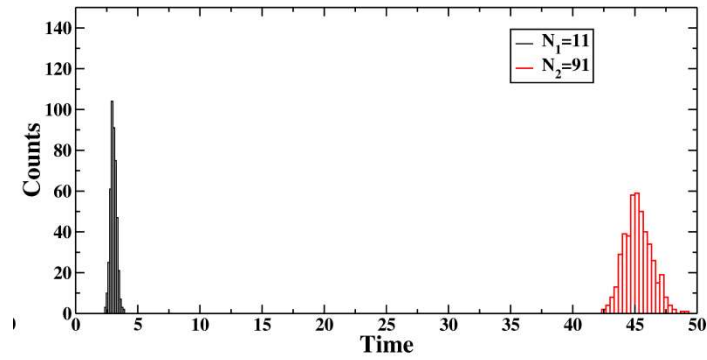
For each the folded segment of the chain, we obtain the histogram of the translocation times, as shown in Fig. 5.2 (a), (b) and (c). From our distribution plots, we obtain the average translocation times as a function of the length of the folded segments. As the folded chain becomes more unsymmetrical, i.e., as we move 51:51 to the 71:31 and then to the 91:11 case, the distribution plots for the folded segments are separated from each other. The distributions for the shorter segments are narrower and the average translocation time of the shorter segment $N_1(\tau_1)$ decreases and that of $N_2(\tau_2)$ increases.



(a)



(b)



(c)

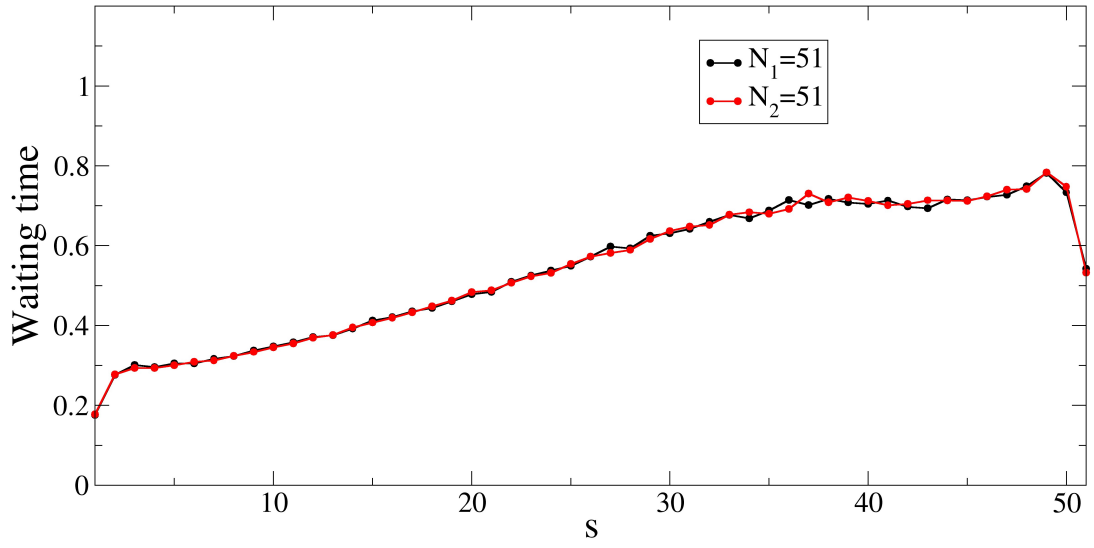
Figure 5.2: The translocation time distributions. (a) 51:51, (b) 31:71 and (c) 11:91

The mean translocations time of the entire chain, τ and the mean time of the different folds τ_1 and τ_2 are shown in Table 5.1. As shown in Table 5.1, The average translocation time is equal to the translocation time of the longer segment τ_2 . This further signifies that when the force is applied at some intermediate bead at the pore, both the folds start moving together followed by the movement of the longer segment through the pore until the last bead of the chain leaves the pore and is on the trans side of the pore.

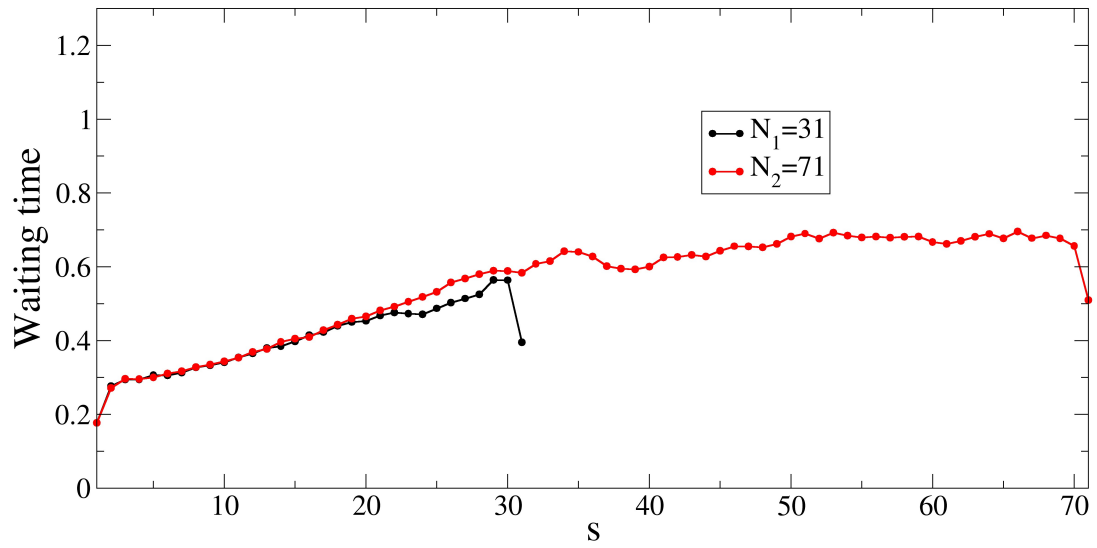
Systems	N_1	N_2	$\langle \tau_1 \rangle$	$\langle \tau_2 \rangle$	$\langle \tau \rangle$
1	-	101	-	46.22	46.22
2	51	51	27.44	27.45	27.63
3	41	61	19.46	34.03	34.03
4	31	71	12.49	39.16	39.16
5	21	81	7.05	42.90	42.90
6	11	91	3.04	45.26	45.26

Table 5.1: Different translocation times of N_1 and N_2 with different branch ratios.

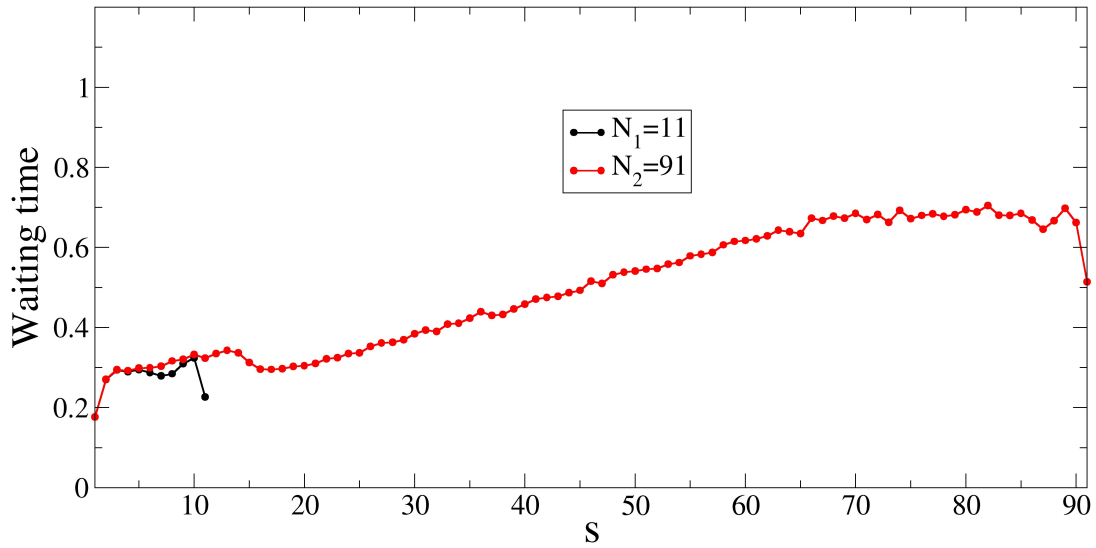
In Figure 5.3, we plot the waiting time distribution for all the folded chains. During the TP stage, the tension propagates along the monomers on both the segments. As time progresses, more and more monomers are in the TP regime, and the waiting time increases. After a certain time, the tension has propagated to till the last bead of the smaller segment N_1 , after which it is quickly pulled through the pore and its waiting time decreases. During the post propagation regime of the shorter chain, the tension continues to propagate along the longer chain segment, and the waiting time increases. Once the shorter segment leaves the pore, there is a small dip in the waiting time due to a transient decrease in the pore friction as now only one monomer bead is occupying the pore. The waiting time is at a maximum when the tension reaches the end of the longer segment, after which it reaches a plateau during the PP regime, which indicates that all the monomers of the chain N_2 are moving with the same velocity.



(a)



(b)



(c)

Figure 5.3: Waiting time distributions of the monomers. (a) 51:51, (b) 31:71 and (c) 11:91

The waiting time distribution and translocation time suggest that the translocation of the shorter segment occurs first followed by that of the longer chain. The tension propagation on the shorter segment finishes first while in, the longer chain, the tension continues to increase for some time. The whole process of folded translocation is represented in Figure 5.4.

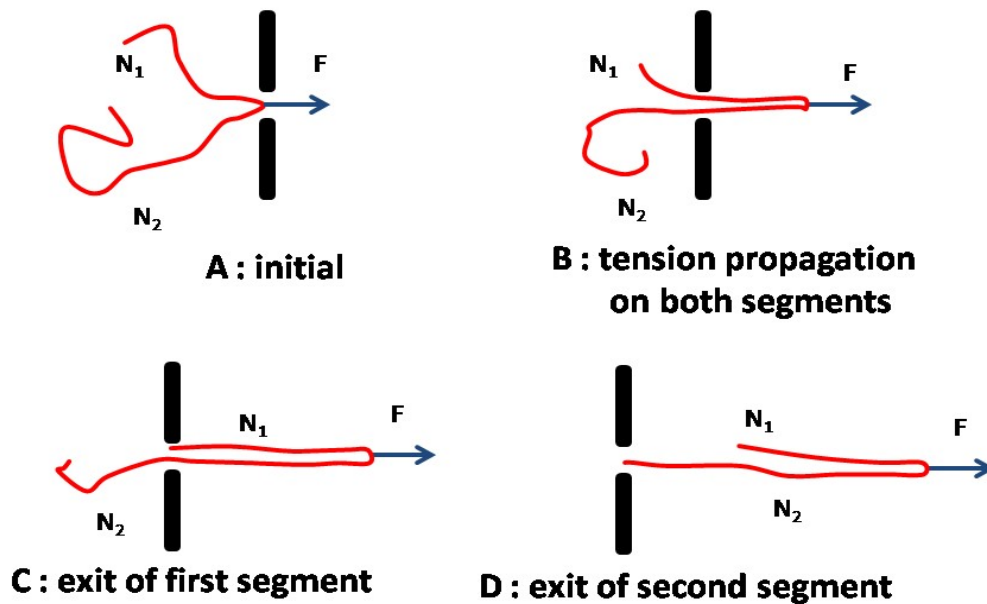
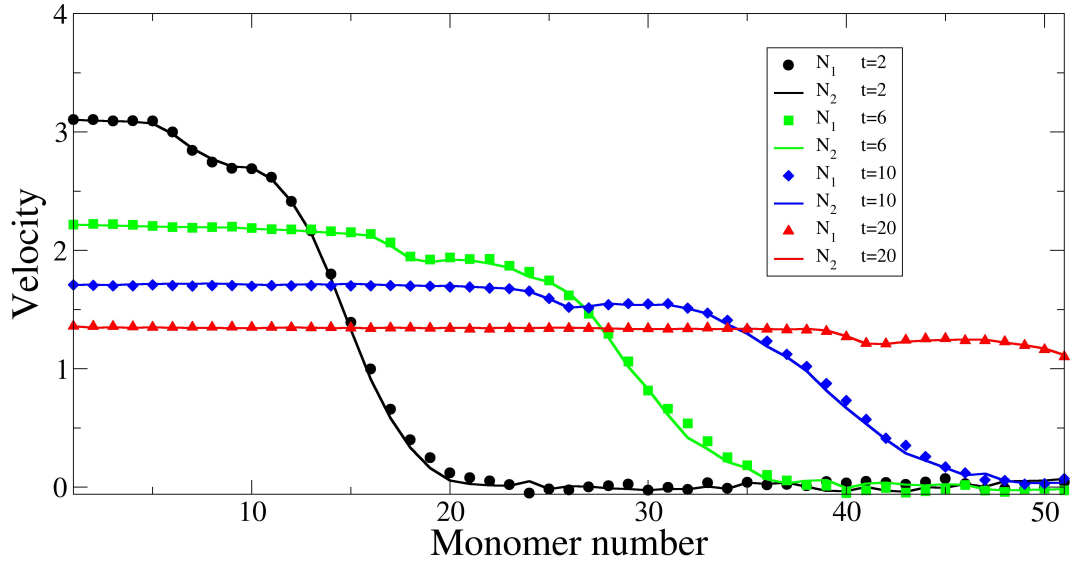


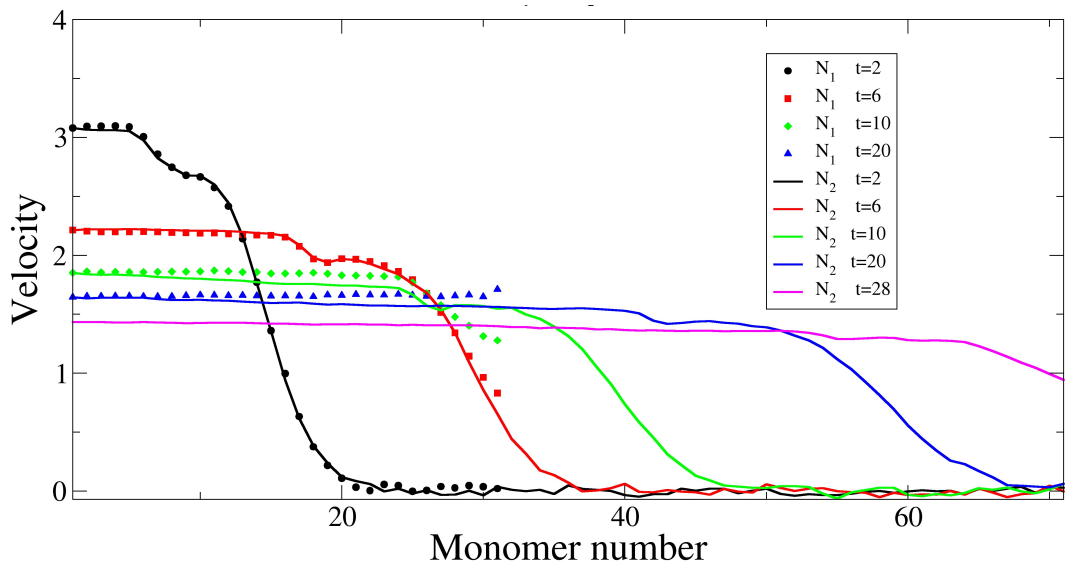
Figure 5.4: The stages of the translocation.

(b) Monomer velocity:

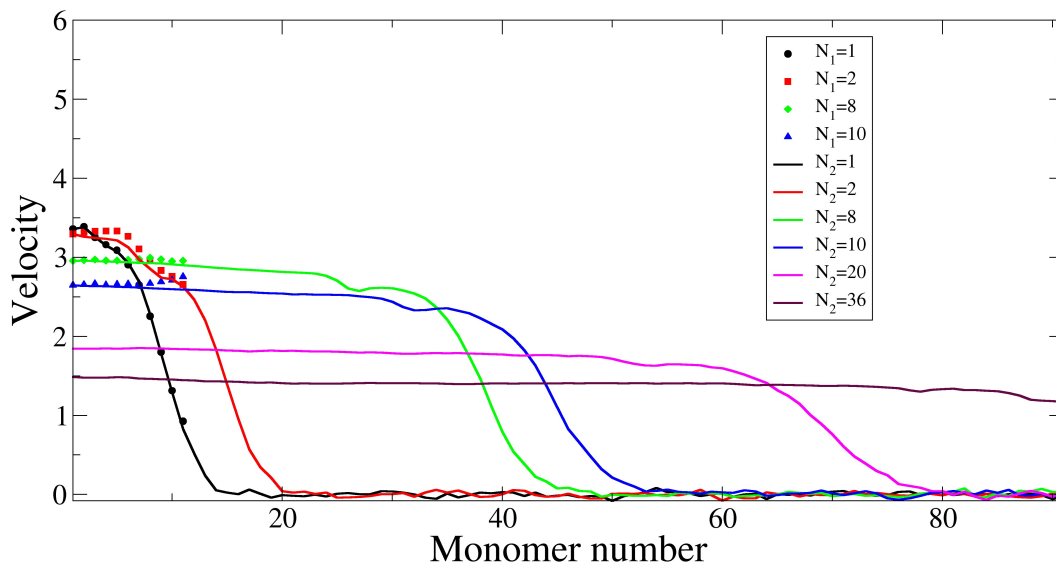
The monomer velocities (averaged over 300-500 successful translocation runs) were calculated in the strong force limit from Langevin dynamics simulation to study the dynamics at different stages of the translocation. The individual monomer velocities perpendicular to the wall (velocity in the direction of the applied driving force, here x-axis) of the two folded segments are plotted against the monomer number in Figure 5.5.



(a)



(b)



(c)

Figure 5.5: The monomer velocities. (a) 51:51, (b) 31:71 and (c) 11:91

At each time, the velocities of the monomers that have moved to the *trans* side of the pore have a constant value since the chain is on the strong stretching regime on the *trans* side due to the strong pulling force. After this, there is a drop in velocity during the TP stage for both the chain segments and for the non-moving part of the chain; the velocity is zero. With the progress of time, the TP of the shorter chain N_1 ends early, and the monomers of the shorter chain start moving with a constant non-zero velocity. During this time, tension is still propagating through the longer segment. This is evident from the fact that the drop in velocity continues along the longer chain and at long times, its velocity finally becomes equal to that of the *trans* side sub chain. For the symmetrical 50:50 folded chain, the monomer velocity is the same, and the tension propagation occurs in an identical manner for both the folded segments.

5.4 Conclusion

We have studied the translocation dynamics of a folded polymer chain using extensive Langevin dynamics simulations by applying a pulling force on some intermediate monomer bead. We calculate the waiting time per monomer defined as the time that an individual monomer spends inside the pore. This is done for both the folded segments of the chain. The time evolution of the tension front gives the contribution of the *cis* side subchain to the effective friction as described in Eq. 4.1. As the folded chain translocate, the tension propagates along both the folds, the effective friction increases, and the translocation slows down. For the shorter fold, during the PP stage, the tail retracts, and a translocation speed up a bit but the tension propagation continues along the longer segment until it reaches the last monomer bead. As a potential application of our simulation, from the theoretical point of view, one can calculate the pore friction, and take that into account into the IFTP theory while making a quantitative comparison of the waiting time distribution obtained our MD simulations.

5.5 References

1. Ghosh, B.; Chaudhury, S., Influence of the Location of Attractive Polymer–Pore Interactions on Translocation Dynamics. *J. Phys. Chem. B* **2018**, 122, 360-368.
2. Ghosh, B.; Chaudhury, S., Translocation Dynamics of an Asymmetrically Charged Polymer through a Pore under the Influence of Different Ph Conditions. *J. Phys. Chem. B* **2019**, 123, 4318-4323.
3. Kasianowicz, J. J.; Brandin, E.; Branton, D.; Deamer, D. W., Characterization of Individual Polynucleotide Molecules Using a Membrane Channel. *Proc.Nat. Acad. Sci.* **1996**, 93, 13770.
4. Akeson, M.; Branton, D.; Kasianowicz, J. J.; Brandin, E.; Deamer, D. W., Microsecond Time-Scale Discrimination among Polycytidylic Acid, Polyadenylic Acid, and Polyuridylic Acid as Homopolymers or as Segments within Single Rna Molecules. *Biophys. J.* **1999**, 77, 3227-3233.
5. Mathé, J.; Aksimentiev, A.; Nelson, D. R.; Schulten, K.; Meller, A., Orientation Discrimination of Single-Stranded DNA inside the A-Hemolysin Membrane Channel. *Proc.Nat. Acad. Sci* **2005**, 102, 12377.
6. Dekker, C., Solid-State Nanopores. *Nature Nanotech.* **2007**, 2, 209.

7. Storm, A. J.; Chen, J. H.; Ling, X. S.; Zandbergen, H. W.; Dekker, C., Fabrication of Solid-State Nanopores with Single-Nanometre Precision. *Nature Mat.* **2003**, *2*, 537-540.
8. Keyser, U. F.; van der Does, J.; Dekker, C.; Dekker, N. H., Optical Tweezers for Force Measurements on DNA in Nanopores. *Rev. Sci. Instru.* **2006**, *77*, 105105.
9. Heng, J. B.; Aksimentiev, A.; Ho, C.; Marks, P.; Grinkova, Y. V.; Sligar, S.; Schulten, K.; Timp, G., Stretching DNA Using the Electric Field in a Synthetic Nanopore. *Nano Lett.* **2005**, *5*, 1883-1888.
10. Nakane, J.; Akeson, M.; Marziali, A., Evaluation of Nanopores as Candidates for Electronic Analyte Detection. *Electrophoresis* **2002**, *23*, 2592-2601.
11. Kasianowicz, J. J.; Henrickson, S. E.; Weetall, H. H.; Robertson, B., Simultaneous Multianalyte Detection with a Nanometer-Scale Pore. *Anal. Chem.* **2001**, *73*, 2268-2272.
12. Bayley, H.; Cremer, P. S., Stochastic Sensors Inspired by Biology. *Nature* **2001**, *413*, 226-230.
13. Bayley, H.; Martin, C. R., Resistive-Pulse Sensing from Microbes to Molecules. *Chem.Rev.* **2000**, *100*, 2575-2594.
14. Storm, A. J.; Storm, C.; Chen, J.; Zandbergen, H.; Joanny, J.-F.; Dekker, C., Fast DNA Translocation through a Solid-State Nanopore. *Nano Lett.* **2005**, *5*, 1193-1197.
15. Storm, A. J.; Chen, J. H.; Zandbergen, H. W.; Dekker, C., Translocation of Double-Strand DNA through a Silicon Oxide Nanopore. *Phys. Rev. E* **2005**, *71*, 051903.
16. Forrey, C.; Muthukumar, M., Langevin Dynamics Simulations of Ds-DNA Translocation through Synthetic Nanopores. *J. Chem. Phys.* **2007**, *127*, 015102.
17. Kotsev, S.; Kolomeisky, A. B., Translocation of Polymers with Folded Configurations across Nanopores. *J. Chem. Phys.* **2007**, *127*, 185103.
18. Sarabadani, J.; Ghosh, B.; Chaudhury, S.; Ala-Nissila, T., Dynamics of End-Pulled Polymer Translocation through a Nanopore. *EPL* **2017**, *120*.

6. Fluctuation theorems for total entropy production in non-Markovian heat bath

(Rights and Permission)

Reprinted (adapted) with permission from (Physica A: 2017,466, 133-139) **Copyright © 2016**

Elsevier B.V. All rights reserved.

6.1 Introduction

With the recent advent of single molecule experimental techniques, like atomic force microscopy, optical and magnetic tweezers,¹⁻² experimentalists are able to follow biomolecules at the individual level. Such individual characterization is essential in protein folding-unfolding, enzymatic activity, polymer translocation, etc. This kind of individual-level experiments revealed many details of the cellular processes. The single molecules inside the cell matrix are impacted with the random, inhomogeneous environment due to the change in ionic concentration, pH change, and their fluctuations. The motion of these individual molecules is thus important to study when fluctuations are present in the system. Such studies are in the realm of non-equilibrium statistical thermodynamics where many basic questions are still unanswered. The study of the motion of single molecules under fluctuations are important to verify the single-molecule experimental results and non-equilibrium thermodynamics principles.³⁻⁶ Here, in this chapter of the thesis, we present a study on the motion a model particle under thermal fluctuations where fluctuation theorems are invoked.

In the field of statistical mechanics, fluctuation theorems have been a topic of interest for systems driven away from thermal equilibrium by the action of an external time-dependent perturbation.⁷⁻⁹ These theorems have been studied both theoretically and experimentally.¹⁰⁻¹¹ A consequence of the fluctuation theorem is the Jarzynski's equality,¹²⁻¹³ which has been tested in many experiments such as mechanically unfolding a single RNA molecule reversibly and irreversibly between two conformations.¹⁰⁻¹¹ The fluctuation theorem (FT) states that if a system is in a state of thermal equilibrium and if it is driven away from equilibrium by an external force, then some physical quantity X such as heat or work or entropy production associated with it^{8, 14} follows the following relation

$$\frac{P(+X)}{P(-X)} = e^X \quad \dots[\text{Eq. 6.1}]$$

where $P(X)$ refers to the probability densities, the + and - signs refer to the original and the time-reversed process.¹⁵ The probability distributions of the dissipated energy in the study of the non-equilibrium thermodynamics of a metallic single-electron box¹⁶⁻¹⁷ were found to obey the Jarzynski theorem¹² and the Crooks fluctuation theorem.¹⁵ Fluctuation theorems can be of two

types, steady state,¹⁸ and transient.¹⁹ The above equation is most commonly referred to as the detailed fluctuation theorem (DFT). Based on the principles of stochastic thermodynamics for diffusive motion, a proof of this relation was given by Kurchan²⁰ and Spohn *et al.*²¹ In all these cases, entropy production is only associated with the entropy change in the medium, and the above relationship holds asymptotically only in the long-time limit. If one includes the entropy change of the system, then the total entropy production has two contributions. Firstly, the heat dissipated can be associated with the change of entropy in the medium along a single trajectory, and secondly, there is trajectory dependent entropy of the system. The total entropy production is thus a sum of these two quantities. Seifert has shown that the total entropy production along a single trajectory for a system driven out of equilibrium by some time-dependent force follows the integral fluctuation theorem (IFT), $\langle e^{-\Delta s_{tot}} \rangle = 1$.²²⁻²³ The dynamics of such a system has been modeled by the over damped motion of a single colloidal particle governed by the Langevin equation. The fluctuations in the total entropy production have been studied for various systems that are initially in a state of thermal equilibrium with the heat bath.²⁴ It has been shown that the detailed fluctuation theorem holds well when the Brownian particle in a harmonic trap is subjected to an external time dependent force or for a particle in a dragged harmonic oscillator.²⁵ For all these cases, the dynamics of the particle is governed by the ordinary Langevin equation with an additive Gaussian white noise. The distribution of the entropy production has been measured experimentally for a number of systems, such as for a colloidal particle driven by a constant force along a periodic potential.²⁶ It has been verified that if the distribution of the total entropy production, (Δs_{tot}) is Gaussian then the IFT holds good.

In this chapter, we test the validity of the fluctuation theorems for the total entropy production in a system embedded in a non-Markovian heat bath. The validity of the non-equilibrium work fluctuation theorems for oscillators in non-Markovian heat baths has been tested earlier Mai and Dhar by calculating the work distribution functions.²⁷ Very recently Aquino has shown that the transient work fluctuation theorem is valid for a charged Brownian harmonic oscillator embedded in a non-Markovian heat bath and under the action of crossed electric and magnetic fields.²⁸ Also, using the concepts of stochastic thermodynamics, the Jarzynski relation was proved for non-Markovian systems with memory.²⁹ Fluctuation theorems for non-equilibrium quantum processes have been studied using an open system approach. It has been suggested that memory effects lead to the correlation between the single trajectories of

entropy production and result in a correction of the well-known fluctuation theorem for entropy production.³⁰ All such Markovian and non-Markovian contributions are taken into account for deriving the fluctuation theorems for entropy production. In this study, to capture the effects of the non-Markovian nature of the heat bath at a constant temperature, we model the dynamics of the system by the generalized equation motion (GLE) with an associated memory kernel.³¹ We find that in the presence of a non-Markovian heat bath, a renormalized temperature term is necessary to support the validity of the fluctuation theorem of total entropy production.

In Section 6.2, we present our theoretical model to study the dynamics of a single colloidal particle using the GLE with colored noise. We derive the Fokker-Planck(FP) equation and propose its solution. We use this solution to obtain the mean and variances of position and work and calculate the total entropy production. In Section 6.3, we obtain the probability distribution of total entropy production and test the validity of the fluctuation theorems. In Section 6.4, we conclude our results.

6.2 Model

The primary objective of the present study is to probe the validity of the non-equilibrium fluctuation relations for the distribution of the total entropy production along a single trajectory. In order to model non-equilibrium fluctuations in a non-Markovian heat bath, we consider a harmonic oscillator of mass m in thermal contact with a Gaussian colored-noise heat bath and acted upon by a time-dependent force $f(t)$.³² This system serves as a model for an optically trapped colloidal particle dragged through a viscoelastic medium, and its dynamics are defined by the generalized Langevin equation:³²

$$m\ddot{x}(t) = -kx(t) + f(t) - \zeta \int_0^t dt' K(t-t')\dot{x}(t') + \theta(t) \quad \dots[\text{Eq. 6.2}]$$

Here, $x(t)$ is the position of the oscillator at time t , k is the force constant of the harmonic well, ζ is the friction coefficient of the particle, and $\theta(t)$ is a Gaussian random variable with $\langle \theta(t) \rangle = 0$. The memory kernel $K(t)$ satisfies the fluctuation-dissipation relation and is given by

$$\langle \theta(t)\theta(t') \rangle = \zeta k_B T K(|t-t'|), \quad \dots[\text{Eq. 6.3}]$$

where T is the temperature of the reservoir and k_B is the Boltzmann's constant. If $\theta(t)$ were the white noise, and $f(t)$ a force pulling the oscillator at a constant speed u (such that $f(t)$ equal to

ku), Eq. 6.2 (with the inertial term neglected) would describe the model treated by Mazonka and Jarzynski.¹³ As discussed in Section 6.1, the total entropy production involves the entropy of the system as it evolves in response to the effects of the time-dependent force and also the entropy production in the surrounding medium. According to the stochastic thermodynamic approach, the change in the internal energy ΔU and the heat dissipated Q to the bath along a stochastic trajectory $x(t)$ are related by

$$Q = w - \Delta U \quad \dots[\text{Eq.6.4}]$$

where the change in internal energy $\Delta U = U(x, t) - U(x_0, 0)$. This is the first law of thermodynamics.

In this article, we restrict our attention to the thermodynamic work²⁷ defined as $w(t) = -\int_0^t x(t')\dot{f}(t')dt'$ for a given stochastic trajectory for time t . In general, using the method of Laplace transforms, we can solve Eq. 6.2 for $x(t)$ and is given by

$$x(t) = x_0\chi(t) + v_0 \int_0^t dt' \chi(t-t')\xi(t') + \frac{1}{m} \int_0^t dt' \chi(t-t')\lambda(t') + \frac{1}{m} \int_0^t dt' \chi(t-t')\gamma(t') \quad \dots[\text{Eq. 6.5}]$$

where

$\chi(t)$ is the inverse Laplace transform of the function $\hat{\chi}(s) = 1/(s + (k/m)/(s + \zeta\hat{K}(s)/m))$, $\xi(t)$ is the inverse Laplace transform of the function $\hat{\xi}(s) \equiv 1/(s + \zeta\hat{K}(s)/m)$, and the functions $\lambda(t)$ and $\gamma(t)$ are defined as

$$\lambda(t) = \int_0^t dt' \xi(t-t')f(t') \quad \dots[\text{Eq. 6.6}]$$

$$\gamma(t) = \int_0^t dt' \xi(t-t')\theta(t') \quad \dots[\text{Eq. 6.7}]$$

To obtain the Fokker-Planck equation for Eq. 6.2 we define the density distribution function as:

$$P(x, w, t) = \langle \delta(x - x(t))\delta(w - w(t)) \rangle \quad \dots[\text{Eq. 6.8}]$$

Then using the properties of a delta function and differentiating Eq. 6.8 we get

$$\frac{\partial}{\partial t} P(x, w, t) = -\frac{\partial}{\partial x} \langle \delta(x - x(t)) \delta(w - w(t)) \dot{x}(t) \rangle - \frac{\partial}{\partial w} \langle \delta(x - x(t)) \delta(w - w(t)) \dot{w}(t) \rangle$$

...[Eq. 6.9]

From the expression for the evolution of $w(t)$ we have $\dot{w}(t) = -\dot{f}(t)x(t)$ and the equation for $\dot{x}(t)$ is derived from Eq. 6.5. The result is

$$\dot{x}(t) = -\eta(t)x(t) + v_0\mu(t) + \phi(t) + \psi(t)$$

...[Eq. 6.10]

where $\eta(t) = -\frac{\dot{\chi}(t)}{\chi(t)}$

$$\mu(t) = \chi(t) \frac{d}{dt} \int_0^t \frac{\chi(t-t')\gamma(t')}{\chi(t)} dt'$$

$$\phi(t) = \frac{\chi(t)}{m} \frac{d}{dt} \int_0^t \frac{\chi(t-t')\lambda(t')}{\chi(t)} dt$$

$$\psi(t) = \frac{\chi(t)}{m} \frac{d}{dt} \int_0^t \frac{\chi(t-t')\gamma(t')}{\chi(t)} dt'$$

By substituting for $\dot{w}(t)$ and $\dot{x}(t)$ in Eq. 6.9 and using functional methods we obtain the Fokker-Planck(FP) equation associated with the GLE (Eq. 6.4).³¹

$$\begin{aligned} \frac{\partial}{\partial t} P(x, w, t) = & \eta(t) \frac{\partial}{\partial x} xP(x, w, t) - \frac{A(t)}{k} \frac{\partial}{\partial x} P(x, w, t) + \frac{k_B T}{k} \eta(t) \frac{\partial^2}{\partial x^2} P(x, w, t) \\ & + x\dot{f}(t) \frac{\partial}{\partial w} P(x, w, t) \end{aligned}$$

...[Eq. 6.11]

where the function $A(t)$ is defined as

$$A(t) \equiv \frac{k}{m} \chi(t) \frac{d}{dt} \int_0^t dt' \frac{\chi(t-t')\lambda(t')}{\chi(t)}$$

...[Eq. 6.12]

The mean, variances, and cross-correlations of the position and work are obtained from the

following relations:

$$\bar{x}(t) = \int dx \int dw x P(x, w, t) \quad \dots[\text{Eq. 6.13a}]$$

$$\bar{w}(t) = \int dx \int dw w P(x, w, t) \quad \dots[\text{Eq. 6.13b}]$$

$$\sigma_x^2(t) = \int dx \int dw P(x, w, t)(x^2 - \bar{x}^2) \quad \dots[\text{Eq. 6.13c}]$$

$$\sigma_{xw}(t) = \int dx \int dw P(x, w, t)(xw - \bar{x}\bar{w}) \quad \dots[\text{Eq. 6.13d}]$$

$$\sigma_w^2(t) = \int dx \int dw P(x, w, t)(w^2 - \bar{w}^2) \quad \dots[\text{Eq. 6.13e}]$$

These equations can be expressed as ordinary differential equations. Imposing certain initial conditions $\bar{x}(0) = \bar{x}_0$, $\sigma_{x_0}^2 = k_B T/k$ and $\bar{w}(0) = \sigma_w^2(0) = 0$, $\sigma_{xw}^2(0) = 0$, the differential equations can be solved for the moments and is given by

$$\bar{x}(t) = \bar{x}_0 \chi(t) - \frac{1}{k} \int_0^t G(t-t') f(t') dt' \dots[\text{Eq. 6.14a}]$$

$$\sigma_x^2(t) = \frac{k_B T}{k} (1 - \chi^2(t)) \quad \dots[\text{Eq. 6.14b}]$$

$$\bar{w}(t) = \frac{1}{k} \int_0^t dt' \int_0^{t'} dt'' \dot{f}(t') G(t' - t'') f(t'') - \bar{x}_0 \int_0^t dt' \chi(t') \dot{f}(t') \quad \dots[\text{Eq. 6.14c}]$$

$$\sigma_{xw}(t) = - \int_0^t dt' \dot{f}(t') \frac{\chi(t)}{\chi(t')} \sigma_x^2(t') \quad \dots[\text{Eq. 6.14d}]$$

$$\sigma_w^2(t) = -2 \int_0^t dt' \dot{f}(t') \sigma_{xw}(t') \quad \dots[\text{Eq. 6.14e}]$$

where $G(t) \equiv \dot{\chi}(t)$.

The solution of Eq. 6.11 gives the joint probability distribution $P(x, w, t|x_0)$ of arriving at position x and performing work w at time t such that $x=x_0$ at $t=0$ and $w(t=0)=0$ and satisfies the initial condition $P(x, w, t|x_0) = \delta(x - x_0)\delta(w)$. This expression in terms of the moments of position and work is given by³⁵

$$P(x, w, t|x_0) = \sqrt{\frac{c}{2\pi}} \exp \left\{ -\frac{1}{2} \left[D_{11}(x - \bar{x}(t))^2 + 2D_{12}(x - \bar{x}(t))(w - \bar{w}(t)) + D_{22}(w - \bar{w}(t))^2 \right] \right\} \quad \dots[\text{Eq. 6.15}]$$

where the constants D_{ij} are the elements of the matrix

$$D = \begin{pmatrix} C\sigma_w^2(t) & -C\sigma_{xw}(t) \\ -C\sigma_{xw}(t) & C\sigma_x^2(t) \end{pmatrix} \quad \dots[\text{Eq. 6.16}]$$

with $C = \det D = [\sigma_x^2(t)\sigma_w^2(t) - \sigma_{xw}^2(t)]^{-1}$.

6.3 Entropy Production Theorem

The non-equilibrium Gibbs entropy S of the system is defined as²⁵

$$S(t) = - \int dx P(x, t) \ln P(x, t) = \langle s(t) \rangle \quad \dots[\text{Eq. 6.17}]$$

This will give as a definition of the trajectory dependent entropy of the system

$$s(t) = -\ln[P(x, t), t] \quad \dots[\text{Eq. 6.18}]$$

where probability density $P(x, t)$ can be obtained from Eq. 6.15

$$P(x, t) = \int P(x_0, 0)P(x, t|x_0)dx_0 \quad \dots[\text{Eq. 6.19}]$$

The marginal probability distribution $P(x, t|x_0)$ can be obtained by integrating Eq. 6.15 over w such that

$$P(x, t|x_0) = \int P(x, w, t|x_0)dw = \sqrt{\frac{1}{2\pi\sigma_x^2}} \exp\left[-\frac{(x-\bar{x})^2}{2\sigma_x^2}\right] \quad \dots[\text{Eq. 6.20}]$$

where \bar{x} and σ_x^2 are given in Eq. 6.15. The initial distribution of the particle positions $P(x_0, 0)$ at equilibrium is a Gaussian and is given by

$$\lim_{t \rightarrow \infty} P(x_0, 0) = \sqrt{\frac{k}{2\pi k_B T}} \exp\left[-\frac{k(x_0 - \bar{x}_0)^2}{2k_B T}\right] \quad \dots[\text{Eq. 6.21}]$$

where $\sigma_x^2(t \rightarrow \infty) = \frac{k_B T}{k}$ and $\bar{x}(t = 0) = \bar{x}_0$

Using Eq. 6.20 and 6.21 in Eq. 6.20, we have

$$P(x, t) = \sqrt{\frac{k}{2\pi k_B T}} \exp\left[-\frac{k(x-\bar{x})^2}{2k_B T}\right] \quad \dots[\text{Eq. 6.22}]$$

The change in the entropy of the system for a trajectory during time t is given by

$$\Delta S_{sys} = -\ln\left[\frac{P(x,t)}{P(x_0,0)}\right] \quad \dots[\text{Eq. 6.23}]$$

Using Eqs. 6.21 and 6.22 in Eq. 6.23 we have

$$\Delta S_{sys} = \frac{k((x-\bar{x})^2 - (x_0 - \bar{x}_0)^2)}{2k_B T} \quad \dots[\text{Eq. 6.24}]$$

The change in entropy of the surrounding medium over some time interval is

$$\Delta S_{surr} = \frac{1}{T}(w - \Delta U) = \frac{1}{T}\left(w - \frac{1}{2}kx^2 + \frac{1}{2}kx_0^2 + f(t)x\right) \quad \dots[\text{Eq. 6.25}]$$

Assuming that the Boltzmann constant k_B is absorbed in the temperature T , from Eq. 6.24 and 6.25, the total entropy change over a time duration t is given by

$$\Delta S_{tot} = \frac{1}{T}\left(w + \frac{1}{2}k\bar{x}^2 - \frac{1}{2}k\bar{x}_0^2 + f(t)x - kx\bar{x} + kx_0\bar{x}_0\right) \quad \dots[\text{Eq. 6.26}]$$

The mean value of ΔS_{tot} is given by

$$\overline{\Delta S_{tot}} = \frac{1}{T}\left(\bar{w} - \frac{1}{2}k\bar{x}^2 + \frac{1}{2}k\bar{x}_0^2 + f(t)\bar{x}\right) \quad \dots[\text{Eq. 6.27}]$$

where \bar{x} and \bar{w} are defined in Eq. 6.14a and 6.14c.

If we assume that there is no force at $t=0$, then $\bar{x}_0 = f(0)/k = 0$, and the expression for the average total entropy production reduces to $\overline{\Delta S_{tot}} = \frac{1}{T}\left(\bar{w} - \frac{1}{2}k\bar{x}^2 + f(t)\bar{x}\right)$. This is identical to the expression obtained by Saha *et al.*²⁵ in the Markovian limit. The variance in the change of total entropy is given by

$$\sigma_{\Delta S_{tot}}^2 = \overline{\Delta S_{tot}^2} - \overline{\Delta S_{tot}}^2 \quad \dots[\text{Eq. 6.28}]$$

Using Eq. 6.26 and Eq. 6.27 and assuming $\bar{x}_0 = 0$, the variance of the total entropy production can be expressed as

$$\sigma_{\Delta S_{tot}}^2 = \frac{\sigma_w^2}{T^2} + \frac{f^2}{kT} + \frac{2\sigma_{xw}(f-k\bar{x})}{T^2} + \frac{k(\bar{x}^2-2f\bar{x})}{T} \quad \dots[\text{Eq. 6.29}]$$

which is not equal to $2\overline{\Delta S_{tot}}$ as obtained in the Markovian case.²⁵

For stochastic processes in Markovian systems in the white noise limit and also for non-Markovian systems with memory²⁷ the following relations for work fluctuations are obeyed.

$$\sigma_w^2 = 2T \left(\bar{w} + \frac{f^2(t)}{2k} \right) \quad \dots[\text{Eq. 6.30a}]$$

and

$$\sigma_{xw} = \frac{T}{k} (k\bar{x} - f(t)) \quad \dots[\text{Eq. 6.30b}]$$

Substituting the above two relations in Eq. 6.28 we have

$$\sigma_{\Delta S_{tot}}^2 = \frac{2}{T} \left(\bar{w} - \frac{1}{2}k\bar{x}^2 + f(t)\bar{x} \right) \quad \dots[\text{Eq. 6.31}]$$

which is equal to $2\overline{\Delta S_{tot}}$.

Thus, it reduces to the relation as obtained in the white noise limit.

6.4 Total Entropy Distribution Function

It has been shown earlier that the transient fluctuation theorem(TFT) for the probability distribution for the mechanical work holds good for both stochastic Markovian^{9, 13, 15} and non-Markovian systems.²⁷ In this section, we would like to investigate the TFT for the probability distribution of the total entropy production. Following the approach provided by Mazonka and Jarzynski,¹³ the probability of the distribution of the total entropy production is given by

$$P(X) = \int d w \delta(X - \Delta S_{tot}) \int \rho(x_0) \rho(w, t|x_0) dx_0 \quad \dots[\text{Eq. 6.32}]$$

where X is the total entropy change ΔS_{tot} in a finite time segment and $P(X)$ is the distribution of the values of X over many such segments for a finite time interval.

The initial distribution of the particle's position is a canonical distribution,

$$\rho(x_0) = \sqrt{\frac{k}{2\pi}} \exp[-kx_0^2/2T] \quad \dots[\text{Eq. 6.33}]$$

and

$$\rho(w, t|x_0) = \int dx P(x, w, t|x_0) = \frac{1}{\sqrt{2\pi\sigma_w^2}} \exp[-(w - \bar{w})^2/2\sigma_w^2] \quad \dots[\text{Eq. 6.34}]$$

Substituting Eq. 6.33, and Eq. 6.34 in Eq. 6.32

$$P(X) = \int d w \delta(X - \Delta s_{tot}) \frac{1}{\sqrt{2\pi\sigma_w^2}} \exp\left[-\frac{(w - \bar{w})^2}{2\sigma_w^2}\right] \quad \dots[\text{Eq. 6.35}]$$

If $\bar{x}_0 = 0$, then according to Eq. 6.24, $\overline{\Delta s_{sys}} = 0$. Hence $\overline{\Delta s_{tot}} = \overline{\Delta s_{surr}}$.

From Eq. 6.25, w is given by

$$w = \frac{\Delta s_{surr}}{\beta} + \frac{k}{2}(x^2 - x_0^2 - 2f(t)x) \quad \dots[\text{Eq. 6.36a}]$$

$$\text{and} \quad \bar{w} = \frac{\overline{\Delta s_{surr}}}{\beta} - \frac{k\bar{x}^2}{2} \quad \dots[\text{Eq. 6.36b}]$$

where $f(t) = k\bar{x}(t)$.

Substituting these relations in Eq. 6.34 and using $\overline{\Delta s_{tot}} = \overline{\Delta s_{surr}}$ the probability distribution of the total entropy production can be written as

$$P(X) = \frac{1}{\sqrt{2\pi\beta^2\sigma_w^2}} \int d \left(\Delta s_{surr} + \frac{\beta k}{2}(x^2 - x_0^2 - 2f(t)x) \right) \delta \left(X - \left(\Delta s_{surr} + \frac{\beta k}{2}(x^2 - x_0^2 - 2f(t)x + \bar{x}^2) \right) \right) \exp \left[-\frac{\left(\left(\Delta s_{surr} + \frac{\beta k}{2}(x^2 - x_0^2 - 2f(t)x + \bar{x}^2) \right) - \overline{\Delta s_{tot}} \right)^2}{2\beta^2\sigma_w^2} \right] \quad \dots[\text{Eq. 6.37}]$$

Using the properties of the delta function, $\int \delta(x - (a + z)) f(a + z) da = f(x)$, the probability distribution reduces to

$$P(\Delta s_{tot}) = \frac{1}{\sqrt{2\pi\beta^2\sigma_w^2}} \exp \left[-\frac{(\Delta s_{tot} - \overline{\Delta s_{tot}})^2}{2\beta^2\sigma_w^2} \right] \quad \dots[\text{Eq. 6.38}]$$

and

$$\frac{P(\Delta S_{tot})}{P(-\Delta S_{tot})} = e^{\Omega \Delta S_{tot}} \quad \dots[\text{Eq. 6.39}]$$

where $\Omega = \frac{2\overline{\Delta S_{tot}}}{\beta^2 \sigma_w^2}$

Thus, the transient fluctuation theorem for total entropy production has a coefficient Ω which contains a renormalized temperature term. This is the consequence of the non-Markovian characteristics of the heat bath that leads to the deviation in the DFT as described in Eq. 6.1.

For Markovian systems, $\sigma_w^2 = 2T \left(\overline{w} + \frac{f^2(t)}{2k} \right) = \frac{2}{\beta^2} \overline{\Delta S_{surr}}$

Using this relation, Ω reduces to unity in the white noise limit.

6.5 Conclusions

In this work, the motion of a colloidal particle subjected to an external time-dependent dragging force is modeled by the GLE with a memory kernel that accounts for the non-Markovian nature of the heat bath. In the limit of white noise, the mean value of the total entropy production and the variance in the change of total entropy agrees with earlier results for a Markovian system. The probability of total entropy production $P_{\Delta S_{tot}}$ satisfies the TFT with a renormalized temperature term. Experimental measurement of the entropy production distribution for a single colloidal particle in a toroidal geometry has reported the validity of the fluctuation theorems for short trajectories.²⁶ The probability distributions of entropy production were calculated in the presence of a velocity-dependent active force using MD simulations and it was found that these distribution functions obey the corresponding fluctuation theorems.²⁴ In all such studies, the validity of the entropy production FT was tested only in the Markovian limit. Recently Aquino and Velasco³² have studied the total entropy production of a Brownian particle embedded in a non-Markovian heat bath under two physically relevant conditions. It was showed that non-Markovian characteristics of the heat bath lead to non-Gaussian distribution of the production of total entropy and the fluctuation theorems are valid only in the white noise limit. Our analytical results show that the FT for systems with memory contains a renormalized temperature term. If

one considers that the work relations holds good which is true even for the non- Markovian case,²⁷ this term reduces to unity and the well-known TFT is satisfied. Such renormalization term has been found to be useful in verifying fluctuation theorems experimentally in mesoscopic electric circuits.³²

6.6 References

1. Bustamante, C.; Liphardt, J.; Ritort, F., The Nonequilibrium Thermodynamics of Small Systems. *Phys. Today* **2005**, 58, 43-48.
2. Ritort, F., Single-Molecule Experiments in Biological Physics: Methods and Applications. *J. Phys.: Condens. Matt.* **2006**, 18, R531-R583.
3. Ritort, F., The Nonequilibrium Thermodynamics of Small Systems. *Comp.s Rend.Phys.* **2007**, 8, 528-539.
4. Santamaría-Holek, I.; López-Alamilla, N. J.; Hidalgo-Soria, M.; Pérez-Madrid, A., Nonlinear Irreversible Thermodynamics of Single-Molecule Experiments. *Phys. Review E* **2015**, 91, 062714.
5. Bustamante, C., Unfolding Single Rna Molecules: Bridging the Gap between Equilibrium and Non-Equilibrium Statistical Thermodynamics. *Quart. Rev. Biophys.* **2006**, 38, 291-301.
6. Rubi, J. M.; Bedeaux, D.; Kjelstrup, S., Thermodynamics for Single-Molecule Stretching Experiments. *J. Phys. Chem. B* **2006**, 110, 12733-12737.
7. Evans, D. J.; Cohen, G. D.; Morriss, G. P., *Phys. Rev. Lett.* **1993**, 71, 2401.
8. Crooks, G. E., *Phys. Rev. E* **1999**, 60, 2721.
9. Narayan, O.; Dhar, A., *J. Phys. A* **2004**, 37, 63.
10. Ritort, F., Single-Molecule Experiments in Biological Physics: Methods and Applications. *J. Phys.: Condens. Matt.* **2006**, 18, R531.
11. Bustamante, C.; Liphardt, J.; Ritort, F., The Nonequilibrium Thermodynamics of Small Systems. *Phys. Today* **2005**, 58, 43.
12. Jarzynski, C., *Phys. Rev. Lett.* **1997**, 78, 2690.
13. Jarzynski, C., *Phys. Rev. E* **1997**, 56, 5018.
14. Ganguly, C.; Chaudhuri, D., *Phys. Rev. E* **2013**, 88, 032102.
15. Crooks, G. E., Entropy Production Fluctuation Theorem and the Nonequilibrium Work Relation for Free Energy Differences. *Phys. Rev. E* **1999**, 60, 2721.
16. Saira, O. P.; Yoon, Y.; Tanttu, T.; Möttönen, M.; Averin, D. V.; Pekola, J. P., Test of the Jarzynski and Crooks Fluctuation Relations in an Electronic System. *Phys. Rev. Lett.* **2012**, 109, 180601.
17. Koskia, J. V.; Maisia, V. F.; Pekolaa, J. P.; Averind, D. V., Experimental Realization of a Szilard Engine with a Single Electron. *Proc Natl Acad Sci U S A* **2014**, 111, 13786.
18. Gallavotti, G.; Cohen, E. G. D., Dynamical Ensembles in Stationary States. *J. Stat. Phys.* **1995**, 80, 931-970.
19. Evans, D. J.; Searles, D. J., Equilibrium Microstates Which Generate Second Law Violating Steady States. *Phys. Rev. E* **1994**, 50, 1645-1648.
20. Kurchan, J., Non-Equilibrium Work Relations. *J. Stat. Mech. : Theor.Exp.* **2007**, P07005.
21. Lebowitz, J. L.; Spohn, H., A Gallavotti–Cohen-Type Symmetry in the Large Deviation Functional for Stochastic Dynamics. *J. Stat. Phys.* **1999**, 95, 333-365.

22. Seifert, U., Entropy Production Along a Stochastic Trajectory and an Integral Fluctuation Theorem. *Phys. Rev. Lett.* **2005**, 95, 040602.
23. Seifert, U., Stochastic Thermodynamics: Principles and Perspectives. *Eur. Phys. J. B* **2008**, 64, 423-431.
24. Chaudhuri, D., *Phys. Rev. E* **2014**, 90, 022131.
25. Saha, A.; Lahiri, S.; Jayannavar, A. M., Entropy Production Theorems and Some Consequences. *Phys. Rev. E* **2009**, 80, 011117.
26. Speck, T.; Blickle, V.; Bechinger, C.; Seifert, U., Distribution of Entropy Production for a Colloidal Particle in a Nonequilibrium Steady State. *EPL*. **2007**, 79, 30002.
27. Mai, T.; Dhar, A., *Phys. Rev. E* **2007**, 75, 061101.
28. Jimenez -Aquino, J. I., *Phys. Rev. E* **2015**, 92, 022149.
29. Speck, T.; Seifert, U., *J. Stat. Phys.* **2007**, L09002.
30. Leggio, B.; Napoli, A.; Breuer, H.-P.; Messina, A., *Phys. Rev. E* **2013**, 87, 032113.
31. Chaudhury, S.; Chatterjee, D.; Cherayil, B. J., Resolving a Puzzle Concerning Fluctuation Theorems for Forced Harmonic Oscillators in Non-Markovian Heat Baths. *J. Stat. Mech.: Theor. Exp.* **2008**, 2008, P10006.
32. Ghosh, B., Chaudhury, S., Fluctuation theorems for total entropy production in generalized Langevin systems. *Physica A*. **2017**, 466, 133-139.

7. Conclusions

7.1 Conclusions and Future Outlook

The problem of polymer translocation has a multifaceted approach due to the involvement of multiple variables and a probable technological application. In this thesis, we have looked into cases like polymer-pore interactions and end-pulled translocations with simple bead-spring polymer and rigid wall model. Our study mainly focused on mimicking the single molecule experimental situations carried out by external driving forces through voltage differences and optical or magnetic tweezers. The Langevin dynamics simulations revealed the importance of different stages of translocation when the pore and the polymer charge distributions are changed through translocation time calculations and free energy calculations. The pulled translocation showed the quantitative waiting times of the monomer beads on the pore and the tension propagation along the backbone of an uncharged polymer.

The actual process of polymer translocation is complicated by the effects of ions in the solution and the crowding of the other entities in the *in vivo* conditions. The properties of the polymer chains are still quite different in cellular conditions than the one used in our molecular dynamics simulations. They are very sensitive to the minute changes in the environment too.

Broadly, the future theoretical and computational translocation studies will be interesting from three more areas. Firstly, the effect of force on the chain conformations when the polymer is out of its equilibrium configuration. People have so far considered the equilibrated chain and applied a high magnitude of force to drive the translocation. In reality, the polymer chain in experiments and *in vivo* conditions floats around which is impacted by many local effects like shear flow, local ion concentration, electrostatic interaction, etc. Due to such effects, the polymer may remain in an unequilibrated configuration. The dynamics of the polymer translocation remains unanswered when the translocation time of the chain is much faster compared to the chain relaxation time from such an unequilibrated state. In that case, conformational fluctuation rates towards equilibration of the chain will impact the translocation times and the overall translocation dynamics.

The second compelling case would be to study this process in detail, considering a fully atomistic model for various kinds of pore proteins and bio-polymers where more chemical details are included. This will consist of the study of hetero-polymers. The real application of the

translocation study lies in the study heteropolymers as most of the polymers in nature constitutes with different kinds of monomer beads.

The third area is when there are configurational differences in the polymer chain. So far, the translocation problem has been looked into mostly with single file motion of linear chains. But the translocation experiments are envisaged as a useful technique for detection purposes. The various kinds of configurations of the polymers like star polymers, ring polymers, polymers with knots are rarely studied for translocation purposes. In experiments, the detection of such polymers can be done via translocation studies with different current signals.

Overall, the polymer translocation still has few open ends, which are of importance to the theorist and experimentalist due to its potential future application.

Rights and Permissions

5/30/2019

RightsLink® by Copyright Clearance Center



RightsLink®

[Home](#)[Account Info](#)[Help](#)

ACS Publications
Most Trusted. Most Cited. Most Read.

Title: Influence of the Location of Attractive Polymer–Pore Interactions on Translocation Dynamics

Author: Bappa Ghosh, Srabanti Chaudhury

Publication: The Journal of Physical Chemistry B

Publisher: American Chemical Society

Date: Jan 1, 2018

Copyright © 2018, American Chemical Society

Logged in as:

Bappa Ghosh
IISER Pune

[LOGOUT](#)

PERMISSION/LICENSE IS GRANTED FOR YOUR ORDER AT NO CHARGE

This type of permission/license, instead of the standard Terms & Conditions, is sent to you because no fee is being charged for your order. Please note the following:

- Permission is granted for your request in both print and electronic formats, and translations.
- If figures and/or tables were requested, they may be adapted or used in part.
- Please print this page for your records and send a copy of it to your publisher/graduate school.
- Appropriate credit for the requested material should be given as follows: "Reprinted (adapted) with permission from (COMPLETE REFERENCE CITATION). Copyright (YEAR) American Chemical Society." Insert appropriate information in place of the capitalized words.
- One-time permission is granted only for the use specified in your request. No additional uses are granted (such as derivative works or other editions). For any other uses, please submit a new request.

[BACK](#)[CLOSE WINDOW](#)

Copyright © 2019 [Copyright Clearance Center, Inc.](#) All Rights Reserved. [Privacy statement.](#) [Terms and Conditions.](#) Comments? We would like to hear from you. E-mail us at customer@copyright.com



RightsLink®

[Home](#)[Account Info](#)[Help](#)**Title:**

Translocation Dynamics of an Asymmetrically Charged Polymer through a Pore under the Influence of Different pH Conditions

Logged in as:

Bappa Ghosh
IISER Pune[LOGOUT](#)**Author:** Bappa Ghosh, Srabanti Chaudhury**Publication:** The Journal of Physical Chemistry B**Publisher:** American Chemical Society**Date:** May 1, 2019

Copyright © 2019, American Chemical Society

PERMISSION/LICENSE IS GRANTED FOR YOUR ORDER AT NO CHARGE

This type of permission/license, instead of the standard Terms & Conditions, is sent to you because no fee is being charged for your order. Please note the following:

- Permission is granted for your request in both print and electronic formats, and translations.
- If figures and/or tables were requested, they may be adapted or used in part.
- Please print this page for your records and send a copy of it to your publisher/graduate school.
- Appropriate credit for the requested material should be given as follows: "Reprinted (adapted) with permission from (COMPLETE REFERENCE CITATION). Copyright (YEAR) American Chemical Society." Insert appropriate information in place of the capitalized words.
- One-time permission is granted only for the use specified in your request. No additional uses are granted (such as derivative works or other editions). For any other uses, please submit a new request.

[BACK](#)[CLOSE WINDOW](#)

Copyright © 2019 [Copyright Clearance Center, Inc.](#) All Rights Reserved. [Privacy statement](#), [Terms and Conditions](#). Comments? We would like to hear from you. E-mail us at customercare@copyright.com



RightsLink®

[Home](#)[Account Info](#)[Help](#)

Title: Fluctuation theorems for total entropy production in generalized Langevin systems

Author: Bappa Ghosh, Srabanti Chaudhury

Publication: Physica A: Statistical Mechanics and its Applications

Publisher: Elsevier

Date: 15 January 2017

Logged in as:
Bappa Ghosh
IISER Pune

[LOGOUT](#)

© 2016 Elsevier B.V. All rights reserved.

Please note that, as the author of this Elsevier article, you retain the right to include it in a thesis or dissertation, provided it is not published commercially. Permission is not required, but please ensure that you reference the journal as the original source. For more information on this and on your other retained rights, please visit: <https://www.elsevier.com/about/our-business/policies/copyright#Author:rights>

[BACK](#)[CLOSE WINDOW](#)

Copyright © 2019 [Copyright Clearance Center, Inc.](#) All Rights Reserved. [Privacy statement](#), [Terms and Conditions](#).
Comments? We would like to hear from you, E-mail us at customer@copyright.com